UNIVERSITÄTSKLINIKUM HAMBURG-EPPENDORF

Zentrum für Innere Medizin
III. Medizinische Klinik und Poliklinik, Nephrologie, Rheumatologie und Endokrinologie

Prof. Dr. med. Tobias B. Huber

Loss of *P3h2* gene causes thin basement membrane nephropathy in mice

Dissertation

zur Erlangung des Doktorgrades Dr. rer. biol. hum. / PhD
an der Medizinischen Fakultät der Universität Hamburg.

vorgelegt von:

Hande Aypek
aus Bursa/ Türkei

Hamburg 2020

Angenommen von der
Medizinischen Fakultät der Universität Hamburg am: 23.11.2020
Veröffentlicht mit Genehmigung der
Medizinischen Fakultät der Universität Hamburg.

Prüfungsausschuss, der/die Vorsitzende: Prof. Dr. Tobias Huber

Prüfungsausschuss, zweite/r Gutachter/in: Prof. Dr. Heimo Ehmke

Prüfungsausschuss, dritte/r Gutachter/in: _____

Table of Contents

1 Introduction

1.1 Kidney

Kidneys are bean-shaped organs in vertebrates that filtrate blood. In humans, they localize to the retroperitoneal space-left and right of the spine. Each kidney has two main structures named as the kidney cortex and kidney medulla (Figure1A). Kidneys receive blood from the renal arteries and blood exits the kidneys via the renal veins post filtration. Kidneys excrete urine as a waste product of the body. During urine formation, the kidney performs sequential steps of ultrafiltration, reabsorption of nutrients and water, secretion, and excretion of waste products. Besides the filtration of blood, mammalian kidneys have other important functions. They play an active role in blood pressure regulation, acid-base homeostasis, hormone secretion and regulation of osmolality. Blood pressure and osmolality regulation by kidneys are related to salt-water balance and extracellular fluid composition. Reabsorption of phospho and bicarbonate from urine as well as excretion of hydrogen ions into urine keep the acid-base homeostasis in the body [1].

There are several types of kidney diseases being classified as acquired or congenital. Polycystic kidney disease or Alport Syndrome are examples of congenital kidney diseases. Acquired types of kidney diseases can be subdivided as metabolic and auto-immune. Diabetic nephropathy is an example of metabolic and Goodpasture's syndrome can be an example of autoimmune kidney disease. Kidney diseases can also be classified as acute or chronic. Progressive chronic kidney disease (CKD) can lead to end-stage kidney disease (ESKD). These patients require dialysis or kidney transplantation.

The nephron is the functional unit of kidney. There are on average 1 million – 2.5 million nephrons in both adult human kidneys [2]. A nephron is divided into two parts: glomerulus and tubule. The Glomerulus works as the filtration unit and the tubule functions as the reabsorption unit. Primary urine is filtered through the glomerulus and collected in Bowman's capsule. In the following steps, urine passes through the different parts of the tubule: proximal tubule, the loop of Henle, distal tubule, and collecting duct. Tubules are enriched with transporters, ion and water channels to regulate reabsorption of salt and water (Figure 1B)[3] [4].

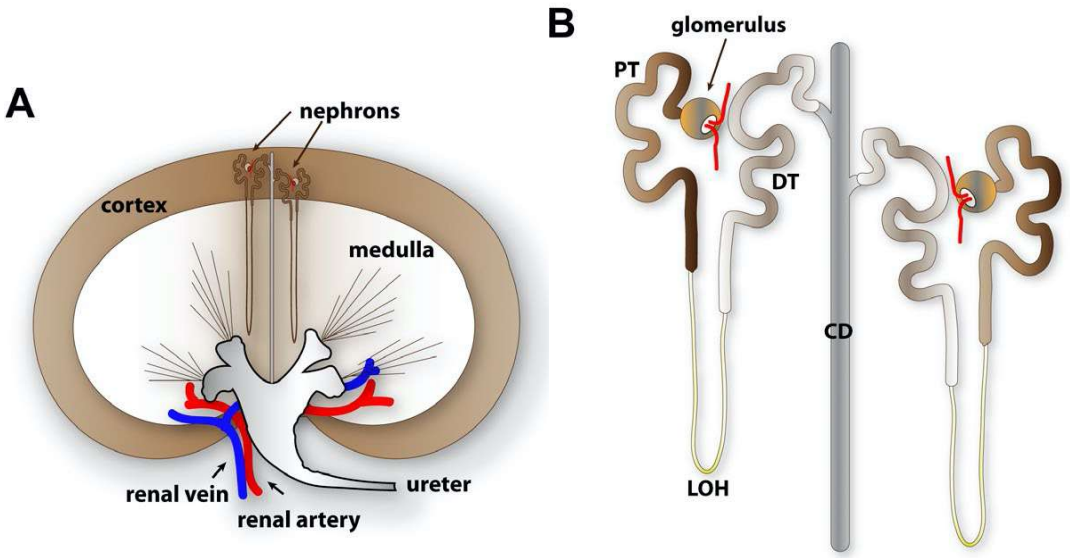

Figure 1: Kidney. A) Anatomic view of a kidney. Kidney cortex and medulla are main structures of the kidney. Renal artery and renal vein are the main blood vessels carrying blood into and out from kidney, respectively. B) Structure of a nephron. A nephron is divided in two parts: glomerulus and tubule. Proximal tubules (PT), loop of Henle (LOH), distal tubules (DT), and collecting duct (CD) are sub-types of the tubules [1].

1.2 Glomerulus

The glomerulus is embedded in Bowman's capsule and consists of small capillaries branched in a parallel fashion and four different types of glomerular cells [5]. Blood enters the glomerulus via the afferent arteriole (AA) and exits via the efferent arteriole (EA). The different types of glomerular cells are named: parietal epithelial cells (PECs), glomerular endothelial cells (GECs), mesangial cells (MCs) and podocytes (Pods) (Figure 2).

1.2.1 Parietal epithelial cells

Parietal epithelial cells (PECs) adhere to the inner wall of Bowman's capsule as a monolayer. There are different types of PECs, presumably having different functions. However, function of PECs is not fully understood but they might have a reparative function by sealing of leakages from the glomerular filter. In case of glomerular injury, PECs are activated and migrate to the glomerular tuft. They increase secretion of

extracellular matrix (ECM) proteins leading to glomerulosclerosis and proliferate ending up in crescent formation [6]. Crescentic glomerulonephritis (CGN) and focal segmental glomerulosclerosis (FSGS) are renal disease entities related to PEC activation and proliferation [7].

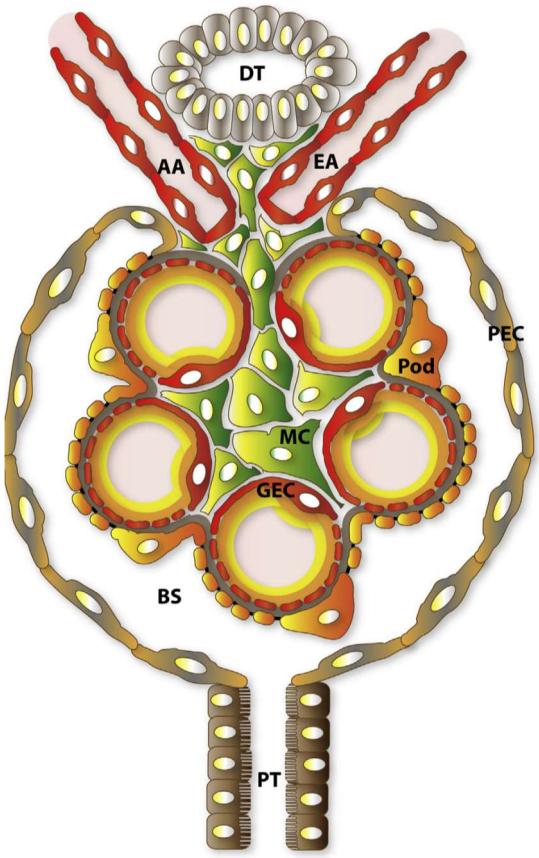

Figure 2: Glomerulus and its components. Parietal epithelial cells (PECs) attach and line the inner wall of Bowman's capsule. Glomerular tuft is composed of mesangial cells (MCs), glomerular endothelial cells (GECs) and podocytes (Pods). Blood enters glomerulus via the afferent arteriole (AA) and leaves via the efferent arteriole (EA). Urine collect at Bowman space and pass through proximal tubules (PT) [1].

1.2.2 Mesangial cells and mesangium

Mesangial cells (MCs) are contractile like smooth muscle cells and have an irregular shape. MCs secrete ECM proteins like fibronectin, laminin and Collagen 1 (Col1) to form the mesangial matrix. MCs and mesangial matrix compose the mesangium which is at the center of the glomerular tuft and maintains the structural architecture of the

glomerulus [8]. MCs control capillary flow via contracting and relaxing regulated by paracrine or autocrine signals to keep hydrostatic pressure in balance. MCs are directly interacting with GECs and have a role in the regulation of the glomerular filtration rate (GFR) [9].

MCs and mesangial matrix play an important role in glomerular injury. They respond to injury with proliferation, excess matrix production, and release of cytokines and chemokines [10]. In addition, GFR is negatively affected by increased activity of MCs which might lead to fibrosis. The proliferation of MCs and an increase in mesangial matrix production are observed in several different glomerular diseases i.e. IgA nephropathy and diabetic nephropathy [11].

1.3 Glomerular filtration barrier

Glomerular Filtration Barrier (GFB) is the site of ultrafiltration of blood via hydrostatic pressure in the glomerulus [12]. The GFB is composed of fenestrated GECs and glycocalyx, glomerular basement membrane (GBM), podocytes, and slit diaphragms (SDs) (Figure 3). These three-layers of the GFB provide ultrafiltration in a size- and charge-selective manner [13]. The GFB is a perm-selective barrier. Water and small molecules can freely pass through the GFB. On the other hand, macromolecules, proteins, and cells cannot pass the GFB under basal conditions. However, when homeostasis of the GFB is disrupted by genetic or environmental factors, proteins or red blood cells (RBCs) can pass through Bowman's capsule leading to albuminuria and hematuria, respectively. Albuminuria and hematuria are indicators of kidney diseases and severe albuminuria can end up with CKD or ESKD [14].

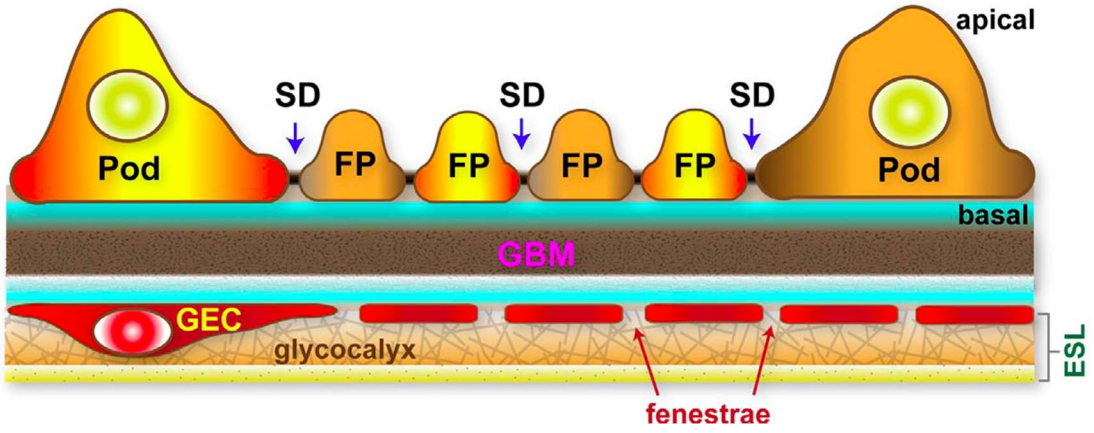

Figure 3: Glomerular filtration barrier. Fenestrated endothelium, glomerular basement membrane (GBM), podocytes and slit diaphragm (SD) between foot processes form the glomerular filtration barrier (GFB). Ultrafiltration of blood occurs at the GFB via hydrostatic pressure. The GFB is a perm-selective barrier and its homeostasis is vital for maintenance of glomerular integrity [1].

Even though each layer of the GFB has been identified and their functional characterization was done in great detail, the mechanism of ultrafiltration at the GFB to date is not fully understood. There are several models trying to explain the process of filtration and the mechanism preventing clogging of the GFB. The heteroporous model was the classical model first suggested in the 1980s and refined over time. It is a mathematical model supported in part by experiments in past years, trying to explain the size permeability of the GFB. This model assumes that the GFB consists of different pores that allow passage of small molecules and prevent the passage of macromolecules and proteins [15]. In this model, there are two parameters; convective flux and diffusive flux. The convection flux is depending on the flow of water passing through the GFB which is proportional to hydrostatic pressure. Diffusion is dependent on the concentration difference of macromolecules in the capillary lumen and filtrated urine at the Bowman's capsule [16].

Another model was suggested by Marcus Moeller and colleagues in 2010. It extended the classical model by adding an electrophoretic effect created during ultrafiltration. In this model, the streaming potential between Bowman's capsule and the endothelial lumen is the driving mechanism for charge selectivity at the GFB. The negative electrical field is

higher in Bowman's capsule than the capillary lumen which prevents the passage of negatively charged macromolecules such as albumin. This extended model is able to explain both size and charge selectivity of the GFB [17].

The most recent model was suggested by William H. Fissell and Jeffrey H. Miner in 2018. They emphasize the role of mechanical forces on the GFB. Compression forces from the foot processes of podocytes prevent the passage of macromolecules from the GBM. In disease conditions, decreased podocyte contractile strength due to foot process effacement leads to a decreased compression level of the GBM and makes it leaky for macromolecules [18].

All approaches were able to explain mechanism of ultrafiltration in a specific manner. However, in each approach, there are still questions which need to be answered.

1.3.1 Glomerular endothelial cells and glycocalyx

Glomerular endothelial cells (GECs) are situated in the inner capillary wall. GECs are flat cells and have 60 nm-100 nm fenestrations to provide passage of water. GECs are covered by a glycocalyx at their luminal side. The glycocalyx is mainly composed of proteoglycans that have negatively charged glycosaminoglycans (GAG) on their cell surface. The glycocalyx regulates interaction of leukocytes with GECs and plays a role in capillary permeability [19]. Initially, it was thought that the glycocalyx allowed free passage of albumin and macromolecules and had no effect on the ultrafiltration process of the GFB [20]. However, recent studies revealed that the membrane of GECs and the glycocalyx are negatively charged; this hinders the passage of albumin and macromolecules[21] [22].

Glomerular injury induces apoptosis of GECs and loss of fenestrations. Damage of the glycocalyx and loss of GAG interaction are further observations. Anti-neutrophil cytoplasmic antibodies (ANCA) -associated glomerulonephritis (GN) and Lupus nephritis are kidney diseases related to GECs and glycocalyx pathology [23].

1.3.2 Podocytes and slit diaphragm

Podocytes (Pods) are a post-mitotic special epithelial cell and they are situated on the outer wall of the glomerular capillaries. Pods are polarized cells which have a large cell body with primary and secondary cellular protrusions. Secondary membrane protrusions are called foot processes (FPs). FPs surround the capillary wall and foot processes of neighboring Pods form a specialized cell-cell junction called the slit diaphragm (SD) [24]. Podocytes are the last layer of the GFB and it is the most vital component of GFB to keep ultrafiltration in balance.

The backbone of FPs is formed by actin cytoskeletal proteins. Actin is one of the key proteins for the maintenance of healthy Pods and structural function of it keeps the FPs in their proper shape as long processes. Quick polymerization and depolymerization dynamics of actin is an advantage for Pods to adapt themselves in response to environmental changes. Dysregulation of actin dynamics in Pods induces foot process effacement (FPE) [25]. Actin is known as essential interactor for SD and focal adhesions (FA) thereby actin can mediate signaling between these two structures [26]. Their interaction with each other determines podocyte response to different environmental stimuli [27]. FAs are enriched with integrins and they have a complex and dynamic structure. FAs are facing the tensile and shear stress from the GBM and have vital roles for podocyte health [28].

Podocyte loss in excess of 20% induces progressive glomerulosclerosis [29]. In stress conditions, actin composition is changed in FPs and induces FPE disrupting the SD structure and causes podocyte loss. Podocyte related gene mutations are mainly found in steroid resistant nephrotic syndrome (SRNS) patients who have a histological diagnosis of FSGS. On the other hand, podocyte injury can be driven in other kidney diseases as well. Defects in any layer of the GFB can induce podocyte injury.

1.3.2.1 Slit diaphragm

Slit diaphragm (SD) is a specialized cell-cell junction between the FPs of adjacent Pods. SD at least anatomically is the outermost part of the filtration barrier and prevents the passage of proteins and cells. Two main SD structural proteins are NPHS1 and KIRREL1. Recently their exact position within the SD was investigated with high-resolution ultrastructural cryo-electron microscopy. It was shown that the KIRREL1 protein localized to the lower part of the SD spanning a width of 23 nm and NPHS1 localized to the apical part of the SD bridging a width of 45 nm [30].

NPHS1 is encoded by the *NPHS1* gene in humans. It is a type 1 transmembrane protein and belongs to the immunoglobulin superfamily. It has eight or nine IgG domains, one fibronectin like domain and a cytosolic tail. A different number of IgG domains were detected at two different groups [30] [31]. Besides its structural function NPHS1 acts as a scaffold protein for actin dynamics. Mutations in the *NPHS1* gene lead to the congenital nephrotic syndrome of the Finnish Type characterized by severe albuminuria and foot process effacement [32].

KIRREL1 is encoded by the *KIRREL1* gene. It is also a type 1 transmembrane protein and has structural homology with NPHS1. It has five IgG-like domains, a transmembrane domain and a short intracellular domain [33]. In humans, a mutation in the *KIRREL1* gene was identified in SRNS patients and mutant KIRREL1 protein failed to localize to the SD [34].

The definitive structure of the SD has not been described yet but a couple of SD associated proteins were identified and investigated in detail for their role in SD maintenance. PODOCIN is encoded by the *NPHS2* gene. It is a stomatin protein family member and localizes to the SD attachment site in the inner cell membrane leaflet. PODOCIN is a kind of scaffold protein for SD assembly and likely to have a role in the signaling of the SD. It recruits NPHS1 to the membrane [35]. *NPHS2* gene mutations cause SRNS and primary FSGS.

Transient Receptor Potential Cation Channel Subfamily C Member 6 (TRPC6) is a calcium channel and has roles in chemo- and mechanosensation. In Pods, it potentially senses environmental changes and induce regulation of actin dynamics in FPs. Mutations in *TRPC6* are linked to FSGS [36]. CD2 Associated Protein (CD2AP) an adaptor protein and links to actin cytoskeleton with NPHS1 and PODOCIN [37]. *Cd2ap* knockout mice histologically have FPE and mesangial matrix expansion leading to nephrotic syndrome [38].

In the majority of glomerular diseases, FPE and SD disruption are the reasons for disease development. Moreover, it has been shown that SD maintenance and podocyte-GBM interaction are two vital mechanisms that keep the GFB in homeostasis. When these two mechanisms are disrupted by genetic or environmental factors, albuminuria and hematuria are induced [39]. Therefore, studying the composition and physiology of podocytes and SD in detail is very important to understand the pathophysiology of kidney diseases [40]. Over the last two decades, Pods and SD structures were investigated in detail to understand the mechanisms of filtration. However, even though there were a lot of new exciting findings, the detailed functional mechanisms of the SD are poorly understood.

1.3.3 Glomerular basement membrane

Glomerular basement membrane (GBM) is an ECM generated by GECs and Pods during glomerular development. There are three functions of the GBM that underline its important role for the maintenance of the GFB. Recently it has been shown that GBM was the most vital component of the GFB. It has both charge and size selectivity for blood filtration. In addition, the GBM is a scaffold that provides attachment sites for GECs and Pods as structural support. It is a key regulator for glomerular cells in basal and disease conditions since it provides cross-talk between GECs and Pods via different signaling pathways [41].

The GBM is a well-structured meshwork and its thickness is approximately 300-350 nm. Four main structural proteins of the GBM are secreted by GECs and Pods. These proteins

are Collagen 4 (Col4) α3α4α5, Laminin-521 (LM-521) α5β2γ1, heparan sulfate proteoglycans (agrin) and nidogens. In the architecture of GBM, there are two-layers of LM-521 under both GECs and Pods. Thick Col4 α3α4α5 layer is localized towards the center of the GBM and thin Col4 α1α1α2 is close to the endothelial site [42].

Laminins are glycoproteins and form heterotrimeric proteins which contain α-, β-, and γ-chains. Laminins harbor two structures: a long and a short arm. A long arm is formed by a coil-coil interaction of αβγ chains generating a cross-shaped composition. Cross-shaped NH2-terminal globular domains from three short arms mediate trimer polymerization. LM-521 is the predominant type of laminins within the GBM. Mutations in the *LAMB2* gene cause Pierson syndrome [43]. Pierson syndrome is classified as a rare, autosomal recessive congenital nephrotic syndrome and patients present with glomerulus sclerosis, ocular abnormalities, and neurological defects [44]. The *Lamb2* KO mouse developed signs of nephrotic syndrome including foot process effacement (FPE) and albuminuria [45].

Nidogens are basement membrane glycoproteins. Nidogen-1 and Nidogen-2 are the two representatives of this protein family in the GBM. They have three globular domains connected by two G-domains [46]. They are bridging proteins between LM521 and Col4 [47]. Single deletion of either *Nidogen-1* or *Nidogen-2* genes doesn't induce any GBM phenotype in mice. However, the deletion of both genes causes perinatal lethality because of disturbed late lung and cardiac development. However, GBM looked normal in these animals which suggests that nidogens might not be vital for GBM formation or their function is compensated by other proteins [48].

Heparan Sulfate Proteoglycans (HSP) are another group of GBM proteins. In the mature form of the GBM, agrin is the dominant type of the HSPs. Two other known HSPs in the GBM are Collagen 18α1 (Col18α1) and perlecan[49]. As nidogens, agrin is also a linker protein between LM521 and Col4. Agrin has sulfated glycosaminoglycan (GAG) side chains with a negative charge. The negative charge of agrin contributes to the negative charge potential of the GBM. However, the effect of agrin on the charge-selectivity function of the GBM is debatable since podocyte-specific *Agrin* KO mice have normal kidney function and proteinuria could not be detected [50].

Matrix metalloproteinases (MMPs) are calcium-dependent zinc-containing proteases. MMPs are a super protein family, divided into many classes such as collagenases, gelatinases, stromelysins, and others. Various MMPs are structurally similar to each other. They contain a pro-domain, a catalytic domain, a hinge region and a hemopexin like domain [51]. They have a role in tissue remodeling in which they degrade all kinds of ECM proteins and thereby modulate the ECM-receptor interaction. The activity of MMPs is regulated by tissue inhibitors of metalloproteinases (TIMPs). There are four families of TIMPs which downregulate the degradative activity of MMPs [52]. Elevated activity of MMPs is observed in kidney diseases enhancing the progression of the diseases via causing GBM abnormalities [53].

1.3.3.1 Collagen 4

Collagen 4 (Col4) is a member of the collagen superfamily and is only expressed in basement membranes. There are six different α-chains of Col4 named: α1, α2, α3, α4, α5, and α6. These alpha chains of Col4 generate three specific heterotrimers: $\alpha1\alpha1\alpha2$, $\alpha3\alpha4\alpha5$, and $\alpha5\alpha5\alpha6$. Their expression profile varies in different tissues. The $\alpha1\alpha1\alpha2$ heterotrimer is expressed in all basement membranes but the heterotrimers $\alpha3\alpha4\alpha5$ and $\alpha5\alpha5\alpha6$ are specifically expressed in the GBM of kidney and the BM of the skin, respectively. Their expression level also changes during development and maturation. The $\alpha1\alpha1\alpha2$ heterotrimer is highly expressed in embryonic GBM and is switched to $\alpha3\alpha4\alpha5$ during maturation. The reason behind this change is not well understood but it is thought that the $\alpha3\alpha4\alpha5$ heterotrimer is less susceptible to proteolytic degradation [54].

Genes encoding for Col4 sub-chains are located on three different chromosomes in humans. *COL4A1, COL4A2* are on chromosome 13, *COL4A3, COL4A4* are on chromosome 2 and *COL4A5, COL4A6* on chromosome X [55]. Col4 sub-chains are composed of a 7S domain, collagenous Gly-X-Y repeats, and a non-collagenous (NC1) domain. The N-terminal 7S domain is rich in cysteine and lysine residues providing the site of interchain crosslinking by disulfide bonds. Gly-X-Y repeats are necessary for molecular flexibility and serve as cell-binding sites [56] [57]. The C-term NC1 domain is

resistant to bacterial collagenase treatment. These NC1 domains are sub-chain specific and important for molecular recognition of Col4 isoforms. Crosslinking of Col4 happens outside the cell in two ways. Secreted Col4 heterotrimers can interact via their NC1 or 7S domain. These two different interaction possibilities provide structural complexity and make the tertiary structure of Col4 more accessible for interactor proteins i.e. nidogen and agrin [58].

Col4 is secreted outside of the cells via the secretory pathway. Col4 chains get all modifications such as hydroxylation of prolines and lysines, glycosylation of specific hydroxy-lysines in the Endoplasmic reticulum (ER)-Golgi network [59].

In the GBM, Col4 is located more at the center but still interacts with a couple of receptors on the podocyte membrane. Members of the integrin family are the most known membrane receptors of Pods. Integrins are transmembrane proteins and work as cell surface receptors for the GBM. They have alpha and beta subunits that form heterodimers at the plasma membrane. There are 18 alpha and 8 beta integrin subunits. Integrins have a large extracellular domain, a short transmembrane segment, and a short cytoplasmic tail. They interact with cytoskeletal proteins via their cytoplasmic tail and with ECM proteins via their large extracellular domain. Therefore they serve as a bridge between the cell and the ECM [60]. Integrin $\alpha 3\beta 1$ is the main type that is found in podocytes and it helps podocytes bind to the GBM. Podocyte-specific deletion of *Itga3* or *Itgb1* in mice leads to severe proteinuria and nephrotic syndrome in mice [61]. In addition, homozygous *ITA3* mutation was previously described in patients diagnosed with FSGS [62].

Discoidin domain receptor tyrosine kinase 1 (DDR1) is another receptor on the podocyte plasma membrane mediating GBM interaction. The DDR1 receptor has an N-terminal discoidin domain, an extracellular juxta membrane (JM) region, a transmembrane helix, a large cytosolic JM domain, and a C-terminal tyrosine kinase domain [63]. The DDR1 receptor is a tyrosine kinase receptor that directly interacts with Col4. Podocyte-specific *Ddr1* deletion in mice induces albuminuria and increases GBM thickness [64].

1.4 Nephrotic syndrome

Nephrotic syndrome (NS) is a kidney disease showing severe dysfunction of the GFB by leaking proteins and macromolecules. Patients with NS have four common symptoms; edema, albuminuria, hypoalbuminemia, and hyperlipidemia [65]. Clinically, a considerable proportion of NS patients are diagnosed with FGSG upon histologic evaluation of their kidney biopsies [66]. Congenital nephrotic syndrome is a special type of NS. The Human Genome Project and advances in sequencing technology have been able to identify more and more disease related genes in these patients (Figure 4). Identified gene mutations dominantly affected Pods. Therefore, researchers focused on this special cell type to understand the mechanisms of NS [67].

There are two types of treatment options for NS patients. These treatment options are immunosuppressive and supportive treatment. Immunosuppressive treatment aims to bring the kidney function as close to its basal level as possible, on the other hand supportive treatment aims to decrease the effect of symptoms caused by the disease. Immunosuppressive treatment includes calcineurin inhibitors (cyclosporine and tacrolimus), corticosteroids (prednisone) and rituximab. Corticosteroids are the most common treatment for childhood nephrotic syndrome having steroid-sensitive nephrotic syndrome (SSNS). Supportive treatment includes angiotensin-converting enzyme (ACE) inhibitors and angiotensin II receptor blockers, statins, prophylaxis for infection, diuretics and anticoagulants. The NS patients can have one or more forms of supportive treatment depending on their blood or urine analysis [68].

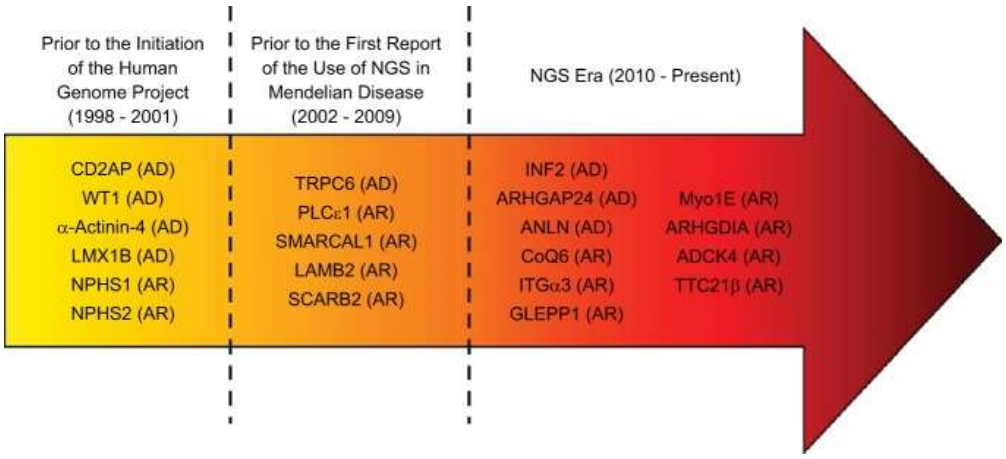

Figure 4: Timeline of discovered gene mutations in nephrotic syndrome. Discovery of gene mutations related with nephrotic syndrome did start with the Human Genome Project (1998-2001). Podocyte-specific gene mutations were identified in this project i.e. NPHS1 and NPHS2. Application of next generation sequencing (NGS) in Mendelian diseases (2002-2009) opened another window for new gene mutation discoveries. The improvement of NGS further enhanced the discovery of novel genes in addition to many new mutations in known genes. [69].

1.5 Glomerular basement membrane diseases

There are certain kidney diseases caused by a mutation in the genes of GBM proteins. Alport syndrome (AS), and thin basement membrane nephropathy (TBMN) are the ones related with *COL4* gene mutations.

1.5.1 Alport syndrome

Alport syndrome is a genetic disease that causes defects in kidney, skin, eye, and ear. Mutation in the genes of *COL4A3*, *COL4A4,* or *COLA5* causes Alport syndrome. There are two types of AS; X-linked and autosomal. *COL4A5* gene localizes to the X chromosome. Therefore, the severity and progression of the disease are different between genders. Males are affected more severely than females. Males progressively develop ESRD while females usually have a mild phenotype which can be explained by having two X chromosomes and random inactivation of one of them. Yet there is a considerable disease spectrum in females and co-factors i.e. hypertension can also cause severe disease in females albeit mostly at a later time point. In general, patients with AS have microhematuria and a lamellated GBM. The mainstay of treatment is ACE

inhibition (Ramipril) to decrease the pressure in glomerular capillaries that directly interferes with the extent of albuminuria [70].

Col4 composition is different in immature and mature GBM. During the early stages of development, GBM is mainly composed of Col4α1α1α2 and during maturation switches to Col4α3α4α5. In the GBM of Alport patient, Col4α3α4α5 is lacking and there is persistence of Col4α1α1α2. This is the molecular reason for a lamellated GBM appearance on EM and basket weave through the GBM to podocytes [57].

1.5.2 Thin basement membrane nephropathy

Thin basement membrane nephropathy (TBMN) is a mild hereditary GBM disease. Heterozygous *COL4A3* and/or *COL4A4* gene mutations cause TBMN. Patients with TBMN have hematuria, microalbuminuria, thinner GBM, and normal renal function. Early AS and TBMN patients have similar symptoms. Therefore, it can be difficult to distinguish between these two diseases. However, patients diagnosed as having TBMN have thinner GBM, and usually, a lamellated GBM isn't observed [71]. TBMN patients are treated with ACE inhibitors quite efficiently. They can live without severe problems for many years. However, in some cases, TBMN can end up with FSGS and ESKD.

1.5.3 Collagen 4 nephropathies and FSGS

AS and TBMN are progressive diseases and in long term patients can develop ESKD. All diseases related to mutations in *COL4A3, COL4A4,* and *COL4A5* are called collagen 4 nephropathies. In the literature, patient cohorts from different populations were investigated for the development of Col4 nephropathies. It was shown that patients diagnosed with both TBMN or AS can develop FSGS throughout their life usually beyond the age of 40. The mechanism behind the progression from TBMN to FSGS is not known but it is thought that modifier genes and environmental factors (e.g. hypertension) might be key for this conversion (Figure 5) [72 73 74 75].

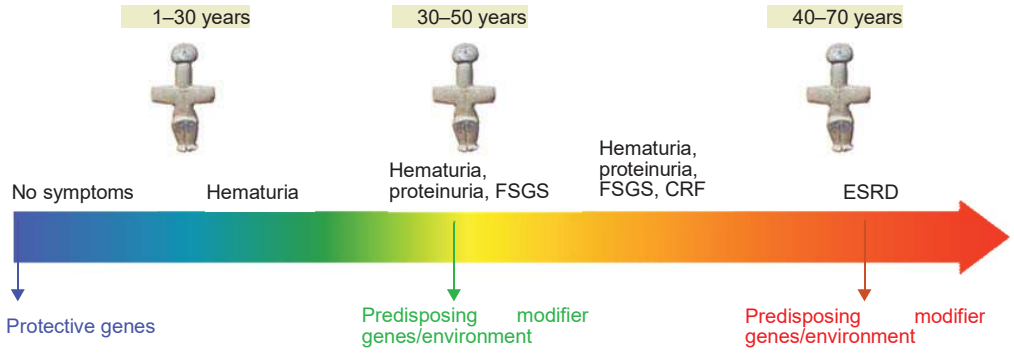

Figure 5: Collagen 4 nephropathies. The phenotype of Col4 nephropathies is variable over a large spectrum from no symptoms to end stage renal disease. Moreover, progression of disease depends on age, genetic and environmental factors. Progression of the patient phenotype is observed over time [76].

ER stress and unfolded protein response (UPR) is a possible mechanism for the development of FSGS. Col4 sub-chains are highly modified by PTMs and all of these PTMs are added to procollagen chains in the ER. Overexpression of the *COL4A3*-G1334E mutant sub-chain in Pods induces ER stress and UPR. Mice with knock-in *Col4α3*-G1334E mutation shows AS-like phenotype with GBM irregularities and has upregulated UPR response [77].

1.6 Prolyl 3-hydroxylase 2

P3H2 encodes prolyl 3-hydroxylase 2 (P3H2) enzyme which is a member of the Leprecan proteoglycan family. P3H2 is a post-translational modifier (PTM) and catalyzes 3' hydroxylation (3Hyp) of proline residues of collagens, especially Col4. Hydroxylation of Col4 is important for chain assembly, crosslinking, stability, and protein-protein interaction [78]. For hydroxylation, P3H2 is targeting a consensus sequence (Gly-P-4HypP). 4Hyp is a vital pre-step for 3Hyp of prolines. 3Hyp is most abundant in Col4 sub-chains and it might increase the flexibility of these chains within the basement membranes. The exact number and localization of 3Hyp sites of Col4 sub-chains are not known completely to date and their effect on Col4 structure and function remains still unclear. On the other hand, detected 3Hyp sites are evolutionarily conserved hence it is hypothesized that they might have a relevant function for collagen structure and synthesis. Hydroxylase activity

of P3H2 is enhanced by 2-oxoglutarate dioxygenases [78]. The chemical process for hydroxylation;

2-oxoglutarate + L-prolyl-[procollagen] + O_2 $\xrightarrow{P3H2}$ CO_2 + succinate + trans-3-hydroxy-L-prolyl-[procollagen] [79].

P3H2 is localized on chromosome 3. It produces 3.4 kb long transcript encoding 708 amino acids; and translated to ~80 kDa protein. The structure of P3H2 consists of a prolyl 4- hydroxylase domain, four tetratricopeptide repeats (TPRs), P-loop, C terminal ER retention signal, and a leucine zipper. N- term TPR provides the protein-protein interaction with a partner protein. TPR motifs are important for many cellular processes such as cell cycle control and chaperone interaction. The Leucine zipper domain is at the center of P3H2 protein and it plays a role in dimerization. Prolyl 4- The hydroxylase domain is the catalytic center of the enzyme. KDEL (ER signal) provides the recycling of the enzyme within the ER-Golgi network. P3H2 is structurally highly similar between mouse and human (92%). P3H2 has 3 potential N-glycosylation sites at Asn449, Asn460, and Asn549 [80].

P3H2 localizes at the ER-Golgi network and it's not secreted. *P3H2* is highly expressed in tissues which have a basement membrane such as kidney and eye. In the Leprecan family, there are two other members besides P3H2. These proteins are P3H1 and P3H3. P3H1 is the first identified Leprecan protein and it is a 3Hyp modifier of fibrillary collagens. The absence of this protein causes Osteogenesis Imperfecta Type, 4. P3H3 is another member of the Leprecan family. This protein has a function as a tumor suppressor gene and is associated with different types of Amyotrophic Lateral Sclerosis [81].

Mutation in the *P3H2* gene is related to high myopia and cataract formation. Myopia (near-sightedness) is an eye disorder characterized by a blurred vision of long-distance objects. It occurs when the eye is longer and cornea is too steep resulting in a focus shift of light rays in front of the retina. It is the most common eye problem. There are mainly two types of myopia according to degree of the refractive error: low or high myopia. High myopia is mainly related to genetic heritage. There are currently three types of high myopia: autosomal dominant, autosomal recessive, and X-linked high myopia. In Chinese and

Israelian myopia patient cohorts, *P3H2* nonsense mutations were detected and classified as a causative gene for myopia [82].

There are more diseases in which the effects of P3H2 were investigated. *P3H2* acts as a tumor suppressor gene in human hepatocellular carcinoma (HCC). *P3H2* overexpression decreases cell proliferation of tumor cells by downregulating of cyclins within the cell cycle [83]. In the literature, *P3H2* expression in the kidney had been shown but its function hasn't been investigated yet [84].

1.7 Aim of the study

A *P3H2* mutation was identified in a young female patient by using an expression-based candidate gene approach. P3H2 is a PTM enzyme and hydroxylases 3Hyp of prolines of Col4. The functional relevance of P3H2 as a Col4 modifier had not been studied in glomeruli before. In recent years, PTMs are getting more attention in different fields since they have vital roles for proper protein function. Their effect on different disease development and progression increase their impact as potential treatment option. Therefore, in our project we aimed to investigate the effect of *P3H2* on GBM, GFB, and glomerular homeostasis. We used two approaches one in-vitro and the other in-vivo to better understand the function of the P3H2 enzyme in kidney. Generation of a *P3H2* human podocyte cell line was our in-vitro approach and generation of podocyte specific *P3h2* KO mice was the in-vivo approach. We aimed to observe effect of *P3H2* deletion on cell matrix interaction and ECM production via in-vitro approach. In-vivo approach was applied to observe its effect on GBM and GFB as well as comparison of mice phenotype with the *P3H2* patient phenotype.

2 Materials and Methods

2.1 Detection of *P3H2* gene

An expression-based candidate gene approach was applied to identify novel genes in a nephrotic syndrome patient cohort. A corresponding Next Generation Sequencing (NGS) -based panel for the parallel analysis of all previously described and potentially new causative genes was established. The candidate genes were selected using a comparative and sequential algorithm from genes heavily expressed in mouse podocytes. With the help of publicly accessible databases, the 750 most enriched transcripts in the mouse were tested for their expression in human kidney cortex, human glomerulus, and their occurrence in the murine podocyte proteome, a significant regulation in human proteinuric diseases or a statistical overrepresentation of the respective "Gene Ontology (GO) term" -based gene clusters. The most promising candidates were chosen according to their scores. After the fragmentation of the genomic DNA, the coding exons, as well as the corresponding exon-intron transitions, were enriched with Roche / NimbleGen technology, amplified and then sequenced simultaneously on an Illumina MiSeq system. The analysis of the NGS data was carried out using in-house established bioinformatics evaluation methods as well as the JSI Medical Systems software (V4.0). Currently, our custom-designed panel contains 258 enriched genes with a total of 3889 exons. *P3H2* gene had one of the highest GO term values on the analysis. A young female patient suffering from FSGS had a homozygous *P3H2* mutation.

2.2 Conditionally immortalized human podocyte cell line

A conditionally immortalized human podocyte cell line was used for in-vitro experiments. The cell line was generated by retroviral transduction including SV40 large T antigen gene to keep the cells in a proliferative status at permissive conditions (33° C). The cell line starts to differentiate at non-permissive conditions (37° C) since the SV40 T antigen is heat-inactivated [85]. RPM1-1640 medium (Sigma Aldrich, R7388) was supplemented with 10% fetal bovine albumin (FBS), 1% Penicillin/Streptavidin (P/S), Moin supplement (1M HEPES, 50 mM Sodium pyruvate and minimum essential medium (MEM)) and 0.1% Insulin Selenite Transferrin (ITS) to make the complete medium. The cell line was

maintained in an incubator at 33° C, 5% CO_2, and was differentiated at 37° C for 12-14 days before experiments. During differentiation, the medium was changed three times a week.

2.2.1 Splitting the cell line for experiments

The cells were washed with 5 ml 1x PBS (Thermo Fisher, 14190136) twice and incubated with 1ml 0.05% Trypsin-EDTA (Thermo Fisher, 25300054) for 5 min at 33° C in an incubator. Detached cells were collected in a 15 ml falcon after inactivating 0.05% Trypsin-EDTA with 5 ml complete medium. Cells were centrifuged at 1200 x rpm for 5 min. The supernatant was aspirated and the pellet was resuspended in 1 ml complete medium. The maintenance dilution of cells was from 1:6 to 1:10 and cells were seeded in a 10 cm cell culture dish.

2.2.2 Counting the cell line for experiments

After cells were resuspended in 1 ml complete medium, 50 µl 0.4% Trypan Blue (Gibco, 15250061) was mixed with 50 µl of the cell suspension. 10 µl was loaded in a cell counting slide and cells were counted by a TC20™ Automated Cell Counter (Bio-Rad, 1450102). The volume of the particular cell number was calculated and cells were seeded in cell culture plates and incubated in a 37° C incubator to start differentiation.

2.2.3 Freezing the cell line in liquid nitrogen vapor

Dimethyl sulfoxide (DMSO) is used as a cryoprotectant to reduce ice formation and keep the cells alive in liquid nitrogen vapor [86]. The freezing medium was prepared with 10% DMSO and 90% complete medium and stored at 4° C. Cells with confluency of 70%-80% in a 10 cm cell culture dish were used to freeze in a single cryovial. The cells were first washed with 1x PBS and incubated with 0.05% Trypsin-EDTA for 5 min at 33° C. Then, they were centrifuged at 1200 x rpm for 5 min. The supernatant was aspirated and the pellet was resuspended in 1 ml freezing medium in the cyrovial. The cryovials were placed in a Corning® CoolCell™ LX Cell Freezing Container (Corning, CLS432002) and stored at -80° C overnight. This container decreases the temperature as 1° C/min to avoid

formation of ice crystals. For long-term storage, the cryovials were transferred into liquid nitrogen vapor following day.

2.2.4 Thawing the cell line from liquid nitrogen vapor

The complete medium was warmed up at 37° C for 30 min and a 15 ml falcon was filled with 7 ml warm complete medium. The cell vial was taken from the liquid nitrogen vapor and incubated in a 37° C water bath for 2 min. After the cells thawed, 1 ml cell suspension was transferred into the 15 ml falcon with warm complete medium. The falcon was centrifuged at 1200 x rpm for 5 min. The supernatant was aspirated to get rid of remaining DMSO and cells were resuspended in fresh 10 ml complete medium. The cell suspension was transferred into a 10 cm cell culture dish and kept in 33° C incubator. The cells were evaluated under the microscope after 24 hours for viability and characteristics.

2.3 Polymerase chain reaction and agarose gel electrophoresis

Polymerase chain reaction (PCR) is used to amplify the target DNA region with polymerase enzymes by target-specific designed primers. Denaturation, annealing, and elongation are the steps of the PCR. Denaturation steps occur at 95° C to disrupt hydrogen bonds between DNA double helix to make it a single strand. During the annealing step, the target-specific primers bind to single-strand DNA at the optimum temperature for this primer pair. During the elongation step, DNA polymerase amplifies the DNA strand at 72° C. To get a sufficient amount of PCR product this reaction is repeated around 35-40 cycles in a thermal cycler.

We used different polymerases, (Phusion, Taq, GoTaq and DreamTaq) in our project. After PCR amplification, the products were run and visualized in a 1.5% agarose gel by electrophoresis. 1.5% agarose gel was prepared by mixing 100 ml Tris-acetate EDTA (TAE) Buffer and 1.5 g agarose (SERVA, 11404.07). The mixture was boiled in the microwave around 2 min until the agarose dissolved completely. Prepared gel was cooled down and 2 µl EtBr was added to the solution. After mixing well, it was poured on the gel tank and dried around 30 min at RT. PCR products were loaded onto the gel and run at

100 V for 40 min. At the final step, DNA bands were visualized under UV light with a wavelength of 366 nm.

2.4 Heat-shock transformation

50 µl DH5-alpha chemically competent bacteria and 5 µl DNA ligation products were mixed and incubated for 30 min on ice. Bacteria and ligation suspension were heat-shocked for 45 sec at 42° C and incubated for 2 min on ice. 450 µl SOC medium was added on transformed bacteria and transformants were incubated at 700 rpm for 1h at 37° C. During incubation, LB-Ampicillin plates were warmed up at 37° C. Bacteria were centrifuged at 2400 x rpm for 5 min and most of the supernatant was aspirated. Bacteria were resuspended with the remaining liquid and 50-100 µl bacterial suspension was spreaded on LB-Ampicillin plates. Plates were incubated overnight at 37° C in an incubator.

2.5 DNA isolation from bacterial cultures

2.5.1 Mini DNA isolation

DNA isolation was done by using the Zyppy™ Plasmid Miniprep Kit (Zymo, D4036) according to the manufacturer's protocol. 600 µl of bacterial culture and 100 µl of 7x Lysis Buffer were mixed by inverting a 1.5 ml Eppendorf 4-6 times to lyse the bacteria. 350 µl of cold Neutralization Buffer was added and mixed on lysed bacteria to stop the lysis reaction. The samples were centrifuged for 2 min at 11.000 x g and the supernatant was transferred into a Zymo-Spin™ IIN column. The samples were centrifuged at 11.000 x g for 15 sec and the flow-through was discarded. 200 µl of Endo-Wash Buffer was added into the column and centrifuged for 30 sec at the same speed. 400 µl of Zyppy™ Wash Buffer was added into the column and centrifuged for 1 min. The column was placed into a clean 1.5 ml Eppendorf and 30 µl of Zyppy™ Elution Buffer was put directly into the column matrix and incubated for 1 min at RT to elute DNA.

2.5.2 Maxi DNA isolation

100 µl mini-culture suspension was inoculated into 100 ml LB-Ampicillin medium and culture was grown overnight at 37° C with 200 x rpm shaking. QIAGEN® Plasmid Maxi Kit (Qiagen, 12263) was used according to the manufacturer's protocol to isolate high concentrated DNA. The overnight bacterial cultures were centrifuged at 6000 x g for 15 min at 4° C. The bacterial pellet was resuspended in 10 ml Buffer P1. Then, 10 ml Buffer P2 was added on bacterial suspension and mixed by inverting 4–6 times and incubated for 5 min at RT to lyse the bacteria. 10 ml pre-chilled Buffer P3 was added on lysed bacteria and mixed by inverting 4–6 times. The lysate was poured into the barrel of the QIAfilter Cartridge and incubated for 10 min. On the other side, a QIAGEN-tip was equilibrated by adding 10 ml Buffer QBT, and the column was allowed to empty by gravity flow. Then, the cap from the QIAfilter Cartridge was removed and the plunger was inserted gently. The cell lysate was filtered into the previously equilibrated QIAGEN-tip and it was allowed to enter the resin by gravity flow. The QIAGEN-tip was washed with 30 ml Buffer QC twice. Elution was performed with 15 ml Buffer QF into a 50 ml falcon. The DNA was then precipitated by adding 10.5 ml 70% isopropanol and centrifuged at 15000 x g for 30 min at 4° C. The DNA pellet was washed with 5 ml 70% ethanol and centrifuged at 15000 x g for 10 mins. It was dried for 10 min at RT and dissolved with 300 µl TE Buffer pH 8.0. The concentration and quality of isolated DNA was measured by NanoDrop (section 2.6).

2.6 DNA and RNA concentration measurement by NanoDrop

The DNA and RNA concentration were measured by Denovix DS-11 spectrophotometer. 2 µl elution buffer was used as blank and then 2 µl DNA or RNA solution was loaded to the machine. Measured concentration was noted as well as 280/260 and 230/260 ratios. For DNA, 280/260 ratio should be around 1.8 which means highly pure DNA. For RNA, 230/260 should be around 2.0 which shows highly pure RNA. If these values are lower, it means that there is residual contamination which might interfere with further experiments.

2.7 In situ Hybridization

In situ hybridization (ISH) is a method that is used to detect RNA localization of genes of interest. In our project, we performed ISH to identify the localization of *P3h2* mRNA in the mouse embryo (E14.5) and P1 kidney.

2.7.1 Probe design

The MluI (ACG CGT) recognition site was attached to the forward primer and the NotI (GCG GCC GC) recognition site was attached to the reverse primer of the *P3h2* gene. 100 pmol /µl primer stocks were diluted in 10mM Tris Buffer pH 8.0. Mouse kidney postnatal day1 RNA was used as a template to clone fragments of mouse *P3h2* by using a one-step PCR kit (Qiagen, 210210) (Table 1). 3 µl PCR product was run on an agarose gel to control PCR efficiency. PCR products were purified by QIAquick® PCR Purification Kit (Qiagen, 28104) as indicated in the manufacturer's protocol. 5 volumes of Buffer PB was added to 1 volume of the PCR reaction and mixed by inverting 4-6 times. A QIAquick column was placed in a 2 ml collection tube and the samples were transferred to the QIAquick column and centrifuged at 11000 x g for 1 min. The column was washed with 750 µl Buffer PE and centrifuged at 11000 x g for 1 min. Flow-through was discarded and the empty column was centrifuged for 1 min. to remove the wash buffer completely. The column was placed in a 1.5 ml Eppendorf tube and 30 µl EB was put into the center of the column to elute the DNA. The column was centrifuged at the same speed for 1 min. and eluted DNA was stored at -20° C until setting up the restriction reaction. A restriction reaction was set for both PCR products and the pBSK II KS vector (Table 2).

One-step qPCR reaction	Volume (µl)
5x buffer	3 µl
dNTPs	0.6 µl
10 µM Primer Mix	1 µl
RNase out (Invitrogen, 10777-019)	0.15 µl
Enzyme Mix	0.6 µl
100 ng RNA	X µl
ddH_20	9.65-x µl
Final volume	15 µl

Temperature (°C)	Duration	Number of cycles
50° C	30 min	1
95° C	15 min	1
94° C	30 sec	40 cycle
60° C	30 sec	
72° C	1 min	
72° C	10 min	1
12° C	∞	1

Table 1. One-step PCR and its thermal cycler reaction.

Restriction reaction	Volume (µl)
Purified PCR product	10 µl
10x Cut smart	2 µl
ddH_20	7 µl
Restriction enzyme	1 µl
Final volume	20 µl

Table 2. Restriction reaction of pBSK II KS vector and PCR products for ISH probes.

After the overnight restriction of PCR products and the pBSK II KS vector, samples were run on the agarose gel. Particular bands were cut and were purified by QIAquick Gel Extraction Kit (Qiagen, 28704) according to the manufacturer's protocol. The gel slice was scaled and incubated with 3 volumes of Buffer QG (100 mg gel ~100 µl) for 10 min at 50° C. During this incubation, the tubes were vortexed every 2-3 min to increase dissolution of the gel. 1 gel volume of isopropanol was added to the sample and mixed. The QIAquick spin column was placed in a provided 2 ml collection tube. The sample was loaded onto the column and centrifuged at 11.000 x rpm for 1 min. The column was washed with 750 µl Buffer PE and centrifuged at 11.000 x rpm for 1 min. Then it was placed into a clean 1.5 ml Eppendorf. 50 µl Buffer EB (10 mM Tris-HCl, pH 8.5) was added to the center of the column carefully to elute the DNA. After centrifugation at 11.000

x rpm for 1 min, cleaned DNA was stored at -20° C until setting a ligation reaction. For cloning, the ligation reaction (Table 3) was set and incubated for 2h at RT.

Ligation	**Volume (µl)**
Ligation buffer	2.5 µl
pBSK II KS vector	0.5 µl
Purified PCR product	5 µl
T4 Ligase (NEB, M0202S)	0.8 µl
ddH_20	21.2 µl
Final volume	25 µl

Table 3. Ligation set up for ISH probes.

Transformation and DNA isolation from bacterial cultures were done as previously described in section 2.4. 5 µl DNA was used for restriction with MluI / NotI and positive colonies were sent for Sanger sequencing (GATC, T7 primer). Maxi-prep DNA isolation was performed from positive colonies as previously described in section 2.5.2 Linearization reaction was set for ISH probes (Table 4).

Linearization	**Volume (µl)**
10x Buffer	10 µl
100x BSA	1 µl
DNA (plasmid, 5µg)	5 µl
20U Enzyme	1 µl
ddH_20	83 µl
Total volume	100 µl

Table 4. Linearization reaction of ISH probes.

The reaction was incubated for 2h at 37° C and checked on the agarose gel. The size of the linearized plasmid was around 3000 bp (pBSK II KS vector + insert size). After cutting the particular band, DNA was purified by using QIAquick Gel Extraction Kit as described previously in this section. Then, the DIG RNA labeling reaction was set as in Table 5.

DIG RNA Labeling	Volume (µl)
RNase free ddH_20	10.5 µl
10x Transcription Buffer	2 µl
10x DIG RNA labeling mix (Roche, 11277073910)	2 µl
1 µg Linearized DNA	4 µl
20U RNase Inhibitor Enzyme	0.5 µl
40U RNA polymerase (T7, T3)	1 µl
Total volume	20 µl

Table 5. DIG RNA labeling for ISH probes.

The samples were incubated for 2h at 37° C. After that, 100 µl TE Buffer pH 8.0, 1 µl glycogen, 10 µl 4M LiCl and 300 µl 100% ethanol was added on the samples and incubated at -20° C overnight. The next day, the samples were centrifuged at max speed for 30 min at 4° C. The supernatant was discarded and 50 µl cold 70% ethanol was added on the samples. After centrifugation and drying on air, the pellet was resuspended in 50 µl TE Buffer pH 8.0 and 50 µl hybridization buffer was added. The probe could be stored in this 50% hybridization buffer for at least several months at -20° C.

2.7.2 In situ Hybridization - Day 1

Solutions for ISH	Recipe
Hybridization Buffer	12.5 ml formamide, 6.25 ml 20x SSC, 1.25 mg yeast RNA, 1.25 ml of 20% SDS, 1.25 mg heparin, 6 ml ddH_20
Wash 1	120 ml formamide, 60 ml of 20x SSC pH 4.5, 12 ml of 20% SDS, 48 ml ddH_20
Wash 2	90 ml formamide, 18 ml of 20x SSC pH 4.5, 72 ml ddH20
Blocking solution	1g blocking reagent (Roche,1096176), 2.5 ml heat-inactivated sheep serum, 500 µL Tween 20, 47 ml TBST
Anti-DIG Antibody solution	2.5 ml heat-inactivated sheep serum, 500 µL Tween 20, 17 µL AP-linked anti-DIG (1:3000 dilution), 47 ml TBST
NTMT	3 mL of 5M NaCl solution, 5 mL of 1M Tris-HCl pH 9.5, 3.75 mL 2M $MgCl_2$ solution, 1.5 ml Tween20, 127 ml ddH_20

Table 6. Recipes of ISH solutions.

The recipes for ISH solutions are listed above in Table 6. Tissues were sliced at 10 µm on a microtome and incubated with RNase free water overnight at 42° C. Dried tissues were evaluated and proper ones were chosen. For embryonic sections, a kidney and complete embryo without any tearing was a prerequisite. For paraffin sections, the deparaffinization procedure was applied as follows. The slides were immersed in the following order: Histo-clear (National Diagnostics, HS-200) for 20 min, 100% ethanol for 20 min, 95% ethanol for 1 min, 90% ethanol for 1 min, 80% ethanol for 1 min, 70% ethanol for 1 min, 50% ethanol for 1 min, 30% ethanol for 1 min and 1x PBS for 5 min. Next, the tissues were fixed with 4% PFA at RT for 15 min. At this point, paraffin and cryotome sections were processed together. The slides immersed in 1x PBS for 5 min, 50 µl Proteinase K (Roche, 3115887001) in 200 ml 1x PBS for 5 min, 2 mg/ml Glycine in PBS for 5 min, 4% PFA for 15 min, 0.25% acetic anhydride (Sigma Aldrich, A6404) in 0.1 M TAE (Sigma Aldrich, T1377) for 10 min and 1x PBS for 5 min. The slide mailer was filled with 7 ml Hybridization Buffer including 7 µl probe and warmed up to 68° C for 15 min. The slides were transferred to the slide mailers and incubated at 68° C for 24 h to 96 h.

2.7.3 In situ Hybridization - Day 2

The samples were taken from 68° C and the procedure described in Table 7 was applied. For every solution around 12 ml was put in the slide mailer.

ISH-Day 2	**Duration (min)**	**Temperature (°C)**
Wash 1	dip	68° C
Wash 1	3 x 15 min	68° C
Wash 2	3 x 15 min	68° C
TBST (Sigma Aldrich, T9039)	3 x 10 min	RT
Blocking reagent	30 min	RT
Anti-DIG Antibody solution	120 min	RT
TBST	4 x 15 min	RT
NTMT	3 x 15 min	RT
BM purple (Roche, 1442074)	1day -4 weeks	RT

Table 7. ISH second day protocol.

2.7.4 In situ Hybridization - Day 3

After the color reaction was checked under the microscope, the slides were washed with 1x PBS for 10 min twice. For dehydration of tissues, the slides were dipped in an ascending ethanol series (30%, 50%, 70%, 80%, 90%, and 95%) for 1 min. The slides then were transferred in 100% ethanol for 10 min twice and subsequently cleaned with xylene for 10 min twice. In the last step, the tissues were covered with Entellan mounting medium (Sigma Aldrich, 1079600500) and a coverslip. The slides were dried overnight under the safety hood and analyzed using a Zeiss Axio Scope.A1 microscope.

2.8 RNA isolation

RNeasy Micro Kit (Qiagen, 74004) was used for RNA isolation according to the manufacturer's protocol. The cell lines were grown on 10 cm cell culture dishes. 70-80% confluent cells were scraped with 5 ml 1x PBS and collected in 15 ml falcon. The cells were centrifuged at 1200 x rpm for 5 min. PBS was aspirated and the cell pellet was lysed with 350 µl Buffer RLT. The lysate was passed at least 5 times through a blunt 20-gauge needle (0.9 mm diameter) for homogenization. 350 µl 70% ethanol was added to the lysate and mixed well by pipetting. The lysate was transferred to a RNeasy MinElute spin column placed in a 2 ml collection tube and centrifuged at 8000 x g for 15 sec. 350 µl Buffer RW1 was added to the column and centrifuged at 8000 x g for 15 sec to wash the column's membrane. 10 µl DNase I (Qiagen, 79254) stock solution was added to 70 µl Buffer RDD and mixed by gently inverting the tube. The 80 µl DNase I mix was put directly to the column membrane and incubated for 15 min at RT. 350 µl Buffer RW1 was put into the column and centrifuged at 8000 x g for 15 sec to wash the column membrane. 500 µl Buffer RPE was added to the column and centrifuged at 8000 x g for 15 sec. 500 µl of 80% ethanol was added to the column and centrifuged at 8000 x g for 2 min. The column was placed in a clean 1.5 ml Eppendorf and 14 µl RNase-free water was added directly to the center of the column membrane and centrifuged at full speed for 1 min to elute the RNA. Isolated RNA was stored at -80° C and the RNA concentration was measured using a Nanodrop device (section 2.6).

2.9 cDNA synthesis and quantitative PCR

Quantitative PCR (qPCR) is a method to measure gene expression at the RNA level with the help of a fluorophore marked nucleotide. For qPCR, isolated RNA was converted to complementary DNA (cDNA) by reverse transcriptase. There are two ways to monitor DNA amplification. These are non-specific fluorescent dyes and sequence-specific DNA probes. In the first method, a fluorescent dye such as SYBR green intercalates with double-stranded DNA. In the second method, DNA probes are already labeled with fluorescent dye being detected after binding its complementary sequence. Housekeeping genes are used to normalize qPCR values [87]. We performed qPCR from the sorted glomerular cells to confirm the absence of P3H2 in podocyte-specific *P3h2* KO mice and evaluate expression profiles of *P3h2* on mouse glomerular cell types.

2.9.1 cDNA synthesis

ProtoScript® II First Strand cDNA Synthesis Kit (NEB, E6560S) was used for cDNA synthesis as the manufacturer's protocol and cDNA synthesis reaction were set as in Table 8.

cDNA synthesis	**Volume (µl)**
Total RNA 1–6µl (up to 1 µg)	6 µl
Random Primer	2 µl
Nuclease-free H_2O	to 8 µl
Incubation 5 minutes at 65°C	
2x ProtoScript II Reaction Mix	10 µl
ProtoScript II Enzyme Mix (10X)	2 µl
Total Volume	20 µl

Temperature (°C)	**Duration (min)**
25° C	5 min
42° C	60 min
80° C	5 min

Table 8. cDNA synthesis set up and cycler reaction.

2.9.2 Quantitative PCR

TaqMan Gene Expression Assays were used for qPCR experiments and reaction was set as in Table 9. Information about the used primers assays can be seen in Table 10. After setting the reaction, the samples loaded on the 96 well plates as duplicate. The plate was sealed with an optical adhesive cover and centrifuged at 5000 x rpm for 2 min. Applied Biosystems QuantStudio.3 Real-Time PCR Machine was used to run the reaction. The standard program (Table 9) was used. The delta-delta Ct method was used to calculate relative RNA level expression of target genes and GAPDH was used as a housekeeping gene. Primers used in TaqMan system are listed in Table 10.

qPCR reaction	**Volume (µl)**
20x TaqMan® Gene Expression Assay Mix	1 µL
cDNA template (10 to 100 ng of cDNA)	5 µL
2x TaqMan® Fast Universal PCR Master Mix	10 µL
RNase-free water	4 µL
Total volume	20 µL

Temperature (° C)	**Duration**	**Number of cycles**
50° C	2 min	1
95° C	10 min	1
95° C	15 sec	40 cycle
60° C	1 min	

Table 9. qPCR set up and reaction for TaqMan settings.

Primer name	**TaqMan ID**
P3h2	Mm01342192_m1
P3h2	Mm00557643_m1
Nphs2	Mm01292252_m1
Gapdh	Mm99999915_g1
Cd31	Mm01242576_m1
Myl9	Mm01251442_m1

Table 10. Primer information used in the TaqMan qPCR system.

2.10 Protein isolation

RIPA lysis buffer (50mM Tris/HCl pH 7.5, 1mM EGTA, 1mM EDTA, 1% (w/v) Triton X-100, 0.1% SDS, 150 mM NaCl and 50mM NaF) was used for protein isolation from both cell lines and glomeruli. Fresh 1 ml RIPA solution was prepared by adding 1µl 0.1% 2-mercaptoethanol (2-ME), 10 µl 1mM sodium orthovanadate, 40 µl protease inhibitor cocktail (Roche, 5892970001) and 50 µl phospho-stop (Roche, 4906837001). The cells were grown in a 10 cm dish until 70%- 80% confluency. They were washed with 5 ml 1x PBS and then, the cells were scraped with 5 ml 1x PBS. The cell suspension was transferred to 15 ml falcon and centrifuged at 1200 x rpm for 5 min. The supernatant was aspirated and the cells were lysed in 300 µl RIPA solution by pipetting. For gloms, the tissue was taken from -80° C and thawed on ice for around 5 min. 5µl RIPA solution/mg was added on gloms and this mixture was transferred to tissue grinders for homogenization. After 30 min incubation on ice, centrifugation was done at 14000 x rpm for 15 min. and the supernatant was collected as a total protein suspension. The protein suspension was cooked with 2x Laemmli at 95° C for 5 min to denature proteins. Isolated protein samples were stored at -20° C. 10 µl protein suspension was taken for protein concentration measurement by BCA Assay (section 2.11).

2.11 BCA assay for protein concentration measurement

Thermo Scientific™ Pierce™ BCA™ Protein Assay kit (Thermo Fisher, 23227) was used to measure protein concentration of isolated total proteins from cell lines, glomeruli, ECM of the cell lines and GBM of mice kidney. Protein suspension was diluted in ddH_2O as a 1:50 ratio. Standards (25, 125, 250, 500, 750, 1000, 1500 µg/ml) were prepared as suggested on the manufacturer's protocol. 10 µl from standards and diluted samples were transferred into a 96-well plate as duplicate. 200 µl Buffer B was mixed with 9.8 ml Buffer A. 100 µl Buffer mixture was added on standards and samples and incubated for 30 min at 42° C. The absorbance was measured at 562 nm in TECAN Sunrise Basic microplate reader and protein concentration was calculated by using the linear standard curve.

2.12 Western blot

Western blot (WB) is a method being used for the identification of target proteins by using an antibody against them in different tissues and cell types. In this procedure, proteins are solubilized by SDS, dithiothreitol (DTT), or 2-ME. The separation of proteins is done by running SDS-PAGE. The separated proteins on SDS gel are transferred to a PVDF or nitrocellulose membrane by an electrical force. All binding sites are blocked with a blocking reagent. The membrane is exposed to the primary antibody for generation antibody-antigen complexes. A secondary antibody with horseradish peroxidase (HRP) was applied to the membrane and proteins were visualized with the Enhanced Chemiluminescence (ECL) solution that activates the peroxidase and starts a chemiluminescence reaction [88].

2.12.1 SDS gel preparation

Fresh 7.5% or 10% SDS gels were prepared for western blot experiments. Stacking gel and resolving gels were prepared separately as indicated in Table 11 and loaded in the Bio-Rad glass gel preparation apparatus. Before preparing SDS gels, the glass and Teflon plates were assembled. Then, both SDS gels were prepared first with resolving gel followed by stacking gel. First, ammonium persulfate (APS) and tetramethylethylenediamine (TEMED) were added to the prepared resolving gel to start polymerization and 5 ml resolving gel solution was poured in the prepared glass gel system. 2 ml Isopropanol was added on top of the resolving gel solution to make the gel line straight. Polymerization took around 15 min at RT. The isopropanol was poured off and the glass dried with tissue paper. The stacking gel was prepared and poured on the resolving gel. The 10 mm comb was inserted immediately. It polymerized for around 30 min at RT. Prepared gels were kept in the running buffer at 4° C until starting WB.

Solutions	10% SDS gel		7.5% SDS gel	
	Resolving gel	Stacking gel	Resolving gel	Stacking gel
Resolving gel Buffer	6 ml		6 ml	
Stacking gel Buffer		2.5 ml		2.5 ml
30% Acyrlamid	4 ml	0.8 ml	3 ml	0.8
ddH20	2 ml	1.7 ml	3 ml	1,7
10% APS	120 µl	50 µl	120 µl	50 µl
TEMED	15 µl	7.5 µl	15 µl	7.5 µl

Table 11. SDS gel recipes for 10% and 7.5% resolving gel and stacking gel.

2.12.2 Running of SDS gels

Solutions for western blot	Recipe
2x Laemmli	33.3 ml 1.5M Tris-HCl pH 6.8, 100 ml 20% SDS, 100 ml Glycerol, 1g Bromophenol bleu, 500 ml dd H_2O
Resolving gel Buffer A (pH 8.8)	180 ml 2M Tris-HCl, 570 ml 2M Trizma Base, 20 ml 20% SDS, 1000 ml dd H_2O
Stacking gel Buffer B (pH 6.8)	242 ml 2M Tris-HCl, 8 ml 2M Trizma Base, 20 ml 20% SDS, 1000 ml ddH_2O
10x Running Buffer	720 g Glycine, 50 g SDS, 150g Trizma Base, 5000 ml ddH_2O
10x Protein Wash Buffer	1530 ml 1M Tris-HCl pH 7.5, 3060 ml 5M NaCl, 153 ml Tween 20, 5000 ml ddH_2O

Table 12. Solution recipes for western blot.

The recipes of WB solutions are listed above in Table 12. To run the protein samples on the western blot system (Bio-Rad), the prepared SDS gels were put in the gel apparatus and placed in the tank. The tank was filled with 1x Running Buffer. 40 µg total protein lysates and 4 µl protein marker were loaded on the gels. For stacking gel, the samples were run at 70 V, 20 mA for 30 min. For resolving gels, the samples were run at 110 V, 20 mA for 2h. After running the samples, the gel was taken out from the glass holders and put in ddH_2O. Trans-Blot® Turbo™ Transfer System (Bio-Rad, 1704150) was used for the blotting of the proteins. The first layer of the transfer system with a PVDF

membrane was put in the cassette. The gel was taken and put on the membrane. Then, the second layer of the transfer system was put on the gel and scrolled to get rid of air bubbles. The lid of the cassette was closed carefully and placed into the machine. The blotting of the samples was done at 20V, 1.3 mA for 10 min. After, the membrane was incubated with 5% Bovine serum albumin (BSA) for 1h at RT on the orbital shaker for blocking. The primary antibody dilution was prepared in a 50 ml falcon by adding 7 ml of washing buffer. For WB, we used the following primary antibodies: guinea pig anti-Nephrin (1:500, Progen, GP-N2), rabbit anti-P3H2 (1:1000, ProteinTech, 15723-1-AP), mouse anti-gamma-tubulin (1:1000, Sigma-Aldrich, T5326), rabbit anti-Collagen 4 (1:1000, Abcam, ab6586), rabbit anti-Col18α1 (1:500, Sigma-Aldrich, HPA011025) and mouse anti-alpha Actinin (1:500, Santa Cruz, sc-166524), rabbit anti-Laminin (1:1000, Abcam, ab11575), mouse anti-alpha tubulin (1:1000, Sigma-Aldrich, T9026). The membrane was put in the primary antibody dilution and incubated overnight at 4° C on a roller shaker. The next day, the membrane was washed with 1x wash buffer three times for 5 min at RT on an orbital shaker. Polyclonal goat Anti-rabbit IgG, HRP-linked Antibody (1:3000, CST, 7074S), polyclonal Rabbit Anti-Guinea Pig Immunoglobulins/HRP (1:8000, Dako, P0141), polyclonal Goat Anti-Mouse Immunoglobulins/HRP (1:10000, Dako, P0447), mouse anti-goat IgG-HRP (1.7000, Santa Cruz, sc-2354) antibodies were used as secondary antibodies depending on the primary antibody host species. The membrane was incubated with secondary antibody dilution for 45 min at RT on a roller shaker. Each membrane was washed with 1x washing buffer three times for 5 min at RT on an orbital shaker. ECL (Thermo fisher, Pierce) was added on the membranes and the protein bands were visualized at Amersham Imager 600, GE Healthcare Life Sciences.

2.13 Generation of *P3H2* knock-out immortalized human podocyte cell lines via CRISPR-Cas9 technology

Clustered regularly interspaced short palindromic repeats (CRISPR) are DNA sequences found in prokaryotes. These sequences have a role in defending prokaryotes against viral infections. CRISPR-associated protein (Cas9) is an enzyme that cleaves the double-stranded DNA (dsDNA) being guided by CRISPR sequences. Recently, the modified CRISPR-Cas9 system has been started to be used in eukaryotes to edit genomes.

Nowadays, this technology is widely applicable to different branches of science and technology and shows a lot of potential. To apply this system, specific guide RNA (gRNA) for target genes has to be designed. gRNA and Cas9 should be introduced in the cell by one of the transfection systems and then the screening of clones is necessary to detect genome-edited cells [89]. In our project, we used CRISPR-Cas9 genome editing technology to generate *P3H2* KO immortalized human podocyte cells line to investigate the effect of P3H2 absence on podocytes and ECM being secreted by them.

In summary (Figure 6A), *P3H2* gene-specific gRNAs were designed and cloned into the Cas9 nuclease vector. Accuracy of individually cloned gRNAs were confirmed by Sanger sequencing (Figure 6B). The immortalized human podocyte cell line was transfected with the gRNAs cloned into the vector encoding the Cas9. This vector has an orange fluorescence protein (OFP) as a reporter gene to control transfection efficiency. The transfected cells were checked under the fluorescence microscope (Figure 6C). The quality of gRNA was evaluated with a restriction enzyme from the isolated genomic DNA from transfected cells. The restriction enzymes were chosen based on the possible editing place at the sequence of the Cas9 protein. Therefore, if there was editing, the restriction enzyme would be unable to cut the DNA since its recognition site was changed by Cas9 editing (Figure 6D). After quality control of the gRNAs, the cells were transfected again and sorted in 96-well plate in a 1 cell per 1 well manner to have pure KO or WT cell lines (Figure 6E). At the final step, the clones were screened for both genomic and protein level KO proof by sequencing and western blot, respectively.

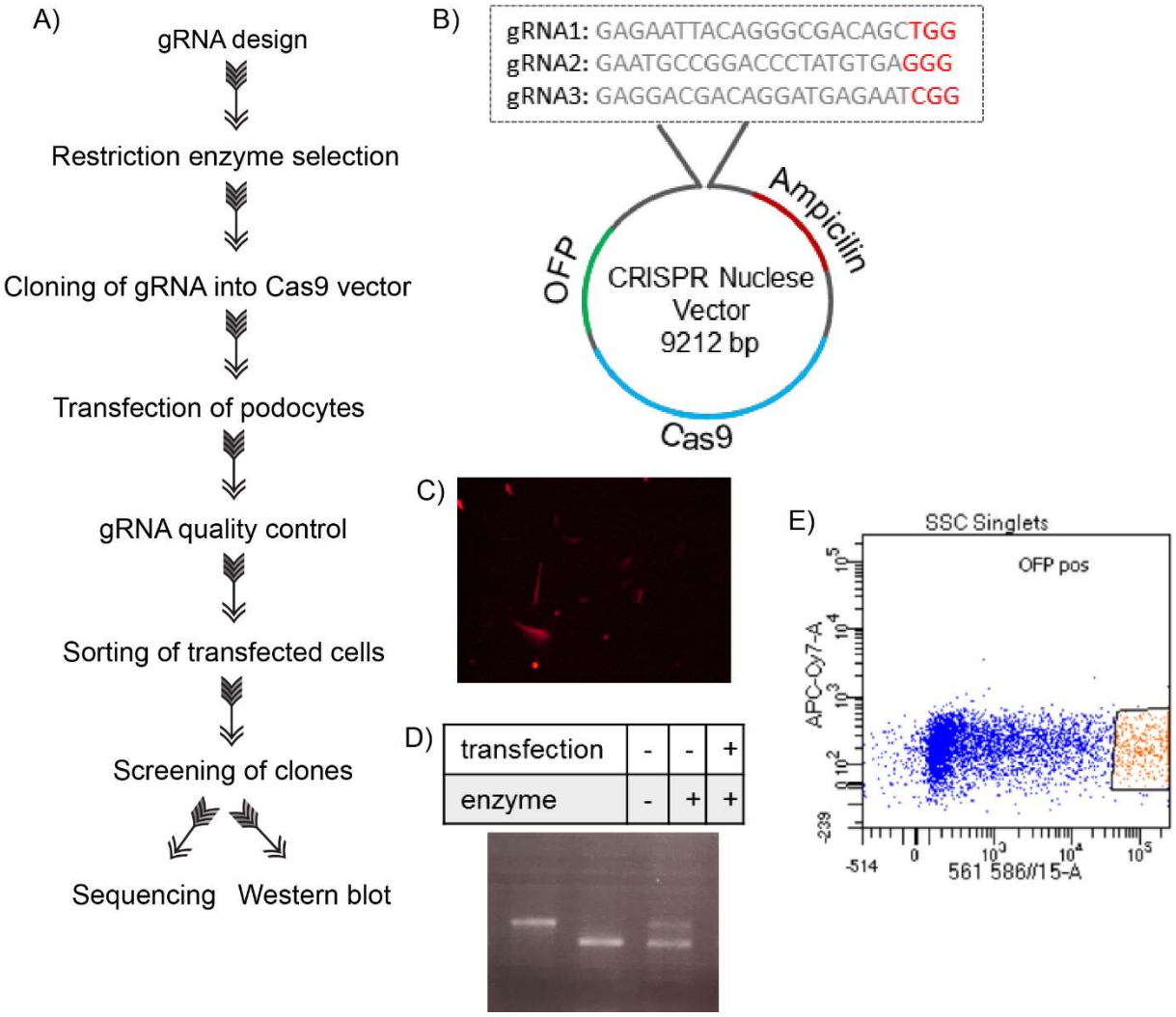

Figure 6: Generation of *P3H2* KO immortalized human podocyte cell lines A) Workflow of the applied CRISPR-Cas9 genome editing technology for the generation of *P3H2* KO clones. B) Individually cloned gRNAs into the Cas9 nuclease vector. C) Immortalized human podocyte cell line transfected by Cas9 plasmid. Orange color indicates transfected cells. D) The quality control of the gRNA by selected restriction enzymes. E) Sorting of OFP positive cells into 96 well plates in a 1 cell per 1 well manner. The cells having strong OFP were gated and sorted in FACS.

2.13.1 Guide RNA design and cloning

Two gRNA designing programs (Chop-Chop and eCRISPR) were used to design *P3H2* gRNAs (Table 13).

Name of gRNA	Designed gRNA sequences	Targeted exon	Restriction enzyme
gRNA1	GAGAATTACAGGGCGACAGCTGG	exon 1	PvuII
gRNA2	GAATGCCGGACCCTATGTGAGGG	exon 4	EcoNI
gRNA3	GAGGACGACAGGATGAGAATCGG	exon7	BsaBI

Table 13. Designed gRNA sequences for *P3H2* gene. Red written nucleotides indicate PAM sequence where Cas9 nuclease cut the dsDNA.

The CRISPR Nuclease Vector Kit (Invitrogen, A21174) was used as described in the manufacturer's protocol to clone gRNAs into the Cas9 nuclease vector. Annealing reaction was set up (Table 14) and double-stranded (ds) gRNAs were generated by heating them for 4 min at 95° C and then cooling down slowly at room temperature (RT). 5 nM ds gRNA working solution was prepared by diluting the stock with ddH_2O. After that, we ligated gRNAs into the Cas9 vector (Table 15) and performed a heat shock transformation as described in section 2.4. Four colonies were chosen from the LB plates and put in 2 ml LB-Ampicillin medium. Colonies were grown in medium overnight at 37° C. The DNA isolation was done by using the Zyppy™ Plasmid Miniprep Kit (section 2.5.1). Eluted DNA samples were sent for sequencing (GATC, U6 primer). After confirmation of the gRNA cloning with sequencing, Maxiprep DNA isolation was performed from positive colonies as described in section 2.5.2.

Annealing procedure	Volume (µl)
Forward strand oligonucleotide (200 µM)	5 µL
Reverse strand oligonucleotide (200 µM)	5 µL
10x Oligonucleotide Annealing Buffer	2 µL
DNase/RNase-Free water	8 µL
Total volume	20 µL

Table 14. Annealing reaction of *P3H2* gRNAs.

Ligation reaction	Volume (µl)
5x Ligation Buffer	4 µL
Linearized GeneArt® CRISPR Nuclease Vector	2 µL
5 nM ds oligonucleotide	2 µL
DNase/RNase-Free water	11 µL
T4 DNA Ligase	1 µL
Total volume	20 µL

Table 15. Ligation reaction of *P3H2* gRNAs into the Cas9 nuclease vector.

2.13.2 Transfection of the immortalized human podocyte cell line

We performed electroporation for the transfection of an undifferentiated immortalized human podocyte cell line. The 35 mm cell culture plate was coated with Col4 for 30 min. at 37° C to increase the viability of cells. The cells were collected at 15 ml falcon and centrifuged at 1200 x rpm for 5 min. 3 µg DNA and 100 µl M1 Buffer were mixed in an Eppendorf tube. Cells were resuspended in prepared DNA and M1 Buffer suspension. The mixture was loaded on the cuvette and the program T20 was applied on the AMAXA Nucleofector® II electroporation device (Lonza). Cells were removed from the cuvette, plated, and put in the 33° C incubator. Transfection efficiency was checked under the fluorescence microscope after 24h. 20-30% transfection efficiency was observed at the control via a fluorescence microscope. After transfection efficiency control, DNA isolation was done by using the Genomic Cleavage Detection Kit (Invitrogen, A24372). Designed PCR primer sequences for gRNAs were listed in Table 16. Phusion PCR reaction (Table 17) was set to check the editing efficiency of gRNA by the respective restriction enzymes. PCR products were purified by QIAquick® PCR Purification Kit (Qiagen, 28104) see detailed protocol in section 2.7.1. Restriction reactions (Table 18) were set and incubated for 3h at 37° C followed by analysis on an agarose gel. Three conditions were checked on the gel: DNA of the WT cells with detection enzyme (DE), DNA of the WT cells without DE, DNA of the transfected cells with DE. When an uncut band was observed at the DNA of the transfected cells with DE condition, it meant the targeted sequence was edited by Cas9 nuclease and mutation occurred at that region (Figure 6D).

Name of gRNA	Forward primer (5`-3`)	Reverse primer (5`-3`)
gRNA1	TGATTGCTTTCTTTGCTGTGC	CACTTAGCTCCCTGTGGTGA
gRNA2	TCCTGAGTCAACAAAAACCCTT	CTCTACAGGAGATAGGCTGGGA
gRNA3	CCTTGCCAAATCTCCACTAACT	CCTAAGGTTACAAAAACGTGGC

Table 16. PCR primers of the targeted exons.

Phusion PCR reaction	Volume (µl)
DNA	2 µl
5x Phusion buffer HF	10 µl
10mM dNTPs	1 µl
Forward primer	1 µl
Reverse primer	1 µl
ddH_20	34.5 µl
Phusion Enzyme	0.5 µl
Final volume	50 µl

Temperature (° C)	Duration	Number of cycles
98° C	30 sec	1
98° C	10 sec	40 cycle
60° C	30 sec	
72° C	30 sec	
72° C	7 min	1
4° C	∞	1

Table 17.Phusion PCR and cycler reaction of targeted *P3H2* gene region.

Restriction reaction	Volume (µl)
Purified PCR product	10 µl
10x Cut smart buffer	2 µl
ddH_20	7 µl
Restriction enzyme	1 µl
Final volume	20 µl

Table 18. Restriction reaction of the amplified targeted *P3H2* gene region for quality control of the gRNAs.

2.13.3 Sorting transfected podocyte cell line into 96 well plates

After 48h transfection, the cells were sorted into 96 well plates as a 1 cell per 1 well manner by a BD Aria-Fusion sorter (FACS sorting Core Facility, UKE). A 100 µM needle was used to sort transfected cells. Firstly, unstained cells were gated, and then, OFP positive cells were detected in transfected cells and gated. After sorting the cells, they

were put into a 33° C incubator. The medium was changed two weeks later and plates were checked under the microscope to detect clones. 1 month after the sorting, the clones were ready for splitting and screening.

2.13.4 Screening of clones

The clones were split into two 96 well plates. 1 plate was frozen into -80° C to keep the clones safe for future experiments. The second plate was used for genomic DNA (gDNA) isolation to screen the clones. The clones were washed with 1x PBS and 100 µl Lysis Buffer (50 mM KCl, 1.5mM $MgCl_2$, 10mM Tris-HCl pH 8.5, 0.45% NP40, 0.45% Tween-20 and 100 µg/ml Proteinase K) was added on the clones for DNA isolation. They were incubated for 1h at 60° C. 1:10 dilution of isolated DNA was prepared for PCR of the clones. The Phusion PCR and restriction assay were performed as described before in section 2.3.2 and analyzed on an agarose gel. After the detection of KO and WT candidates, cloning was performed for confirmation by sequencing. Taq Polymerase PCR reaction (Table 19) was set and TOPO® TA Cloning® Kit for Sequencing (Thermo Fisher, 450030) (Table 20) was used according to the manufacturer's protocol to clone KO and WT candidates.

TOPO TA Cloning reaction was incubated for 5 min at RTwhich was followed by transformation as in section 2.4. DNA isolation was done from growing bacterial colonies with Zyppy™ Plasmid Miniprep Kit (section 2.5.1) and samples were sent for sequencing (GATC, T3 primer). Sequencing results were checked by BLAST at NCBI. In the BLAST, insertion or deletion at the targeted exon was checked around the PAM sequence of the gRNA. Detected mutation sites were controlled at the VectorNTI program to figure out premature stop codon formation. If there was premature stop codon formation, these clones were chosen as KO clones. WT clones had no mutation at the BLAST result. This procedure was the genomic level proof of the clones and the protein level of the candidates were checked with a western blot to show the absence of P3H2 protein in KO clones and presence of P3H2 protein in WT clones.

Taq polymerase PCR reaction	Volume (µl)
DNA	4 µl
10x PCR buffer	2 µl
50 mM $MgCl_2$	0.25 µl
5 mM dNTPs	0.5 µl
Forward primer	1 µl
Reverse primer	1µl
dH20	11.1 µl
Tag Poylmerase	0.2 µl
Final volume	20 µl

Temperature (° C)	Duration	Number of cycles
94° C	5 min	1
94° C	15 sec	30 cycle
60° C	30 sec	
72° C	1 min	
72° C	5 min	1
4° C	∞	1

Table 19. Taq Polymerase PCR set up and cycler reaction.

TOPO TA cloning	Volume (µl)
Taq Polymerase PCR product	4 µl
Salt Solution	1 µl
ddH_2O	0.5 µl
Vector	0.5 µl

Table 20. TOPO TA cloning set up for ligation.

2.13.5 Thawing frozen CRISPR clones from -80° C

After confirming mutations in KO clones and wild type sequences in WT clones, cells were thawed from -80° C to check P3H2 protein expression. Frozen cells were thawed as described in section 2.2.3. The 96 well plates were taken from -80° C and selected wells were thawed and 100 µl cell suspension was put on a clean well of 96 well plates. Clones proliferated around two weeks to get enough cells to perform protein isolation. Protein isolation was done as described in section 2.10 and P3H2 protein abundance was checked by WB as described in section 2.12.

2.14 Adhesion assay

We performed adhesion assay for P3H2 KO clones to analyze the effect of *P3H2* deletion on cell adhesion. 150.000 cells per well were seeded on 24 well plates and incubated for 15 min at 37° C incubator. Next, the cells were washed with 1 ml 1x PBS three times and fixed with 500 µl 4% PFA for 15 min at RT. After washing with 1x PBS three times, the cells were stained with 0.1% Crystal Violet stain for 15 min at RT. The cells were washed with water four times. Stained cells were checked under the light microscope. The membrane of the cells was permeabilized with 0.5% TritonX-100 for 30 min at RT on the orbital shaker. At this step, Crystal Violet dye was excreted out of the cells. After, this solution was collected to 96 well plates, and absorbance was measured at 570 nM in a TECAN Sunrise Basic microplate reader. The absorbance value of the collected suspension provided indirect information regarding the adhesion of the cells.

2.15 Migration assay

We performed a migration assay to better understand the effect of *P3H2* deletion on the moving capacity of KO clones as compared to WT clones. 20.000 cells per well were split on a culture-Insert 2 Well in µ-Dish 35 mm (Ibidi, 81176) and filled with 75 µl medium. The next day, the splitting rubber was taken and the gap between cells was generated. Images were taken at 0h, 3h, 6h, and 9h. Then the cell free area was measured by the ImageJ program to calculate migrated area. The values were exported to Microsoft Excel for statistical analysis.

2.16 Extracellular matrix isolation

The *P3H2* KO and WT immortalized human podocyte cell lines were differentiated on a 10 cm cell culture plate for 12 days at 37° C. 50 µg/ ml Ascorbic acid was added to the medium of the cells every 2nd day. Ascorbic acid is necessary to stabilize ECM being secreted from the cells. After differentiation, the cells were lysed with 1 ml Lysis solution (20mM NH_4OH and 0.5% v/v TritonX-100 in PBS) for 1 min at 37° C. Lysis suspension was removed very carefully and cell plates were washed with 10 ml 1x PBS three times. Denuded ECM was incubated with 10µg/ml DNase I for 1h at 37° C and washed with 10

ml 1x PBS three times. In the final step, denuded ECM was scraped into 500 µl Reducing Buffer (50mM Tris-HCl, 10% w/v Glycerol, 4% SDS, 8% 2-ME and 0.004% bromophenol blue) and was cooked for 20 min at 70° C. The samples stored at -20° C and protein concentration was measured by BCA Assay (section 2.11).

2.17 Quantitative proteomics of GBM and ECM

We performed quantitative proteomics of ECM of the immortalized *P3H2* KO human podocyte cell lines and GBM of *P3h2*$^{\Delta Pod}$ and *P3h2*$^{fl/fl}$ mice to detect regulated ECM and GBM proteins. We used the Mass Spectrometric Proteomics core facility, UKE.

2.17.1 Sample preparation

Isolated ECM and enriched GBM were prepared using the optimized SP3 sample preparation protocol [90]. In brief, 10 µg of ECM or GBM protein were taken per sample, and disulfide bonds reduced in the presence of 10 mM DTT at 60° C for 30 min at RT. Cysteine residues were then alkylated in the presence of 20 mM iodoacetamide (IAA) at 37° C for 30 min in the dark. 2 µL (20 µg/µL) of a 1:1 mix of carboxylate-modified paramagnetic beads (Sera-Mag Speed-Beads (Hydrophilic), and Sera-Mag Speed-Beads (Hydrophobic) were added to each sample. Acetonitrile (ACN) was added to a final concentration of 70% (v/v) ACN and samples were shaken at 900 x rpm at RT and then placed on a magnetic rack. The supernatant was removed, the beads were washed with 70% (v/v) ethanol, and then with 100% ACN. Beads were resuspended in 10 µL trypsin solution (1:50 Enzyme to protein ratio, 50 mM NH_4HCO_3) and samples were digested at 37° C for overnight by shaking at 700 x rpm. After digestion, ACN was added, to a final concentration of 95% (v/v) ACN. After a brief incubation, samples were placed on a magnetic rack, the supernatant was removed, and beads were rinsed with 100% ACN. Peptides were eluted from the beads in 20 µL of a 2% (v/v) DMSO and transferred into a new tube. Samples were dried in a vacuum centrifuge.

2.17.2 LC-MS/MS measurements

For LC-MS/MS analysis, samples were resuspended in 0.1% FA at a concentration of 1 µg/µl. LC-MS/MS measurements were performed on a Quadrupole Orbitrap hybrid mass spectrometer (Q Exactive, Thermo Fisher) coupled with a UPLC system (nanoAcquity, Waters). For analysis, 1 µg of peptides were loaded by autosampler injection onto a C18 reversed-phase (RP) trap column (Symmetry C18 trap column, 100 Å pore size, 5 µm particle diameters, 180 µm x 20 mm) and separated on a 20 cm C18 RP (Peptide BEH C18 column, 130 Å pore size, 1.7 µm particle diameters, 75 µm x 250 mm). Trapping was done for 5 min at a flow rate of 15 µl per min with 99% solvent A (0.1% FA) and 1% solvent B (0.1% FA in ACN). Separation and elution of peptides were achieved by a linear gradient from 1 to 30% solvent B in 60 min.

The eluting peptides were transferred in an Orbitrap Q Exactive mass spectrometer. MS1 scans were performed in positive mode over a scan range of 400-1300 m/z. The Orbitrap resolution was set to 70.000 with an AGC target of $1x10^6$ and a maximum injection time of 240 ms. Peptides with charge states between 2+ - 5+ above an intensity threshold of 100.000 were isolated with a 2 m/z isolation window in Top12 mode and fragmented with a normalized collision energy of 28%. The fragments were measured with an Orbitrap resolution of 17.500, AGC target of $1x10^{5,}$ and 50 ms maximum injection time. Already fragmented peptides were excluded for 20 sec.

2.17.3 LC-MS/MS Data Processing

The collected raw files were searched against the reviewed mouse protein database downloaded from Uniprot (release January 2019 with 20,399 protein sequences) processed with the Andromeda Algorithm included in the MaxQuant Software (Max Plank Institute for Biochemistry, Version 1.6.2.10). All samples were handled as individual experiments. The label-free quantification option with the match between runs was used. Trypsin was selected as digest enzyme to generate peptides, allowing a maximum of two missed cleavages. A minimal peptide length of 6 amino acids and maximal peptide mass of 6000 Da was defined. Oxidation of methionine and proline (hydroxylation), acetylation of protein N-termini, and the conversion of glutamine to pyro-glutamic acid were set as

variable modifications. The carbamidomethylation of cysteines was selected as a fixed modification. The error tolerance for the first precursor search was 20 ppm, for the following main search 4.5 ppm. Fragment spectra were matched with 20 ppm error tolerance. The false discovery rate for peptide spectrum matches and proteins was set to 1%. For Quantification, all identified razor and unique peptides were considered.

The ProteinGroups.txt result files from MaxQuant were loaded into Perseus software (Max Plank Institute for Biochemistry, Version 1.5.8.5). The quantitative LFQ Intensity values for protein groups were used as main columns. The quantitative values for all protein groups were transformed into log2 values and normalized by the median. Hierarchical clustering, student's t-test, and principal component analysis (PCA) were performed.

2.18 Generation of a floxed allele *P3h2* podocyte-specific KO mouse

A conditional P3H2 (*P3h2*) KO mouse was generated from embryonic stem (ES) cells of the UC Davis KOMP (Knock-out Mouse Project) repository (P3h2 tm1aWtsi) (Figure 7). ES cells were injected into blastomere of the foster mother (Dresden, Dr. Ronald Naumann). The chimeras were bred with C57BL/6 WT mice and pups were screened for germline transfer. The positive mice were bred with the FLP deleted line to get rid of FRT sites. Floxed allele *P3h2* (*P3h2*$^{fl/fl}$) mice were bred with *hNphs2Cre*$^{+/wt}$ (TghNphs2-cre295^{Lbh}) to generate podocyte-specific *P3h2* KO (*P3h2*$^{\Delta Pod}$) mice.

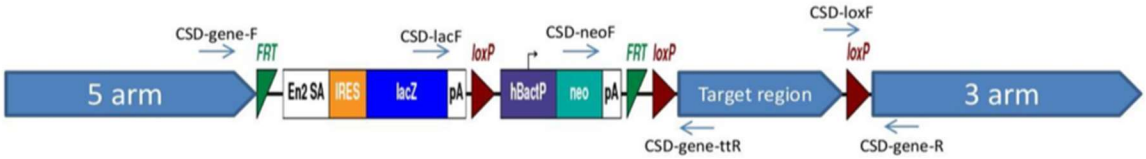

Figure 7: Primer strategy of *P3h2*$^{fl/fl}$ mouse generation. After germ line transfer, positive pups were bred with a FLP deleter line to get rid of FRT sites (green). *P3h2*$^{fl/fl}$ mice were bred with *hNphs2Cre*$^{+/wt}$ mice to get rid of loxP site (dark red) to generate podocyte-specific *P3h2* KO (*P3h2*$^{\Delta Pod}$) mice.

2.18.1 Genotyping

Tail biopsies were taken from 3w old pups and gDNA isolation was done. 75 µl alkaline lysis buffer (25 mM NaOH, 0.2 mM Na_2-EDTA) pH 12.0 was added to the tails and they were lysed for 30 min at 95° C. The reaction was stopped by adding 75 µl neutralization buffer (40 mM Tris-HCl) pH 5.0 and gDNA were stored at 4° C. Primer sequences (Table 21) and expected DNA band size (Table 22) are listed below. The Dream Taq Polymerase and cycler PCR reaction were used for the genotyping of *P3h2*$^{\Delta Pod}$ and *P3h2*$^{fl/fl}$ mice (Table 23).

Primer name	**Primer Sequence**
CSD-lac-F	GCTACCATTACCAGTTGGTCTGGTGTC
CSD-neo-F	GGGATCTCATGCTGGAGTTCTTCG
CSD-lox-F	GGGATCTCATGCTGGAGTTCTTCG
CSD-*P3h2*-R	GAAACAACATTCTCAAGTATCATAAGCC
CSD-*P3h2*-ttR	AGGAAAGCACAGGACAGTAATGAGG
CSD-*P3h2*-F	TCATGGCTACAGTAAGTATTGTTTCCC

Table 21. Designed primer sequences for *P3h2*$^{\Delta Pod}$ and *P3h2*$^{fl/fl}$ mouse genotyping.

Genotype	**Forward Primer**	**Reverse primer**	**Amplicon size (bp)**
Floxed	CSD-lox-F	CSD-*P3h2*-R	377
PreCre	CSD-neo-F	CSD-*P3h2*-ttR	627
PostCre	CSD-lac-F	CSD-*P3h2*-R	675
Wild-type	CSD-*P3h2*-F	CSD-*P3h2*-ttR	316
PostFlp	CSD-*P3h2*-F	CSD-*P3h2*-ttR	507
PostFlp & Cre	CSD-*P3h2*-F	CSD-*P3h2*-R	604

Table 22. Primer pairs for the generation of *P3h2*$^{\Delta Pod}$ and *P3h2*$^{fl/fl}$ mice.

Dream Taq PCR	Volume (µl)
DNA	2 µl
2x Dream Taq Master Mix	7 µl
Forward primer	1 µl
Reverse primer	1 µl
dH_20	3 µl
Final volume	14 µl

Temperature (° C)	Duration	Number of cycles
94° C	5 min	1
94° C	15 sec	30 cycle
60° C	30 sec	
72° C	1 min	
72° C	5 min	1
4° C	∞	1

Table 23. DreamTaq PCR set up and PCR reaction for genotyping of *P3h2*$^{\Delta Pod}$ and *P3h2*$^{fl/fl}$ mice.

2.19 Tissue preparation

Mice were euthanized after anesthesia by cervical dislocation. Subsequently, the abdomen was opened using a median laparotomy, the intestinal loops were mobilized and the kidney-vascular package was taken. This was followed by transfer of the entire kidney-vascular package to a cell culture dish with warm 1x HBSS pH 7.4.

2.19.1 Paraffin-embedded tissue

Small pieces of kidney tissue were cut and put in 2 ml Eppendorf with 2 ml 4% PFA and fixed overnight at 4° C on a roller shaker. The next day, the fixed tissue was washed with 10 ml 1x PBS four times for 30 min at RT. The automated tissue processor (Histokinette) was used for the preparation of tissue for embedding. In this machine, the tissue was incubated in an ascending ethanol series of 70%, ethanol, 80% ethanol, 95% ethanol, 100% ethanol and in the final step, incubated with xylene for 1h. Then, the tissue was embedded with liquid paraffin in a cassette on the paraffin embedding station. After paraffin polymerization, the extra paraffin was cleaned from the cassette, and the sample was stored at RT.

2.19.2 Frozen tissue preparation by optimal cutting temperature compound embedding medium

Small pieces of kidney tissue were cut and put in medium sized cryomolds (Tissue-Tek, 4566) and filled with Optimal Cutting Temperature Embedding Medium (OCT) (Tissue-Tek, 4583). The specimen was slowly frozen on the vapor interface of liquid nitrogen and subsequently stored at -80° C.

2.19.3 Tissue fixation for transmission electron microscopy

Very small pieces of kidney tissue were cut and put in 2 ml Eppendorf with 4% PFA and 1% glutaraldehyde in 1x PBS. The tissues were fixed overnight at 4° C on a roller shaker. On the following day, the fixative solution was diluted in 1:10 with 1x PBS and the tissues handed over to the EM facility, UKE for further processing.

2.20 Immunofluorescence staining

We performed immunofluorescence (IF) staining of paraffin-embedded and frozen tissues and cell lines to detect the localization or co-localization of different proteins in the kidney, glomeruli, and podocytes.

2.20.1 Immunofluorescence staining of paraffin-embedded tissue

Tissue was sliced at 2 µm and dried at 37° C overnight. The next day, tissues were deparaffinized and rehydrated. The slides were immersed in xylol for 20 min, and a descending ethanol series (100% ethanol for 10 min, 90% ethanol for 2 min, 80% ethanol for 2 min, 70% ethanol for 2 min, 50% ethanol for 2 min, 30% ethanol for 2 min) and washed with 1x PBS for 2 min. Heat-induced epitope retrieval was performed with Citrate Buffer pH 6.0 or TRIS/EDTA Buffer pH 9.0 for 30 min in a cooker followed by a cool down on ice for around 30 min. The slides were washed with 1x PBS three times for 3 min and blocked with 5% BSA in 1x PBS for 1h at RT. For IF staining, the following primary antibodies were used. Guinea pig anti-NPHS1 (1:200, Progen, GP-N2), rabbit anti-P3H2 (1:100, ProteinTech, 15723-1-AP), guinea pig anti-Synaptopodin (1:200, SYSY, 163004),

rabbit anti-DACH1 (1:100, Sigma Aldrich, HPA012672), rabbit anti- phospho-S6 Ribosomal Protein (1:100, Cell signaling, 2211). The particular primary antibody was incubated on tissues for 45 min at RT. The slides were washed with 1x PBS three times for 5 min. We used the following secondary antibodies: Alexa Fluor™ 488 Phalloidin (1:1000, Thermo Fisher Scientific, A12379), Alexa Fluor® 647 anti-mouse/human CD44(1:50, BioLegend, 103018), Alexa Fluor 555 donkey anti-rabbit IgG (H+L) (1:1000, Thermo Fisher Scientific, A31572), Alexa Fluor 488 goat anti-guinea pig IgG (H+L) (1:1000, Thermo Fisher Scientific, A11073), Alexa Fluor 488 donkey anti-mouse IgG (H+L), (1:1000, Thermo Fisher Scientific, A21202) based on primary antibody host. The 4′, 6-diamidino-2-phenylindole (DAPI) (1:1000) was incubated on tissues for 30 min at RT in the dark. The slides were washed with 1x PBS three times for 5 min. 11 µl Prolong Gold Antifade Mountant put on the tissues and covered by the cover glass (18x18mm). The slides were dried at RT overnight. The next morning, they were sealed with nail polish to fix the coverslip on the slide and stored at 4° C until imaging. Images were taken at 20x and 63x magnification on a Zeiss Axiovert M200 microscope with an ApoTome using different channels for fluorophores.

2.20.2 Immunofluorescence staining of frozen tissue

Tissue was sliced freshly at 4 µm and kept on -20° C until starting the protocol. The tissues were fixed with 2% PFA for 1.5 min or methanol or acetone for 10 min at -20° C. The slides were washed with 1x PBS three times for 3 min. Free aldehydes were saturated with 50mM Ammonium chloride (NH_4Cl) for 7 min at RT. The slides were washed with 1x PBS three times for 3 min and blocked with 5% BSA in 1x PBS for 1h at RT. The same primary and secondary antibodies were used as in section 2.20.1 and the rest of the protocol was also performed as in that section.

2.20.3 Immunofluorescence staining of immortalized cell lines

Cells growing on a coverslip were fixed with 4% PFA for 10 min at RT and washed with 1x PBS three times. Cells were permeabilized with 0.1% TritonX-100 for 15 min at RT and then, blocked with 5% BSA for 1h at RT. The same primary and secondary antibodies

were used as in section 2.20.1 and the rest of the protocol was also performed as described in that section.

2.21 Podocyte morphometrical analysis

We performed podocyte morphometrical analysis (podometrics) to observe the effect of *P3h2* deletion on podocyte number, density, and average podocyte cell volume. We used *P3h2*$^{\Delta Pod}$ and *P3h2*$^{fl/fl}$ mice for this analysis.

2.21.1 Confocal Imaging

IF staining of paraffin-embedded mice kidney tissue was performed as described in section 2.20.1. The tissues were stained with synaptopodin (SYNPO) as a podocyte cytoplasmic marker, DACH1 as a podocyte nucleus marker, and DAPI as a general nucleus marker. Images were taken at 63x magnification with a Zeiss Confocal Laser Scanning Microscope 800.

2.21.2 Model-based stereology

Podocyte number, podocyte density, and average podocyte cell volume (aPCV) per glomerulus were calculated by model-based stereology [91]. 6 mice per group were analyzed and 20 glomeruli per section were randomly taken with the confocal microscope. Fiji imaging software ((Max Planck Institute of Molecular Cell Biology and Genetics, Dresden, Germany) was used to measure the area of the glomerular tuft, podocyte nuclear number, and podocyte nuclear and cellular area in the sections. Measured area and podocyte numbers were used in model-based stereology to transform 2D information to 3D to the approximate calculation of podocyte number, podocyte density and aPCV of each glomerulus. Each glomerulus was accepted as a single observation and median values were used for statistical analysis and data presentation.

2.22 Immunohistochemistry – Periodic acid–Schiff staining

We performed Periodic acid–Schiff (PAS) staining for *P3h2*$^{\Delta Pod}$ and *P3h2*$^{fl/fl}$ mice *P3h2* podocyte-specific KO mice to observe glomerular structural changes. PAS staining was done for 3 different time points (at the age of 6w, 28w, and 48w) in both genotypes.

Paraffin sections were sliced at 2 µM. Deparaffinization and rehydration steps were done as previously described in section 2.20.1. Then, the slides were immersed in 1% periodic acid solution for 15 min at RT and washed under running water for 3 min. Slides were stained with Schiff's reagent for 45 min at RT and washed under running water for 7 min. For counterstain, slides were stained with haematin for 3 min at RT and washed under running water for 2 min. Then, the slides were dipped in HCl-Alcohol solution three times and washed under running water for another 2 min. The slides were immersed in 50% ethanol, 70% ethanol, 95% ethanol, 100% ethanol, and covered with Eukitt to fix the staining. After overnight drying of slides, images were taken at 20x and 40x magnifications at the Zeiss Axio Scope.A1 microscope.

PAS, Acid Fuchsin Orange G (AFOG), Methenamine Silver (MET), and Hematoxylin and eosin (HE) staining of the patient kidney biopsy were performed at the pathology department of the University Medical Center Freiburg.

2.23 Transmission electron microscopy

The transmission electron micrographs shown in this work were taken in cooperation with PD. Dr. Oliver Kretz from the EM facility, UKE.

For transmission electron microscopy (TEM), tissue blocks were washed after post fixation in 0.1M phosphate buffer (PB), and 50 mm sections of the kidney were cut by using a vibratome. The sections were incubated in 1% Osmium tetroxide (OsO_4) and they were stained with uranyl acetate. After dehydration, the tissues were embedded in epoxy resin (Durcupan ACM, Fluka, Sigma-Aldrich, Gillingham, UK). 40 nm ultrathin sections were cut and analyzed using a Phillips CM 100 transmission electron microscope [92].

2.23.1 Measurement of GBM and foot process width thickness

The thickness of the GBM was measured by using TEM micrographs for both *P3h2*$^{\Delta Pod}$ and *P3h2*$^{fl/fl}$ mice kidney tissue. For quantitative analysis, four mice for each time point and genotype were analyzed. 15 to 20 random images of glomeruli were taken at a magnification of 2900x using a Phillips CM 100 transmission electron microscope. Determination of foot process width was performed as follows: Total length of the GBM in each image was measured and the number of foot processes in that region was counted. A foot process was defined as any connected epithelial segment butting on the basement membrane between two neighboring filtration slits. Foot process width was calculated as follows: foot process width = length of GBM / FP number /4*PI. Approximately 50 µm GBM or 1000 foot processes were analyzed per animal. For GBM or Bowman's capsule thickness a 1µm mesh grid was placed as an overlay on each image and measurements were performed at each crossing point of the GBM with the grid lines. For image analysis either ITEM software (Olympus) or ImageJ software were used [93].

2.24 Urine collection

To collect the mouse urine, the animals were held over a petri dish and slight pressure was exerted manually on the bladder from the outside. The urine collected in the petri dish was picked up with a pipette and transferred into a 1.5 ml Eppendorf tube. The urine was then stored at -20° C until further evaluation.

2.25 Albumin ELISA

Enzyme-linked immunosorbent assay (ELISA) is a method to determine quantitative protein concentration from plasma, serum, or urine in 96-well plate. ELISA was used for albumin measurement for the urine of mice. High binding 96 well plates (Sarstedt, 82.1581.200) were coated with goat anti-mouse albumin antibody (Bethyl, A90-134A) in coating buffer (0.05M Carbonate-bicarbonate pH 9.6) as 1:100 dilution overnight at 4° C. The next day, a coated plate was warmed-up for 1h and the rest of the protocol was done at RT. The plate was rinsed with washing buffer (50mM TBS, 0.05% Tween20 pH 8.0) three times and it was incubated with a post coat solution (50mM TBS, 1%BSA pH 8.0)

for 30 mins. Urine was diluted at 1:100-1:600 with sample diluent (50mM TBS, 1% BSA pH 8.0, 0.05% Tween20). After post coating and washing, samples were incubated in the 96 well plates for 1h on an orbital shaker. Then, the plate was rinsed with wash buffer five times and secondary antibody, goat anti-mouse Albumin-HRP, (Bethyl, A90-134P) at a dilution of 1:20.000 was added. The plate was incubated for 1h. After washing three times, TMB substrate (Biomol, E102) was incubated for 3 min and the reaction was stopped by stop solution (2N H_2SO_2). The absorbance was measured at 450 nm in ELx808™ Absorbance Microplate Reader, Biotek Instruments. Albumin concentration of the urine samples was calculated by using the logarithmic standard curve.

2.26 Creatinine assay

A Creatinine measurement kit (Labor und Technik, LT-CR 0106) was used for this assay according to the manufacturer's protocol for mouse urine. The mouse urine was diluted 1:40 in ddH_2O. Diluted urine was put on 96 well plate (Sarstedt, 82.1582) with standards. 100 µl of solution 1 was added to the urine and incubated for 5 mins at RT. Then, 50 µl solution 2 was added and the first measurement was taken at 562 nm in a TECAN Sunrise Basic microplate reader. The plate was incubated in the machine for 20 min at 25° C and the second measurement was taken at the same absorbance. The creatinine concentration of samples was calculated by using the linear standard curve.

2.27 Hematuria

Mouse urine was collected as explained in section 2.24. Urine was centrifuged at 2000 x rpm for 5 min and the supernatant was aspirated. The pellet was resuspended in 20 µl urine supernatant removed one step previously. 5 µl were taken and put on a slide and red blood cells were counted under a microscope. Similarly, 5 µl undiluted urine was put on a dipstick and incubated 2 min at RT and checked for the appearance of blue spots on the dipstick.

2.28 Glomeruli isolation without digestion

We isolated glomeruli without digest solution to perform GBM isolation and total protein extraction from glomeruli. The animals were euthanized as described in section 1.4. The aorta was opened along its longitudinal axis to provide access to the orifices of the renal arteries. Kidneys were perfused with 4 ml warm magnetic nanoparticle solution (Dynabeads) via the renal arteries. 37.5 µl of Dynabeads® M-450 Tosylactivated and 37.5 ul Dynabeads® M-450 Epoxy were mixed in 4 ml 1x HBSS/ mice. A Magnet (DynaMag ™ -2 Magnet) was used to wash the magnetic nanoparticles solution twice with 2 ml 1x HBSS and then resuspended in 4.5 ml 1x HBSS. The magnetic nanoparticles were unable to pass and concentrate in the capillary loops of the glomeruli due to their size. After perfusion, the kidney cortex was separated and placed in a cell culture dish on ice.

Mouse kidney cortex was cut into small pieces on ice. Kidney tissue was divided into two and transferred to Precellys tubes (size 2.8mm). 1 ml cold 1x HBSS was added and mixed for 15 sec at 5000 x rpm in the Minilys tissue homogenizer. A 100 µm cell strainer was placed on a 50 ml falcon. Homogenized tissues were put on a cell strainer and pestled with a 1 ml insulin syringe. The cell strainer was washed with 1x HBSS until all tissue passed through the mesh. Tissue suspension was centrifuged at 2000 x rpm for 5 min at 4° C and the supernatant was discarded. The pellet was resuspended in 3.5 ml 1x HBSS and transferred to 2 ml Eppendorf tubes. The tubes were put in a magnet to collect glomeruli and mixed at least ten times. The supernatant was discarded and the attached glomeruli were washed with 1x HBSS to get rid of adherent tubular fragments. The glomerular pellet was scaled and flash-frozen in liquid nitrogen. Isolated glomeruli were stored at -80° C.

2.29 Glomerular basement membrane isolation

This procedure to isolate GBM from glomeruli was adapted from Lennon et al., JASN, 2014 [94]. Isolated mouse glomeruli were incubated with extraction Buffer (10 mM Tris, 150 mM NaCl, 1% Triton X-100, 25 mM EDTA, 25 µg/ml leupeptin, 25 µg/ml aprotinin, 0.5 mM 4-(2-Aminoethyl) benzene sulfonyl fluoride hydrochloride) for 30 min to solubilize cellular proteins. The samples were centrifuged at 14.000 x g for 10 min to yield fraction 1. The

pellet was incubated for 30 min in alkaline detergent Buffer (20 mM NH_4OH, 0.5%Triton X-100 in PBS) to further solubilize cellular proteins and disrupt the cell–ECM interaction. The samples were centrifuged at 14.000 x g for 10 min to yield fraction 2. The pellet was incubated for 30 min in 10 mg/ml DNase I (Roche, 10104159001) to degrade DNA. The samples were centrifuged at 14.000 x g for 10 min to yield fraction 3. The final pellet was resuspended in reducing sample buffer (50 mM Tris-HCl pH 6.8, 10% glycerol, 4% SDS, 0.004% bromophenol blue, 8% 2-ME) to yield the ECM fraction. Samples were stored at -80° C.

2.30 Coomassie blue staining

SDS PAGE was done as described in section 2.12. The SDS gel was taken out from the glass covers and placed in a 10 ml fixing solution (50% methanol and 10% glacial acetic acid) for 1h on an orbital shaker. The gel was stained with 10 ml staining solution (0.1% Coomassie Brilliant Blue R-250 in 50% methanol and 10% glacial acetic acid) for 20 min on an orbital shaker. Destaining was done with a 10 ml destaining solution (40% methanol and 10% glacial acetic acid) and the solution was refreshed until the background of the gel was transparent. The gel was stored in 10 ml storage solution (5% glacial acetic acid) at 4° C. Coomassie blue staining was performed to control isolated GBM before performing quantitative GBM proteomics.

2.31 FACS of mouse glomerular cells

We isolated mouse glomerular cells (Pods, GECs and MCs) from bead perfused glomeruli to confirm that podocytes of generated *P3h2*$^{\Delta Pod}$ mice didn't express *P3h2*. We also checked *P3h2* expression level in these three glomerular cell types to determine the one having the highest *P3h2* expression.

2.31.1 Glomeruli isolation with collagenase V digestion

Glomerulus perfusion was done as previously explained in section 2.28. Beside the bead perfusion, 250 µl/kidney collagenase II (Col II) digestion solution (100 mg/ml Col II, 20 mg/ml Pronase E, 50 mg/ml Dispase II, 10U/µl DNase I) was perfused as well. The mouse

cortex was cut into small pieces on ice. Tissues were transferred to c-tube and 5 ml collagenase V (Col V) (5.5 ml HBSS+5.5 ml DMEM/F12+27.5 mg BSA+11 mg Col V) digestion solution was added. Tissue was digested for 5 min at 37° C and homogenized by using a gentleMACS™ dissociator. Tissue was digested for 5 more min at 37° C and homogenized by using a gentleMACS™ dissociator. A 100 µm cell strainer was placed on a 50 ml falcon. Homogenized tissues put on cell strainer and pestle with 1m Insulin syringe. Cell strainer was washed with 1x HBSS until all tissue passed through the mesh. Tissue suspension was centrifuged for 5 min at 4° C, 300 g, and the supernatant was discarded. The pellet was resuspended in 3.5 ml 1x HBSS and transferred to 2 ml Eppendorf tubes. The tubes were put in the magnet to collect glomeruli and were turned at least ten times. The supernatant was discarded and glomeruli were washed with 1x HBSS to get rid of tubules.

2.31.2 Digestion of glomeruli

The isolated glomerular pellet was resuspended in 2 ml Collagenase II solution and split into two Eppendorf tubes. They were incubated for 40 min at 37° C on a thermomixer shaking at 1400 x rpm per min. During incubation, different mechanical stresses were applied to detach cells. Isolated gloms were sheered with a 27G needle attached to a syringe at 15 min of incubation. Then they were mixed by pipetting at 5, 10, 20, 25, and 35 min during incubation. Podocytes were loosened at 10, 20, 30 min by vortexing once. Digested gloms were pipetted up and down five times with a 200 µl pipette attached to a 1000 µl pipette at 30, and 40 min. Digestion efficiency was controlled under a microscope and digestion was stopped after approx. 40 min.

Digested cells were sieved with a 1 ml pipette through a 40 µm cell strainer on a 50 ml Falcon. Mesh was washed with 10 ml 1x HBSS and the cell suspension was centrifuged at 400 x g for 4 min at 4° C. The supernatant was discarded and cells were resuspended in 2 ml Staining Buffer and transferred to 2 ml Eppendorf tubes and put in the magnet to get rid of beads. Supernatant including all glomerular cells was taken and passed through a 35 µm cell strainer on a FACS tube. Cells were centrifuged at 400 x g for 4 min at 4° C. The supernatant was discarded and cells were resuspended in 500 µl Staining Buffer.

2.31.3 Staining of glomerular cells and FACS

An antibody mixture was prepared with 1µl antibody in 100 µl Staining Buffer. Two antibodies were used simultaneously to stain cells. Those antibodies were PODXL-AF647 (R&D, FAB1556R) for endothelial and podocytes as well as CD105-PE (BioLegend, 120407) for mesangial and endothelial cells. The antibody mix was added to the cell suspension and incubated for 30 min at 4° C in the dark. After staining, cells were washed with 1ml Staining buffer and centrifuged at 400 x g for 4 min at 4° C. The supernatant was discarded and the cell pellet was resuspended in 200 µl Staining Buffer.

We used the BD AriaFusion Sorting device at the FACS Sorting Core Unit, UKE to sort the cells. Before sorting 1 µl DAPI (20 µg/ml) was added to the cells to detect dead cells. First, unstained cells were counted and proper gating was established. After that, samples and 1.5 ml Eppendorf tubes containing 350 µl RNA Lysis Buffer were loaded to the sorter and 10.000 cells were counted. 30.000 podocytes and endothelial cells and 10.000 mesangial cells were sorted in Eppendorf tubes. After sorting, the cell suspension was vortexed for 30 sec and RNA isolation was performed as explained in section 2.8.

2.32 Statistical analysis

The data in the diagrams of the results section is shown in different types of plots. All plots were prepared by using GraphPad Prism (v8.4.0). The data are presented as mean with SD or median with interquartile range (IQR). This software was used for statistical analysis of plots as well. The unpaired 2-tailed t-test, multiple t-test, and the Mann Whitney's U test were used to determine the significance between experimental and control groups. A p-value of $p < 0.05$ (*) was set for the significance level. A p-value of $p < 0.01$ (**) was found as very significant and a p-value of $p < 0.001$ (***) and $p < 0.0001$ (****) were found as highly significant.

3 Results

3.1 Detection of a *P3H2* gene mutation in a nephrotic syndrome patient cohort

The aim of using an expression-based approach was to identify novel candidate genes causing nephrotic syndrome. In this approach, potential candidate genes were detected in a nephrotic syndrome patient cohort by probing a correlation of highly expressed mouse podocyte genes. The identified candidate genes were scored according to expression, detection by proteomics, identification in human expression data sets as well as enrichment in respective GO terms. The *P3H2* gene was identified in a human glomerular expression database and enriched in GO terms related to matrix biology. Subsequently a homozygous nonsense mutation was identified in a young female patient.

3.1.1 Clinical history and phenotype of the patient with a *P3H2* mutation

The *P3H2* mutation at exon 4 caused a transition from cytosine (C) to thymidine (T) at position 1213. This transition induced a premature stop codon formation at amino acid position 405 coding arginine (Arg) (Figure 8A). After identification of the *P3H2* mutation, the family of the patient was examined as well. The patient was the second child of a consanguineous marriage. She had a brother that passed away when he was six years old suffering from FSGS as well (Figure 8B).

According to the clinical history of the patient, she was diagnosed with FSGS after histological examination of her first kidney biopsy in 2011. She was treated with steroids with little benefit but suffered a lot from side effects such as glucose intolerance and severe lactate acidosis. She was subsequently diagnosed as SRNS. The treatment was continued with cyclosporine-A but proteinuria didn’t improve. Then, treatment was switched to Enalapril and Losartan reducing proteinuria. However, kidney function started to decrease and the treatment regime was switched to cyclosporine-A and Enalapril until start of hemodialysis. Besides kidney disease, she also had cataracts and myopia. A lens extraction had to be done in 2013. In the same year, a second kidney biopsy was done because of increasing proteinuria and decreasing renal function. 6 months after the

second biopsy, hemodialysis was started and she was listed for kidney transplantation (KTx). In 2017, she had a KTx. (Table 23).

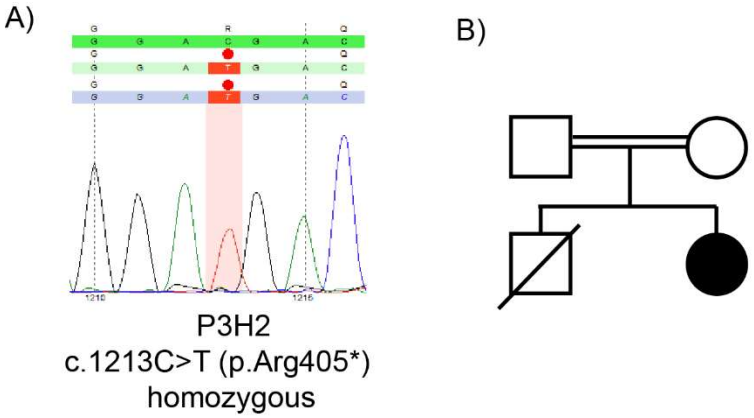

Figure 8: A *P3H2* gene mutation was detected in one patient of a nephrotic syndrome patient cohort. A) Position of the *P3H2* mutation in the patient genome. A nonsense mutation was detected at exon 4 with transition from cytosine (C) to thymidine (T) at position 1213 leading a premature stop codon formation. B) Pedigree of the patient. She had a brother who has FSGS diagnosis, already passed away and parents has consanguineous marriage.

Patient	
Gender, age of diagnosis	Female, 6-year-old
Clinical presentation	Proteinuria 3.2 g/d
1st biopsy (02/11) and diagnosis	Histologically FSGS, clinically SRNS
Operation (10/13)	Lens extraction of left eye because of cataract, myopia
2nd biopsy (10/13) and diagnosis	Progressive FSGS, increasing proteinuria, decreasing renal function
Treatment	Cyclosporin A (+Coenzym-Q10) between 04-08/11 Enalapril + Losartan between 08/11- 07/13 Cyclosporin A + Enalapril between 07/13 – 05/15 Hemodialysis between 05/15 – 04/17 Kidney transplantation 04/17

Table 24. Clinical history of the patient.

3.1.2 Analysis of the patient's kidney biopsy

The patient was biopsied twice before starting hemodialysis. The second kidney biopsy tissue was kindly supplied by Prof. Kerstin Amann (Department of Pathology, University of Erlangen-Nurnberg, Erlangen, Germany). PAS, AFOG, MET, and HE staining were performed to observe histological changes in the kidney. In addition, the biopsy section was examined with transition electron microscopy (TEM) to check the ultrastructural state of the GFB components.

The images of the IHC staining were taken under a light microscope and representative images are shown below. Partial sclerosis in glomeruli was observed in the PAS staining of the patient biopsy (Figure 9A). In FSGS, partial glomerular sclerosis is one of the hallmarks. Fibrosis and GBM thickening of the glomerulus were detected in AFOG and MET staining, respectively (Figure 9B and C). Furthermore, glomerular damage was observed in the HE staining (Figure 9D). In TEM micrographs of the patient, foot process effacement (FPE) of Pods and GBM irregularities were observed. GFB was severely injured explaining the high proteinuria (Figure 9E). Clinical follow-up showed that the progressive FSGS ended up in end-stage kidney disease (ESKD).

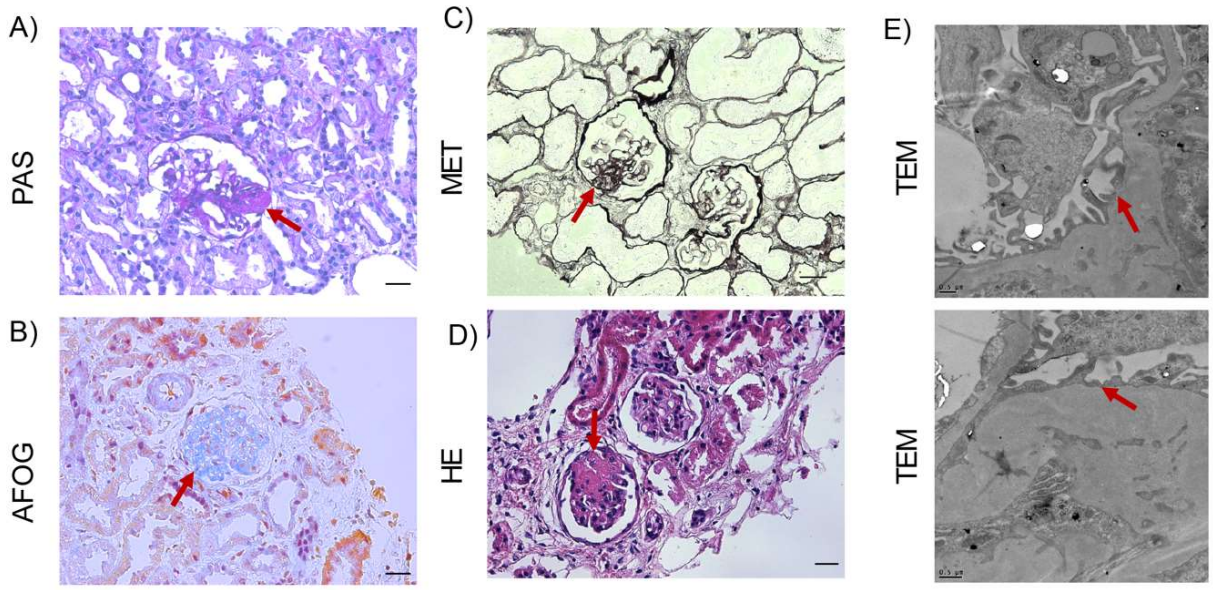

Figure 9: Histology examination of the patient with a *P3H2* gene mutation. A) Representative PAS image shows focal glomerulosclerosis (red arrow). B) Fibrosis was observed in AFOG images (red arrow). C) Representative Met images show thickened GBM (red arrow). D) Glomerular damage was examined in HE images (red arrow). Scale bars, 20 µm. E) FPE, irregular and thickened GBM were observed on TEM micrographs (red arrows) of the patient biopsy. Scale bar, 0.5 µm.

3.2 Expression of *P3H2* in glomeruli of human, rat and mouse.

We aimed to identify the expression profile of the *P3H2* gene in glomeruli of humans and mice. We also aimed to find out the glomerular cell type that has the highest abundance of P3H2. The RNA expression of *P3h2* was checked in mouse embryo, mouse kidney by ISH, and in FACS sorted mouse glomerular cell types by qPCR. The P3H2 protein abundance was examined in human glomeruli, rat glomeruli, mouse glomeruli and immortalized human podocyte cell line by IF staining and WB. We performed the expression analysis in a large spectrum of species and cells as we aimed to use these model organisms for further characterization of the *P3H2* gene.

We examined RNA localization of *P3h2* in the mouse embryo at embryonic day 14.5 (E14.5) and mouse P1 kidney. *P3h2* RNA wasn't detected in mouse embryo tissue (Figure 10A). In P1 mouse kidney, glomerular localization of *P3h2* RNA was detected. The staining was at the outer layer of the glomeruli where podocytes localize within the

glomerulus (white arrow, Figure 10B). The ISH data showed that *P3h2* gene expression coincides with glomerular maturation.

We sorted the glomerular cells, Pods, GECs, and MCs to find out which cell type has the highest expression profile of the *P3h2*. These cell types were sorted by staining of cell-specific antibodies using FACS. Two fluorophore-conjugated antibodies (podocalyxin-AF647 and CD105-555) were selected for sorting these cells types. Podocalyxin is a marker for podocytes and GECs. CD105 is a marker for GECs and MCs. Therefore, staining of cells with these antibodies gave us the possibility to sort these three glomerular cells types. Cells only stained with podocalyxin were Pods. Double stained cells were GECs since they express both proteins. Only CD105 positive cells were MCs. The mRNA level of *P3h2* was evaluated on sorted glomerular cell types by qPCR. The graph of the qPCR showed that Pods had significantly higher expression of *P3h2* mRNA when compared with GECs and MCs. In the graph, *P3h2* expression was normalized to 100 percent for representation. The Pods had 100% (n=3), the GECs had 0.09% ± 0.03 (n=3) and MCs had 3.9% ± 1.1 expression (n=3) (Figure 10C). qPCR data indicated that Pods were the main cell type expressing *P3h2*.

We performed IF staining and WB analysis to characterize the abundance of P3H2 protein in glomeruli and Pods. Paraffin-embedded kidney tissue of human and mice were stained with NPHS1 (podocyte marker), P3H2 and DAPI and images were taken under a fluorescence microscope. In addition, protein abundance of P3H2 was evaluated in protein lysate of rat glomeruli, mouse glomeruli, and immortalized human podocyte cell line by WB. 40 mg protein was loaded on the gels and gamma-tubulin was used as a loading control.

The images of the IF staining showed co-localization of P3H2 with NPHS1 in all tissues (Figure 10D). The membrane images of the WB showed that there was P3H2 protein in all samples and its abundance was highest in immortalized human podocytes. The band in mouse glomeruli was weaker than rat glomeruli and cell line because the antibody was specific to human (Figure 10E). All in all, the expression data indicated that *P3H2* expression and P3H2 abundance was highest in Pods within glomerular cells.

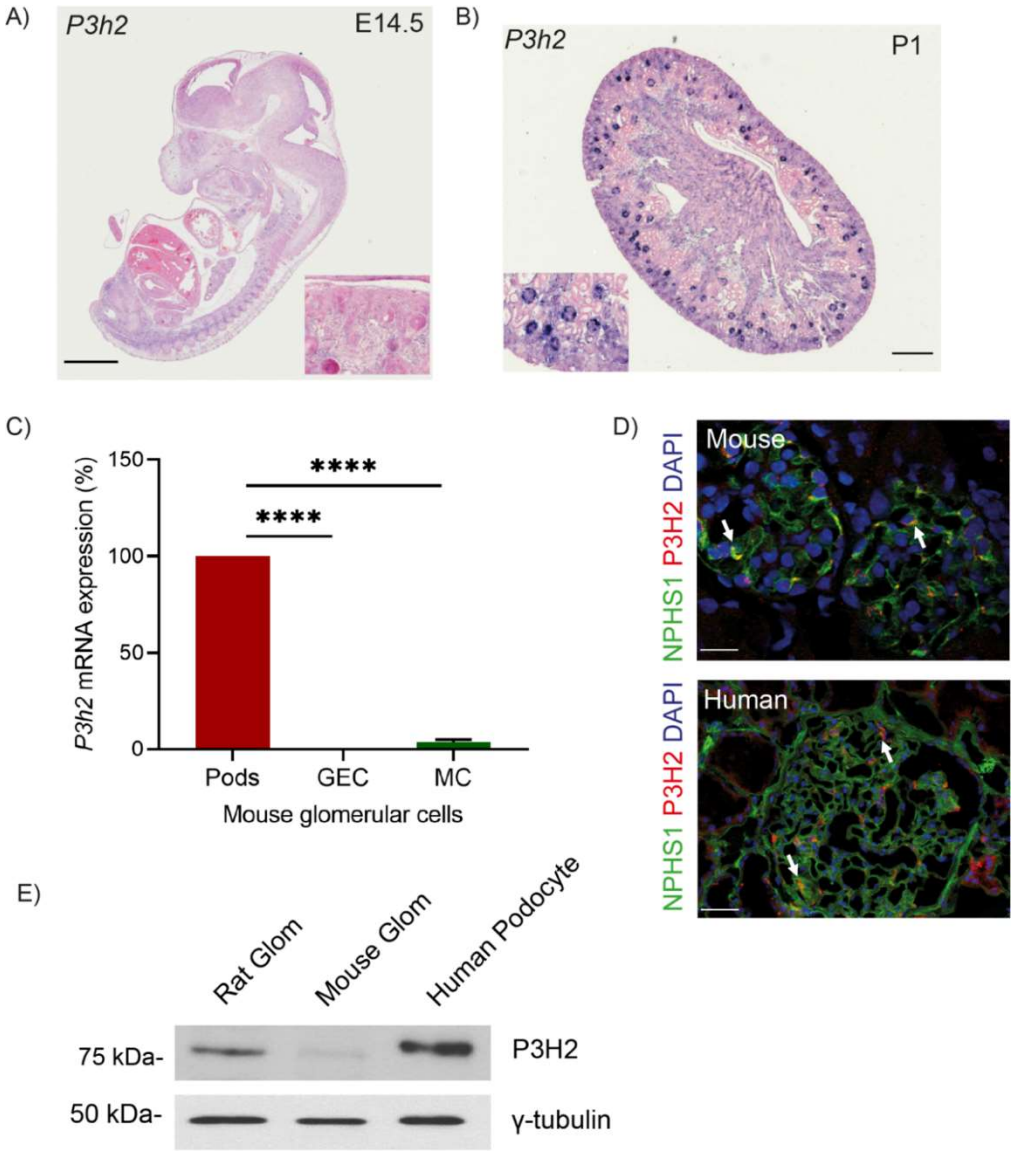

Figure 10: *P3h2* expression in kidney. A) ISH of E.14 mice embryo for *P3h2. P3h2* RNA localization couldn't be observed in kidney at E14.5. Scale bar, 2 mm. B) ISH of P1 mice kidney for *P3h2*. *P3h2* RNA was localized in the outer layer of glomeruli. Scale bar, 500 µm. C) *P3h2* mRNA expression in sorted mouse glomerular cell types via qPCR. Pods have the highest expression level of *P3h2*. Graph shows mean ± SD, n=3, unpaired 2-tailed t-test, p-value ****< 0.0001. D) IF staining of human and mice paraffin-embedded kidney tissue with P3H2, NPHS1, and DAPI. White arrows indicate the co-localization of P3H2 and NPHS1 in both species. Scale bar, 20 µm. E) P3H2 protein expression was detected in rat glomeruli, mouse glomeruli and an immortalized human podocyte cell line via WB.

3.3 Generation and characterization of the *P3H2* knock-out immortalized human podocyte cell lines

P3H2 knock-out (KO) immortalized human podocyte cell lines were generated to investigate the effect of the deletion of *P3H2* gene on cell matrix interaction and ECM production. CRISPR-Cas9 genome editing technology was used to edit the genome of the immortalized human podocyte cell line. Clones were generated by targeting different exons to minimize off-target effects of the Cas9 enzyme. We used three different gRNAs. KO clone 1 and the WT clone were generated by using gRNA1. For the generation of KO clone 2, we used both gRNA2 and gRNA3 to create a larger mutation at the targeted site. The clones were screened by restriction assay and candidate clones were evaluated on genomic and protein level by sequencing and WB, respectively. KO clones were chosen after screening and characterized by adhesion and migration assay for their cell-matrix interaction. In addition, the ECM was isolated and quantitative ECM proteomics were performed to identify affected proteins in the absence of P3H2 protein.

3.3.1 Generation of the *P3H2* knock out podocyte cell lines

The generation of clones was done as explained in section 2.13. After genomic level confirmation of WT and KO clones by Sanger sequencing, protein level confirmation of WT and KO clones were proven by WB. We used unsorted WT human immortalized human podocytes as a control group to check for off-target effects on generated cell lines.

The DNA sequence alignment of *P3H2* KO clone 1 with WT sequence indicated that there was a 2 base-pair (bp) deletion in one allele and a 5 bp deletion in the other allele inducing premature stop codon formation (Figure11A). The KO clone 2 was transfected with gRNA2 and gRNA3 to generate a large deletion. The DNA sequence alignment of *P3H2* KO clone 2 with the WT sequence indicated that the size of the deletion was around 9610 bp (Figure 11B). The alignment of the P3H2 WT clone with the WT sequence showed that there was no mutation in the targeted region (Figure 11C).

A) P3H2 KO clone 1, allele 1

```
P3H2_WT  517  AGCTTAACCAGCTCGAAAAAGCAGTGGAAGCAGCTCACACATTTTTCGTGGCTAACCCTG
576           ||||||||||||||||||||||||||||||||||||||||||||||||||||||||||||
P3H2_KO  779  AGCTTAACCAGCTCGAAAAAGCAGTGGAAGCAGCTCACACATTTTTCGTGGCTAACCCTG
838
P3H2_WT 577  AGCACATGGAAATGCAGCAGAACATTGAGAATTACAGGGCGACAGCTGGTGTTGAAGCAT
636           |||||||||||||||||||||||||||||||||||||||||||||      ||||||||||||
P3H2_KO 839  AGCACATGGAAATGCAGCAGAACATTGAGAATTACAGGGCGAC-----GTGTTGAAGCAT
893
P3H2_WT  637  TGCAGTTGGTAGACAGAGAAGCCAAGCCACACATGG  672
              |||||||||||||||||||||||||||||||||||
P3H2_KO  894  TGCAGTTGGTAGACAGAGAAGCCAAGCCACACATGG  929
```

P3H2 KO clone 1, allele 2

```
P3H2_WT  447  AGCTTAACCAGCTCGAAAAAGCAGTGGAAGCAGCTCACACATTTTTCGTGGCTAACCCTG
506           ||||||||||||||||||||||||||||||||||||||||||||||||||||||||||||
P3H2_KO  215  AGCTTAACCAGCTCGAAAAAGCAGTGGAAGCAGCTCACACATTTTTCGTGGCTAACCCTG
274
P3H2_WT  507  AGCACATGGAAATGCAGCAGAACATTGAGAATTACAGGGCGACAGCTGGTGTTGAAGCAT
566           ||||||||||||||||||||||||||||||||||||||||||||  ||||||||||||||||
P3H2_KO  275  AGCACATGGAAATGCAGCAGAACATTGAGAATTACAGGGCG--AGCTGGTGTTGAAGCAT
332
P3H2_WT  567  TGCAGTTGGTAGACAGAGAAGCCAAGCCACACATGG  602
              |||||||||||||||||||||||||||||||||||
P3H2_KO  333  TGCAGTTGGTAGACAGAGAAGCCAAGCCACACATGG  368
```

B) P3H2 KO clone 2, deletion 1

```
P3H2_KO  3          TTACAAAANCGTGGCAGGAAGAGCTGGGACCTGGATGCAGAGCTCCTAATTCAGAGCTTA  62
                    |||||||| |||||||||||||||||||||||| ||||||||||||||||||||
P3H2_WT  189984374  TTACAAAAACGTGGCAGGAAGAGCTGGGACCTGGATGTAGAGCTCCTAATTCAGAGCTTA
189984433
P3H2KO   63         GAATTATTTTATTATATCTCCTTGCCTATTTCATAGAGCTACATTTCTCTATGATAGGTT  122
                    ||||||||||||||||||||||||||||||||||||||||||||||||||||||||||||
P3H2_WT  189984434  GAATTATTTTATTATATCTCCTTGCCTATTTCATAGAGCTACATTTCTCTATGATAGGTT
189984493
P3H2_KO  123        ATGACACTAAGTATTTCTCCTCATAAAAAAACCAGTTTGCATTCTGAATGGACTTACCGAT  182
                    ||||||||||||||||||||||||||||||||||||||||||||||||||||||||||||
P3H2_WT  189984494  ATGACACTAAGTATTTCTCCTCATAAAAAAACCAGTTTGCATTCTGAATGGACTTACCGAT
189984553
P3H2_KO  183        TC  184
                    ||
P3H2_WT  189984554  TC  189984555
```

P3H2 KO clone 2, deletion 2

```
P3H2_KO  184        CATAGGGTCCGGCATTCTGTATCTTCAACGAAATATTCTCTTAAGGCTTGTTCGAAATGC  243
                    |||||||||||||||||||||||||||||||||||||||||||||||||||||||||| |||
P3H2_WT  189994165  CATAGGGTCCGGCATTCTGTATCTTCAACGAAATATTCTCTTAAGGCTTGTTCGAAGTGC
189994224
P3H2_KO  244        CTGATAGCCATCTCAAAGTCATCAGCCTCATAATGTTTAACTCCTGCATTGTAACTCTCC  303
                    ||||||||||||||||||||||||||||||||||||||||||||||||||||||||||||
P3H2_WT  189994225  CTGATAGCCATCTCAAAGTCATCAGCCTCATAATGTTTAACTCCTGCATTGTAACTCTCC
189994284
P3H2_KO  304        TGTAATgaaacagacaagaaaaaacaaacaaactaacaaacaaacaaacaaacaaaaaaa  363
                    ||||||||||||||  |||||||||||||    ||||||||||||||||||||||||||
P3H2_WT  189994285  TGTAATGAAACAGACGGGAAAAAACAAACA----AACAAACAAACAAACAAACAAAAAAA
189994340
P3H2_KO  364        cCCCTATTTTCAAAGAGAAGGGTTTTTGTTGACTCAGGA  402
                    ||| ||||||||||||||||||||||||||||||||||
P3H2_WT  189994341  CCCTTATTTTCAAAGAGAAGGGTTTTTGTTGACTCAGGA  189994379
```

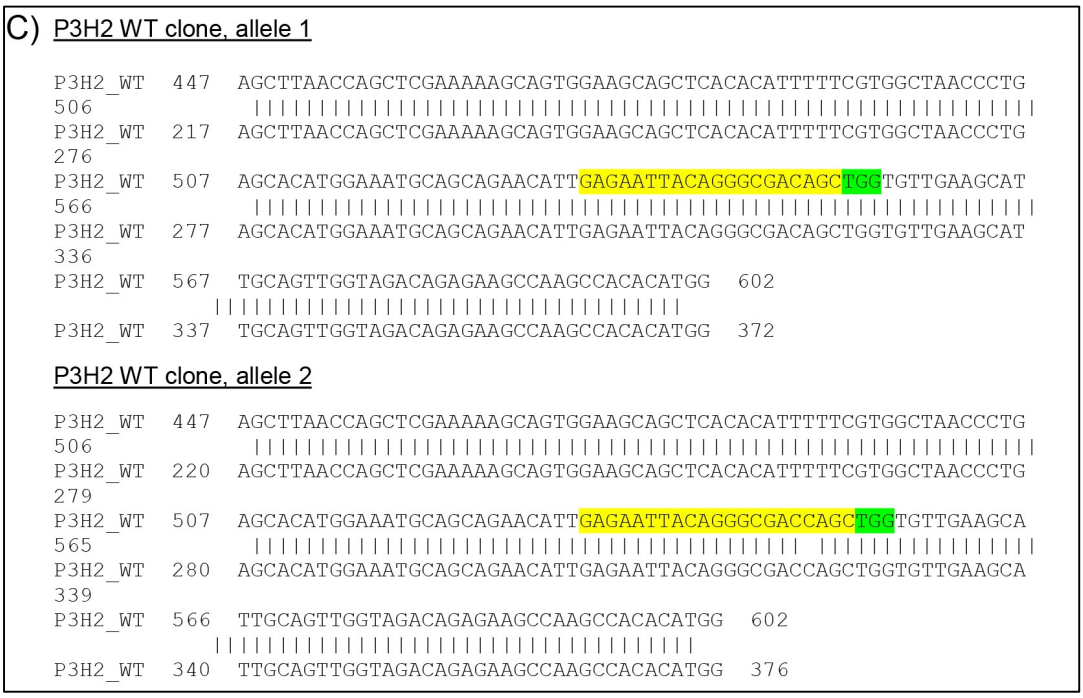

Figure 11: Genomic level confirmation of the generated WT clone and KO clones. A) DNA sequence alignment of the P3H2 KO clone 1 with WT sequence. There was a 2 bp deletion on one allele and a 5 bp deletion in another allele. The gRNA1 was outlined with yellow color and the PAM sequence was highlighted in green. The deleted sequences were highlighted in red color B) DNA sequence alignment of the P3H2 KO clone 2 with WT sequence. There was a 9610 bp deletion as a result of double gRNA transfection. The green-labeled numbers highlighted the position of the mutation in P3H2 KO clone 2. The yellow-colored numbers highlighted the position of the mutation in the P3H2 WT genome C) DNA sequence alignment of the P3H2 WT clone with WT sequence. There was no mutation between the WT clone and the WT sequence. The color indication is same as with the KO clone 1 alignment.

Selected clones were assessed for protein level confirmation by WB and IF staining. The WB analysis indicated that there was no expression of P3H2 protein in KO clones when compared with unsorted WT and WT clone. (Figure 12A). Images of the IF staining indicated that there was no P3H2 protein staining in KO clones when compared with WT showing ER-like localization. There was only nonspecific nuclear staining of P3H2 in KO clones (Figure 12B). Therefore, these results proved the lack of P3H2 in generated KO clones at the genomic and protein level.

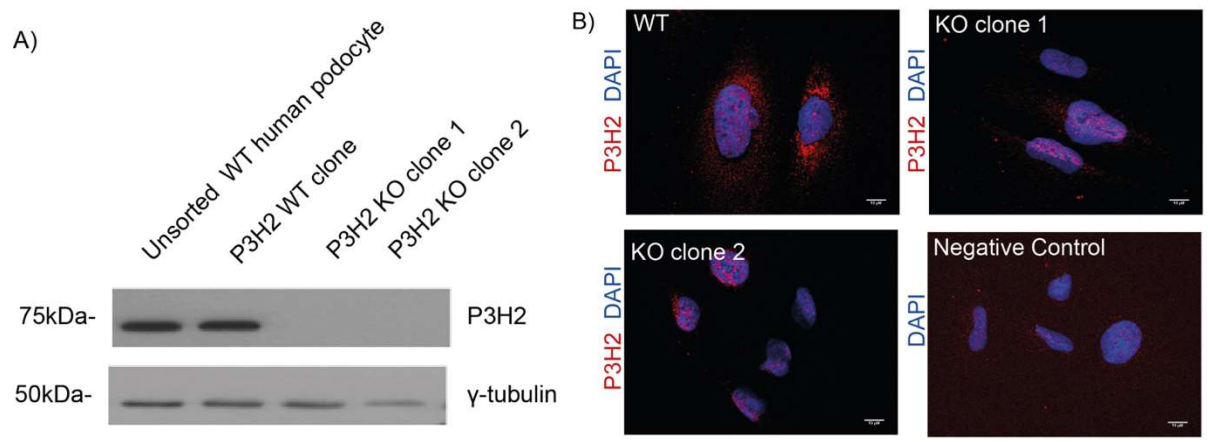

Figure 12: Protein level confirmation of P3H2 absence in KO clones. B) WB analysis of WT and KO clones for P3H2 protein expression. There was no protein expression in KO clones when compared to WT and WT clone. C) IF staining of WT and KO clones with P3H2 and DAPI. ER-like localization of P3H2 was lacking in KO clones when compared with WT. Scale bar, 10 µm.

3.3.2 Characterization of the *P3H2* knock-out podocyte cell lines

We aimed to characterize generated clones by cellular assays and quantitative proteomics of the ECM. Adhesion and migration assays were performed to observe changes in cell-matrix interaction in KO clones. Quantitative proteomics was used to detect changed protein abundances in ECM of generated cell lines.

3.3.2.1 Cell-matrix interaction of *P3H2* knock-out podocyte cell lines

Adhesion assay was performed for WT and KO clones. 150.000 cells per well were seeded on a 24 well plate and after 15 mins, cells were fixed by 4% PFA. Crystal violet was used to stain cells which were subsequently permeabilized by Triton-X. The collected cellular solution was measured at 570 nm. The absorbance values gave an indirect measure of the adhesion capacity of cells. We seeded equal amounts of cells of both WT and KO clones so that the absorbance difference showed more or less attached cells within 15 min incubation.

The results of the adhesion assay indicated that the KO clones had a significantly higher adhesion capacity than WT and WT clone (Figure 13). The values of the absorbance were 0.03 ± 0.01 for WT, 0.06 ± 0.02 for WT clone, 0.14 ± 0.05 for KO clone 1 and 0.10 ± 0.01

for KO clone 2 (n=4). The elevated adhesion capacity might be an indication of podocyte stress.

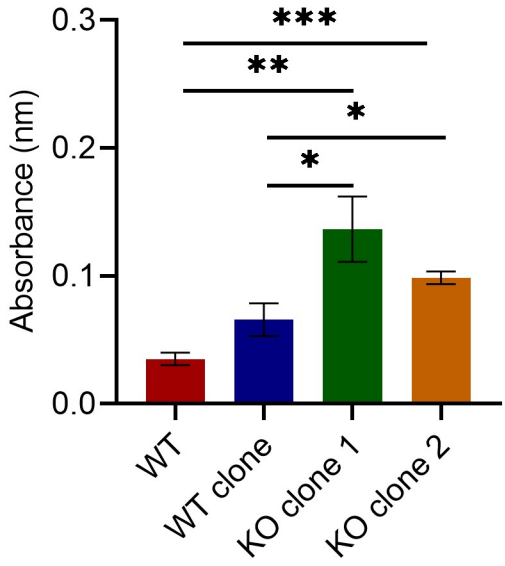

Figure 13: Adhesion assay of the *P3H2* KO and WT podocyte cell lines. KO clones had higher adhesion capacity then unsorted WT and WT clone. Graph shows mean ± SD, n=4, unpaired 2-tailed t-test, p-value * < 0.05, ** <0.01, *** <0.001.

A migration assay was performed to assess migration ability of WT and KO clones by calculating the migrated area. 75.000 cells were seeded per well of Ibidi migration assay channels. After 24h, the rubber separating two channel parts was removed and migration of cells was started. Images were taken at 0h, 3h, 6h, and 9h. For analysis, ImageJ software was used to calculate the cell covered area (µm^2).

The migration assay showed that WT and KO clones had similar migration capacities. The migrated area for each condition was similar and differences were not significant. The representative images show the migration capacities of the WT, WT clone, KO clone 1, and KO clone 2 (Figure 14A). The migrated area was measured and quantified for every time point. At 3h, the migrated area for WT was 60238.6 ± 10968.2 µm^2, for WT clone 58166 ± 20708.9 µm^2, for KO clone 1, 49674 ± 9988.3 µm^2 and for KO clone 2, 30082.6 ± 6664.4 µm2. At 6h, the migrated area for WT 114735 ± 51393.7 µm^2, for WT clone 103579 ± 22129.2 µm^2, for KO clone 1 126544.7 ± 24637.1 µm^2 and for KO clone

2, 89380.6 ± 12100.6 μm^2. At 9h, the migrated area for WT was 216042.7 ± 43823.9 μm^2, for WT clone, 166029.3 ± 24375.6 μm^2, for KO clone 1, 186985.5 ± 28523 μm^2 and for KO clone 2, 127423.9 ± 28850.2 μm^2 (n=4) (Figure 14B). The quantification of cell covered area from the images indicated that there were no significant changes regarding the migrated area of the KO clones when compared with WT and WT clone 1.

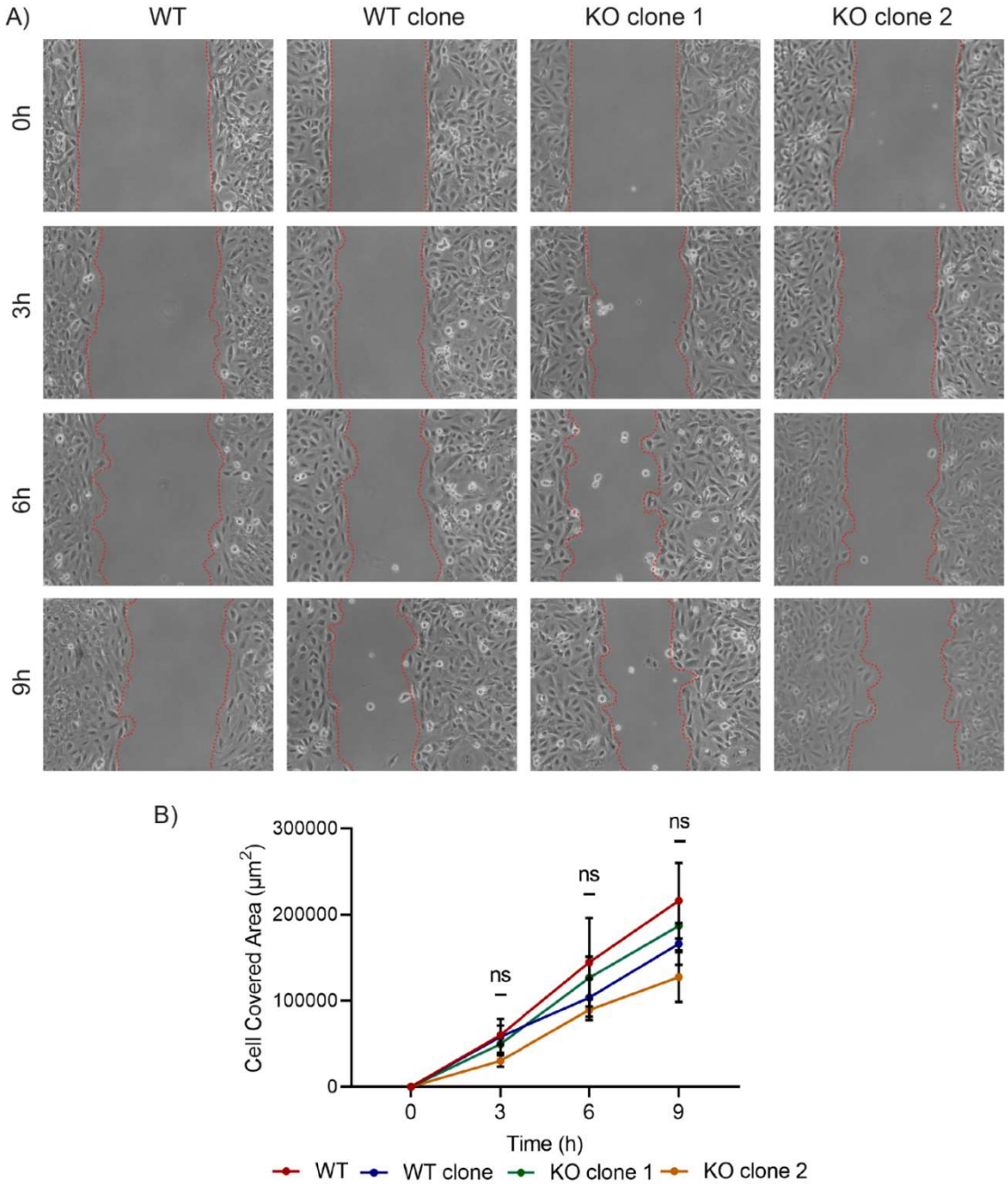

Figure 14: Migration assay of *P3H2* WT and KO podocyte cell lines. A) Representative images of the cell migration at 0h, 3h, 6h, and 9h. Red dashes show the cell borders. B) Quantification of the migrated area. There was no significant difference between KO clones and WT and WT clone regarding cell covered area during 9h migration. Graph shows mean ± SD, n=4, multiple t-test analysis, p-value ns > 0.05.

3.3.2.2 Quantitative extracellular matrix proteomics of the *P3H2* knock-out podocyte cell lines

We applied quantitative proteomics for ECM of the cells to find out changes in the secreted ECM composition. ECM isolation was performed by lysing cells and denuding ECM afterwards. Quantitative proteomics was performed for isolated ECM of the cells.

The analysis was presented in the volcano plot. The x axis represents the log2 fold change difference of regulated protein between WT and KO ECM. The Y axis represents the p-values of the proteins. The left side of the plot shows downregulated proteins in KO ECM and right part of the plot shows upregulated proteins in KO ECM. The volcano plot of the quantitative ECM proteomics indicated that Col4α1, and Col4α2 proteins were significantly downregulated in KO ECM compared with WT ECM. Moreover, downregulation of Col18α1 an interactor of Col4 was identified in KO ECM as well. This data showed that P3H2 enzyme had an effect on Col4 and Col18α1 abundance in the ECM.

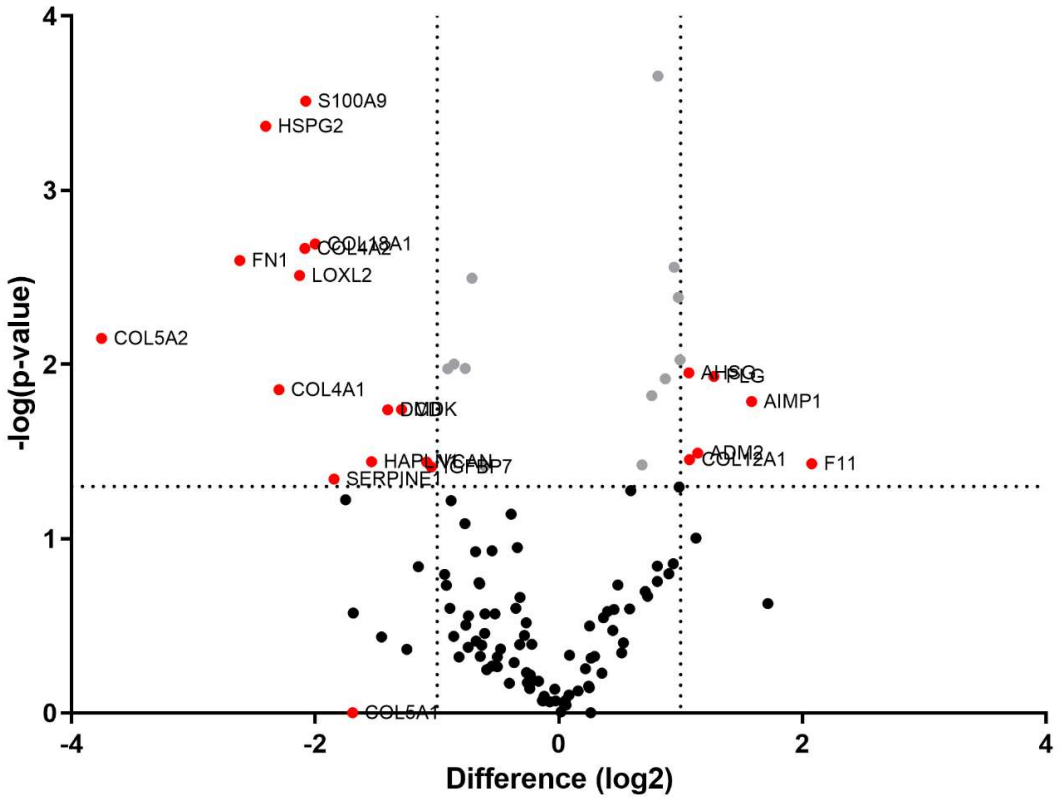

Figure 15: Quantitative ECM proteomics of the *P3H2* KO and WT clones. Volcano plot of ECM proteomics. The x axis represents the log2 fold change difference of regulated proteins between WT and KO ECM. The Y axis represents the p-values of the proteins. The volcano plot shows downregulation of Col4α1, Col4α2 and Col18α1 in KO ECM.

Our in-vitro approach, the generation of *P3H2* KO immortalized human podocytes cell lines, indicated that KO clones had different cellular behavior and abundance of Col4 sub-chains as well as interacting proteins were negatively affected by its absence. Even though we could answer several questions, there were limitations related to the in-vitro system so we further continued with *P3h2*$^{\Delta Pod}$ mice as an in-vivo approach.

3.4 Generation of podocyte-specific floxed *P3h2* knock-out mice

P3h2$^{\Delta Pod}$ mice were generated to investigate the effect of P3H2 on GBM and GFB homeostasis. *P3h2*$^{fl/fl}$ mice were bred with *hNphs2Cre*$^{WT/+}$ mice to delete the *P3h2* gene only in podocytes and both mouse lines were on a C57BL/6J background. *P3h2*$^{fl/fl}$ mice

without Cre recombinase were used as WT controls in experiments. Three-time points (6w, 28w, and 48w) were chosen for further characterization.

3.4.1 Confirmation of gene knock-out by analyzing sorted podocytes

To prove lack of *P3h2* expression in the generated *P3h2*$^{\Delta Pod}$ mice, qPCR and IF staining were performed in sorted podocytes and paraffin-embedded kidney tissue, respectively. To sort podocytes, glomeruli isolation was performed by bead perfusion and purified glomeruli were digested to the single-cell level. The same staining procedure was applied as explained in section 2.31. The stained cells were sorted in a FACS after proper gating (Figure 16A & B). Total RNA isolation was performed and the RNA level expression of *P3h2* was checked in sorted KO and WT mice podocytes. For IF staining, the paraffin-embedded kidney tissues were stained with NPHS1, P3H2, and DAPI in *P3h2*$^{\Delta Pod}$ and *P3h2*$^{fl/fl}$ mice.

The qPCR analysis indicated that the *P3h2* RNA level was highly significantly lower when compared with sorted WT podocytes (Figure 16C). The WT mice podocytes had 100% (n=3) and KO podocytes had 1.6% ± 0.7 (n=3) *P3h2* mRNA expression. There was co-localization of P3H2 and NPHS1 in WT podocytes (Figure 16D) which could not be demonstrated in KO podocytes. Both qPCR and IF staining data showed that the generated *P3h2*$^{\Delta Pod}$ mouse line lacked *P3h2* expression in podocytes.

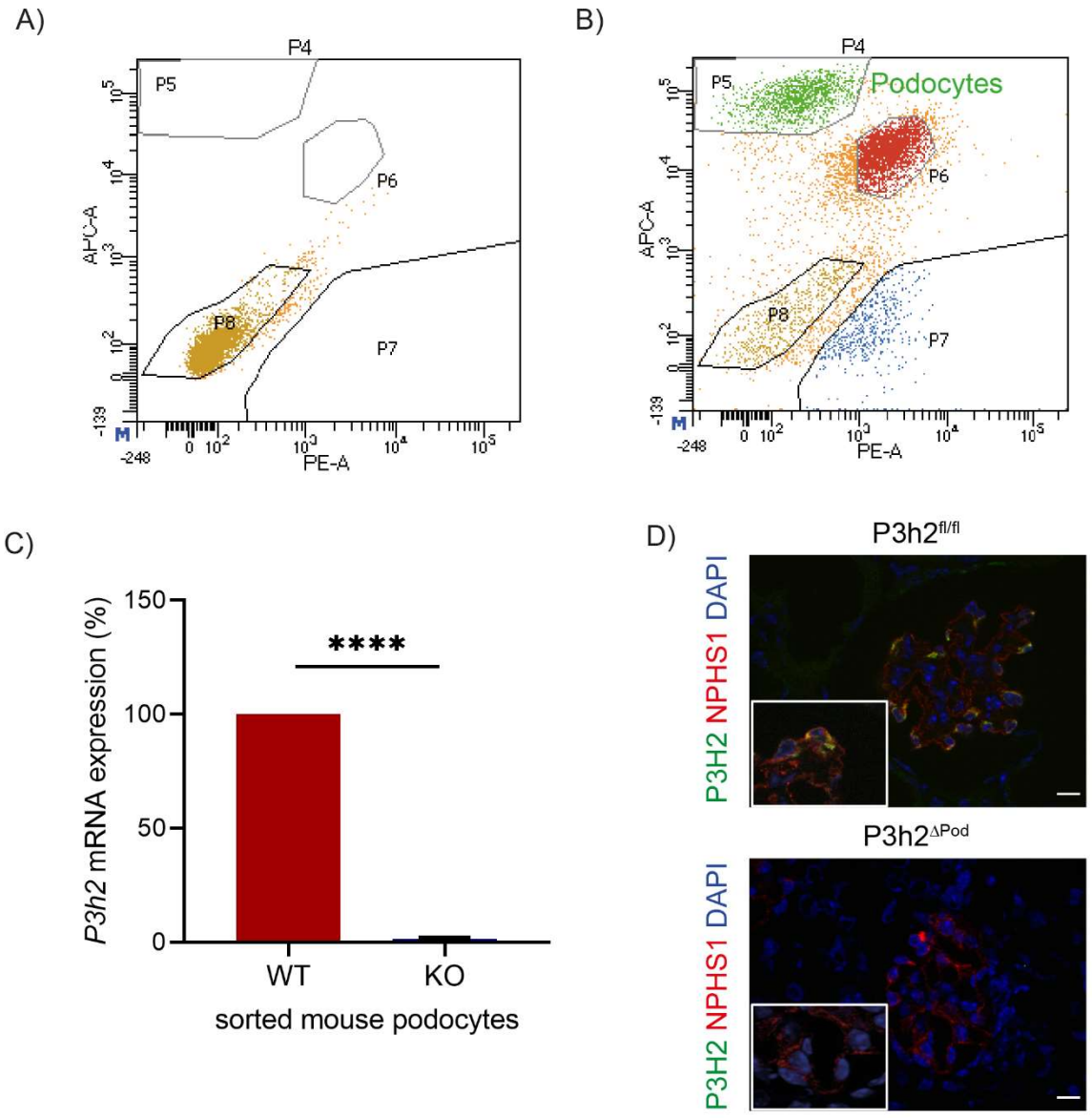

Figure 16: KO confirmation of the *P3h2*$^{\Delta Pod}$ mice. A) FACS graph of unstained cells. Unstained cells were necessary for gating of stained cells. B) Gating of stained cells via podocalyxin-647 and CD105-555 antibodies. P5 gating represents podocytes. C) *P3h2* mRNA expression analysis of sorted podocytes from WT and KO mice by qPCR. *P3h2* RNA level was 99% downregulated in *P3h2*$^{\Delta Pod}$ mice compared with RNA level of *P3h2*$^{fl/fl}$ mice. Graph shows mean ± SD, n=3, unpaired 2-tailed t-test, p-value ****< 0.0001. D) IF staining of WT and KO mice kidney tissue with P3H2, NPHS1, and DAPI. There was no P3H2 localization in *P3h2*$^{\Delta Pod}$ mice podocytes. Scale bar 10 µm.

3.4.1.1 Characterization of *P3h2*$^{\Delta Pod}$ mice

We characterized *P3h2*$^{\Delta Pod}$ mice to investigate its relevance for GBM composition and glomerular homeostasis. For characterization of the generated line, urine analysis, histological and ultrastructural examination, podocyte morphological analysis, and GBM proteomics were performed.

3.4.1.2 Development of albuminuria in *P3h2*$^{\Delta Pod}$ mice over time

The first step of the characterization of *P3h2*$^{\Delta Pod}$ mice was the measurement of body weight and urine albumin creatinine ratio (UACR) analysis over time to observe signs of glomerular disease development. *P3h2*$^{\Delta Pod}$ and *P3h2*$^{fl/fl}$ mice were examined between 5w till 48w of age. Albumin concentration in urine was measured with ELISA and creatinine was measured by an enzymatic kit.

Body weight of KO and WT animals were close to each other at every time point of the measurement period. Mean body weight of the KO mice was nominally higher than WT mice at 36w and 48w but these differences were not significant. At 36w, KO animals were 38.5 ± 10.1 g (n=9) and WT animals were 32.1 ± 9.4 g (n=9). At 48w, KO animals were 41.8 ± 10.8 g (n=9) and WT animals were 36.9 ± 10.5 g (n=9) (Figure 17A).

The graph of the UACR shows that KO mice started to present with albuminuria at the age of 36w. At all earlier time points, KO mice didn't have albuminuria and their UACR was similar to the UACR of WT mice. Mean albuminuria of 36w old KO mice was 50.1 ± 12.7 mg/g (n=8). WT animals had a mean of 28.4 ± 16.4 mg/g (n=8). At 48 weeks, the albuminuria of KO mice increased to a mean of 107.7 ± 10.3 mg/g (n=8). WT animals had a mean UACR of 38.1 ± 21.3 mg/g (n=8). The difference between WT and KO mice UACR was highly significant and KO mice showed progressive albuminuria (Figure 17B). These UACR data highlight that KO mice started to leak albumin at 36w which further increased at 48w indicating development of progressive glomerular damage.

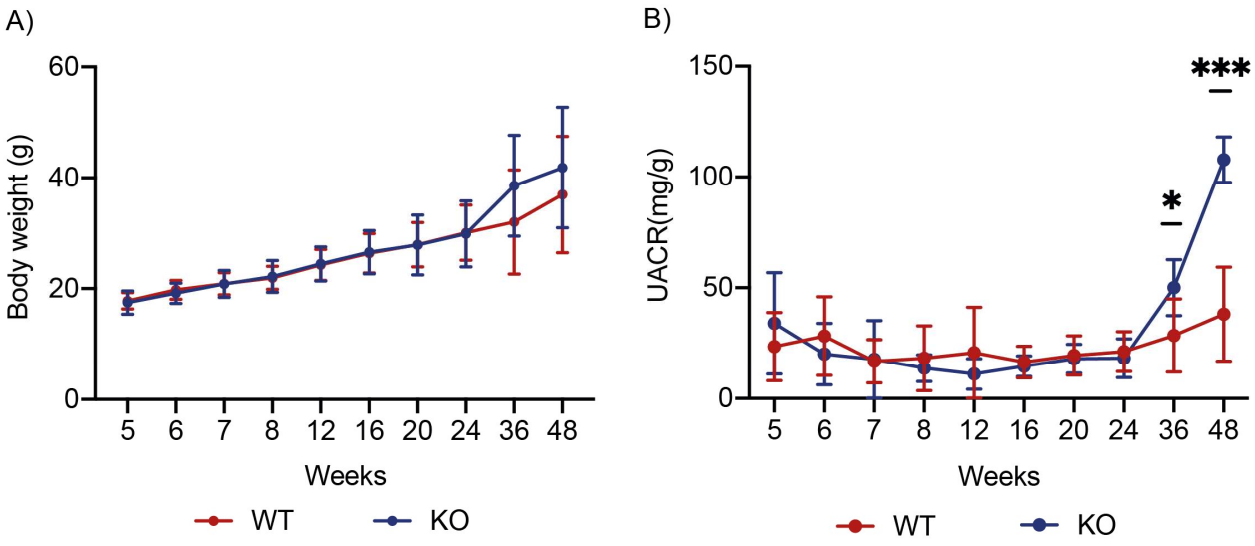

Figure 17: Body weight and UACR of *P3h2*$^{\Delta Pod}$ and *P3h2*$^{fl/fl}$ mice. A) Body weight of WT and KO mice were measured starting from 5w till 48w of age. There was no significant difference at any time point of the body weight measurements between *P3h2*$^{\Delta Pod}$ and *P3h2*$^{fl/fl}$ mice B) UACR of WT and KO mice. KO mice started to present albuminuria at 36w of age and it increased at 48w of age. Graphs show mean ± SD, n ≥ 8, Mann Whitney U test, p-value * < 0.05, ***< 0.001.

3.4.1.3 Histological phenotype of *P3h2*$^{\Delta Pod}$ mice

The histological phenotype of *P3h2*$^{\Delta Pod}$ mice was examined by PAS staining. Paraffin-embedded kidney tissues were collected at 6w, 28w, and 48w and stained to assess glomerular structure in *P3h2*$^{\Delta Pod}$ mice and *P3h2*$^{fl/fl}$ mice.

Analysis of the sections indicated that glomeruli in *P3h2*$^{\Delta Pod}$ mice appeared normal in 6w and 28w old mice. There were no observed histological differences between *P3h2*$^{\Delta Pod}$ and *P3h2*$^{fl/fl}$ mice at 6w and 28w. At 48w, *P3h2*$^{\Delta Pod}$ glomeruli had glomerulosclerosis and showed signs of podocyte injury. In *P3h2*$^{fl/fl}$ mice, glomeruli looked normal and healthy at 48w (Figure 18A). Quantification of glomerulosclerosis showed that *P3h2*$^{\Delta Pod}$ mice had significantly more glomerulosclerosis than *P3h2*$^{fl/fl}$ mice. The mean value of the percentage of glomerulosclerosis in KO glomeruli is 35.8 % ± 10.6 (n=5). For WT mice, it is 10.4% ± 5.1 (n=5). Focal sclerosis was also observed and focal glomerulosclerosis is indication hallmark of FSGS (Figure18B).

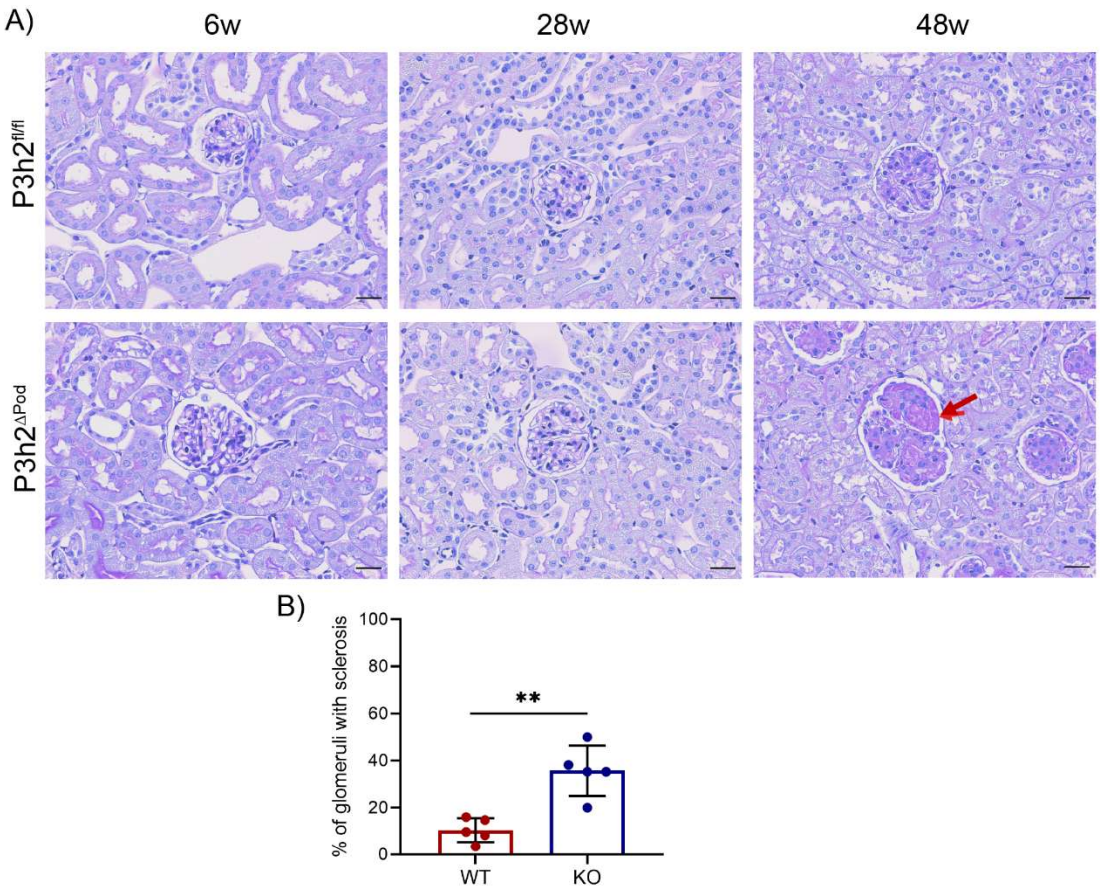

Figure 18: Histological phenotype examination of *P3h2*$^{\Delta Pod}$ and *P3h2*$^{fl/fl}$ mice by PAS staining. A) PAS staining was performed at three different time points at 6w, 28w, and 48w. At 6w and 28w, glomerular morphology was normal in *P3h2*$^{\Delta Pod}$ mice. At 48w, glomerulosclerosis and podocyte injury were observed in *P3h2*$^{\Delta Pod}$ kidney tissue (red arrow). Scale bar, 20 µm. B) Quantification of glomerulosclerosis of *P3h2*$^{\Delta Pod}$ and *P3h2*$^{fl/fl}$ mice at 48w. *P3h2*$^{\Delta Pod}$ mice had significantly more glomerulosclerosis than *P3h2*$^{fl/fl}$ mice. Graph shows mean ± SD, n = 5, unpaired 2-tailed t-test, p-value ** < 0.01.

3.4.1.4 Ultrastructural analysis of the glomeruli of *P3h2*$^{\Delta Pod}$ mice

We next examined the glomeruli of *P3h2*$^{\Delta Pod}$ mice and *P3h2*$^{fl/fl}$ mice by ultrastructural analysis. Kidney tissue at 6w, 28w, and 48w of age were fixed, embedded, and cut for transmission electron microscopy (TEM). Podocytes, foot processes, GBM and Bowman's capsule was examined in detail. Quantification was done for GBM thickness and foot process width (FPW) for *P3h2*$^{\Delta Pod}$ and *P3h2*$^{fl/fl}$ mice at all time points.

GBM irregularities especially partial thickening, thinning or loosely packaged GBM were observed in *P3h2*$^{\Delta Pod}$ mice glomeruli at 6w and 28w (red arrows, Figure 19A). Whereas,

P3h2$^{fl/fl}$ mice had conserved healthy glomeruli. At 48w, foot process effacement, thickening of GBM and Bowman's capsule, glomerulosclerosis was observed in *P3h2*$^{\Delta Pod}$ mice glomeruli.

Quantification of the TEM images showed that the KO mice had thinner GBM than WT mice at 6w and 28w indicating a symptom for thin basement membrane nephropathy (TBMN). At 6w, thickness of the GBM for *P3h2*$^{\Delta Pod}$ mice was 124.7± 12.8 nm (n= 4) while that of *P3h2*$^{fl/fl}$ mice was 154.1 ± 15.3 nm (n=4). At 28w thickness of the GBM for *P3h2*$^{\Delta Pod}$ mice was 149.9 ± 9.1 nm (n=4) and that for *P3h2*$^{fl/fl}$ mice was 195.2 ± 7.5 nm (n=4). At 48w, the thickness of the GBM increased significantly as a result of sclerosis. The thickness of the GBM for *P3h2*$^{\Delta Pod}$ mice was 387.5 ± 34 nm (n=4) and for *P3h2*$^{fl/fl}$ mice 230 ± 8.1 nm (n=4) (Figure 19B).

Quantification of FPW indicated that there was no difference at 6w between KO and WT mice. The mean foot process width was 311.9 ± 35.5 nm (n=4) for KO mice and 310.8 ± 21.9 nm (n=4) for WT mice. At 28w FPW was significantly higher in KO mice indicating foot process effacement (FPE). The mean values of the FPW for KO mice were KO 499.9 ± 98.9 nm (n=4) and for WT 317.7 ± 21.5 nm (n=4). At 48w, the mean values of the FPW for KO mice were 409.9 ± 25.5 nm (n=4) and for WT 343.7 ± 19.2 nm (n=4) (Figure 19C). In addition, Bowman's capsule (BC) thickness was quantified at 48w. There was a significant increase in thickness of BC in KO mice indicating PEC activation. The mean values of BC thickness for KO and WT mice were 1065 ± 224.2 nm (n=4) and 455 ± 66.1 nm (n=4), respectively (Figure 19D). In conclusion, TEM data proved that *P3h2* deletion affected the GBM of the mice as early as 6w. Mice developed a severe phenotype at later stages of life indicating progressive glomerular disease.

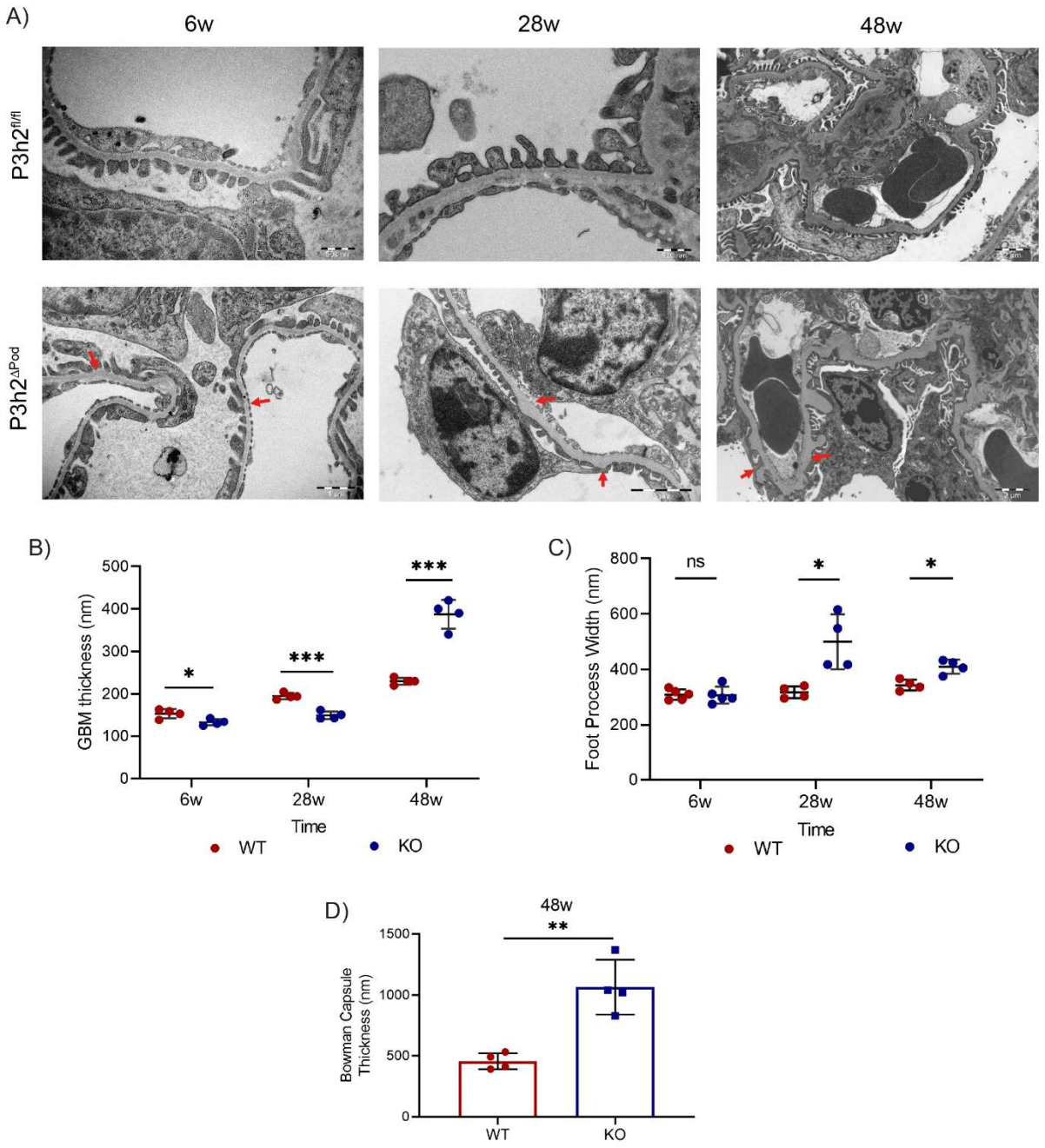

Figure 19: Ultrastructural analysis of *P3h2*$^{\Delta Pod}$ and *P3h2*$^{fl/fl}$ mice. A) TEM micrographs of WT and KO mice at 6w, 28w and 48w. Red arrows indicate abnormal GBM structure. Scale bars, 500 nm and 1µm. B) Measurement of GBM thickness on TEM micrographs. At 6w and 28w, KO mice had thinner GBM and at 48w, KO mice had thicker GBM when compared with WT mice C) FPW measurement of WT and KO podocytes on TEM micrographs. FPW was increased at 28w and 48w old KO mice when compared to WT indicating FPE. D) BC thickness measurement of the TEM micrographs of *P3h2*$^{\Delta Pod}$ and *P3h2*$^{fl/fl}$ at 48w.Thickness of BC was increased significantly in KO mice indicating PEC activation. Graphs show mean ± SD, n=4, unpaired 2-tailed t-test, p-value ns >0.05, * < 0.05, **< 0.01 ***< 0.001.

3.4.1.5 Urinary abnormalities in *P3h2*$^{\Delta Pod}$ mice

The observation of a thinner basement membrane in *P3h2*$^{\Delta Pod}$ mice led us to check for hematuria. Hematuria is one of the clinical features of TBMN. Spot urine was collected from *P3h2*$^{\Delta Pod}$ and *P3h2*$^{fl/fl}$ mice at the age of 48w. Hematuria was first checked with a dipstick and subsequently red blood cells (RBCs) were counted under a light microscope.

Malformed RBCs were detected in the urine of KO mice and there was considerably less or none RBCs in WT urine (Figure 20A). There were 14 ± 7 cells per µl (n=4) in KO urine while there were only 2 ± 1 cells per µl in WT urine (n=4, Figure 20B). Microhematuria of *P3h2*$^{\Delta Pod}$ mice represents another symptom of TBMN.

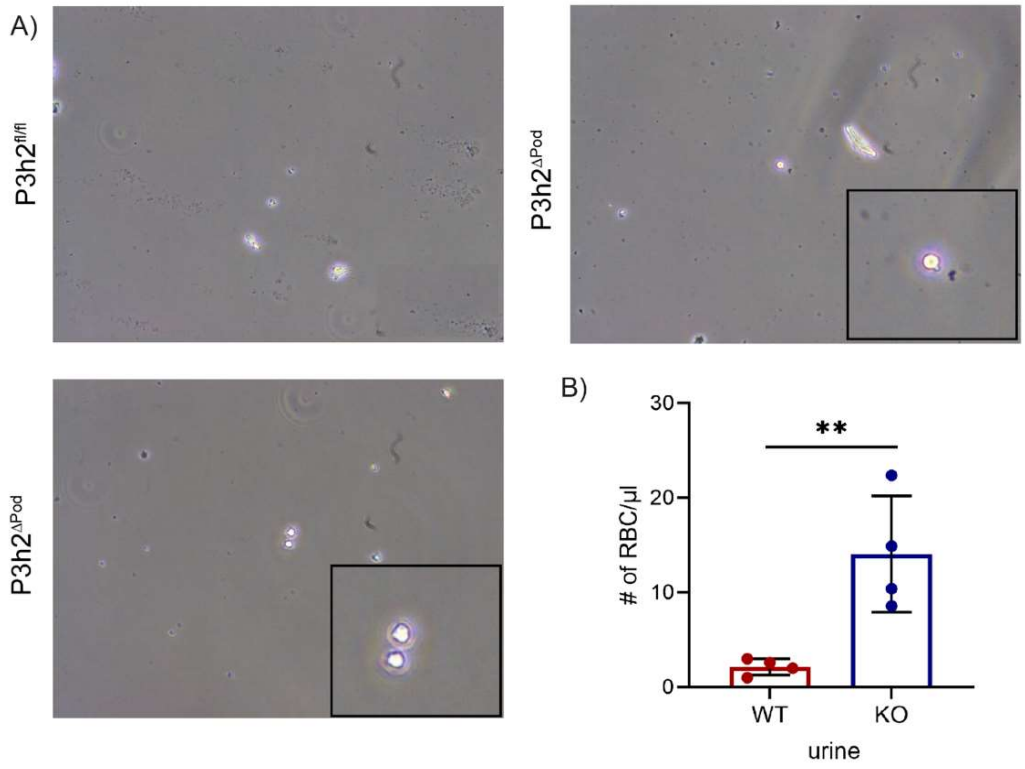

Figure 20: Observation of hematuria in spot urine of *P3h2*$^{\Delta Pod}$. A) Representative images of mice urine. There was no RBCs in WT mice urine. However, malformed RBCs were detected in KO mice urine. B) Quantification of counted RBCs in urine under the light microscope. Graph shows mean ± SD, n=4, unpaired 2-tailed t-test, p-value **< 0.01.

3.4.1.6 Morphological analysis of podocytes in *P3h2*$^{\Delta Pod}$ mice

Podocyte morphometric analysis (podometrics) was performed to evaluate podocyte injury in *P3h2*$^{\Delta Pod}$ mice at the age of 48w. In the workflow of this analysis, paraffin-embedded kidney sections were immuno-stained with SYNPO as a podocyte cytoplasm marker, DACH1 as a podocyte nucleus marker, and DAPI as a general nucleus marker. Images of 20 glomeruli were randomly taken under a confocal microscope. These images were used to measure the area of the glomerular tuft, podocyte cytoplasmic and nuclear area and to count the podocytes by FIJI software. A model-based stereology formula was used to convert 2D information to 3D information. Thereby, we could calculate podocyte number, podocyte density and average podocyte cell volume (aPCV) of each glomerulus.

The representative IF staining images indicated that KO mice had less podocytes and an increased glomerular tuft volume. In WT glomerulus, in ten cells DACH1 and DAPI co-localized and were surrounded by the SYNPO signal, therefore representing podocytes. However, in KO glomerulus, the podocyte number was eight (Figure 21A). The podocyte number was significantly decreased in KO glomeruli when compared with WT glomeruli. The median values for KO glomerulus were 80 podocytes (n=6) and 87 podocytes for WT glomerulus (n=6) (Figure 21B). Podocyte density in a glomerulus was significantly decreased in KO glomerulus as well. Podocyte density was 23.3 per μm^3 (n=6) in KO and 36.7 per μm^3 (n=6) for WT (Figure 21C). The glomerular volume was not significantly changed in KO glomeruli when compared with WT glomeruli. The median values for KO glomerular volume was 3.16 $x10^5$ μm^3 (n=6) and 2.95 $x10^5$ μm^3 (n=6) for WT glomerular volume (Figure 21D). In the last graph, aPCV was calculated by dividing the calculated total podocyte cell volume (TPCV) to the podocyte number (PN). This data indicated that there was a significant increase in the aPCV in KO podocytes. aPCV of the KO podocytes was 296.8 μm^3 (n=6) while it was 256 μm^3 in WT podocytes (n=6) (Figure 21E). Increased aPCV is a sign for podocyte hypertrophy. These data showed that KO glomeruli were losing podocytes and pointed towards podocyte hypertrophy as a sign of glomerular injury.

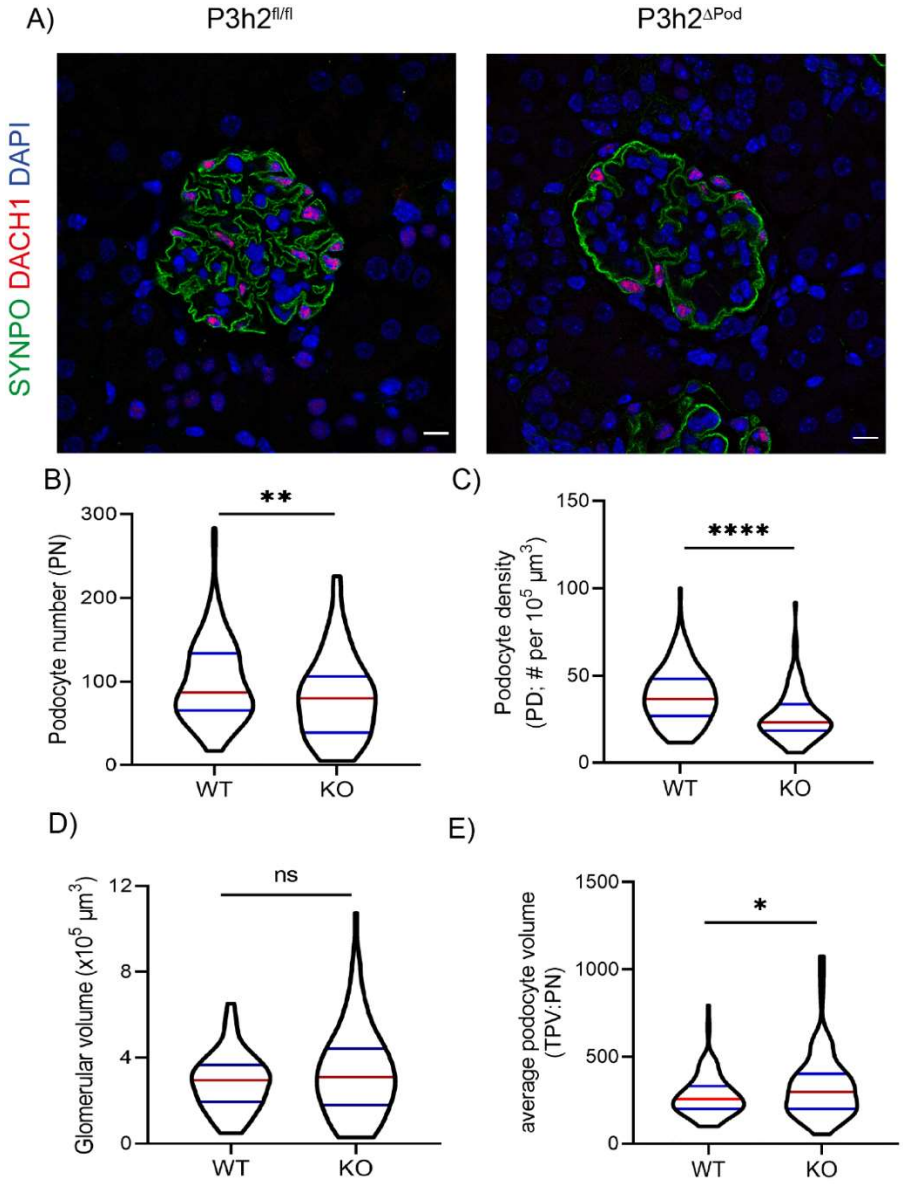

Figure 21: Podocyte morphometric analysis of *P3h2*$^{\Delta Pod}$ and *P3h2*$^{fl/fl}$ mice. A) Representative IF images of WT and KO mice paraffin-embedded kidney tissue with SYNPO, DACH1, and DAPI. The images were used for podocyte number (PN), podocyte density (PD), glomerular volume, and average podocyte volume (aPCV: TPV/PN) measurements. Scale bar 10 µm. B) Podocyte number of WT and KO mice. PN was significantly decreased in KO mice glomeruli indicating podocyte loss. C) Podocyte density of WT and KO mice. In KO mice glomeruli, PD was decreased significantly in comparison to WT mice glomeruli indicating podocyte loss. D) Glomerular volume of WT and KO mice. There was no significant difference between the glomerular volume of WT and KO mice. E) aPCV of the WT and KO mice. Significant increased aPCV was observed in KO mice glomeruli indicating podocyte hypertrophy. Graphs show median ± interquartile range, n ≥ 6, Mann Whitney U test, p-value ns > 0.05, *< 0.05, **< 0.01, ****< 0.0001.

3.4.1.7 Podocyte hypertrophy in *P3h2*$^{\Delta Pod}$ mice

We aimed to further characterize the state of hypertrophy of podocytes in *P3h2*$^{\Delta Pod}$ mice at the age of 48w. We observed increased aPCV in podometric analysis and corroborated this finding by IF staining using a podocyte hypertrophy marker. Podocytes become hypertrophic when there is podocyte loss in the glomeruli. Remaining podocytes are trying to close the denuded are on the GBM. This event is protective until a certain level but after approx. more than 20% of podocytes are lost, podocyte hypertrophy and activated PECs induce sclerosis within the glomerulus [91]. Paraffin-embedded kidney sections of 48w old mice were stained with phosphorylated ribosomal protein S6 (Rb-pS6), a podocyte hypertrophy marker. The images were taken under a confocal microscope and quantification was done by FIJI software analysis.

We could detect podocyte hypertrophy in both genotypes. Representative images of IF images show podocyte hypertrophy (green) in WT and KO glomeruli (Figure 23A). A certain level of podocyte hypertrophy is expected in WT glomeruli since the mice were at 48w of age. Podocyte are post-mitotic cells and by aging podocyte loss occurs in glomeruli and remaining podocytes become hypertrophic to compensate the loss of detached podocytes. Quantification of IF images indicated that the percentage of glomeruli having hypertrophic podocyte is significantly higher in KO mice (Figure 23A). The mean percentage value of glomeruli having podocyte hypertrophy in KO mice is 50.8% ± 9.9 (n=6) and for WT mice it is 34.1% ± 10.4 (n=6). This data confirmed the podometrics finding which indicated increased podocyte hypertrophy in KO mice glomeruli.

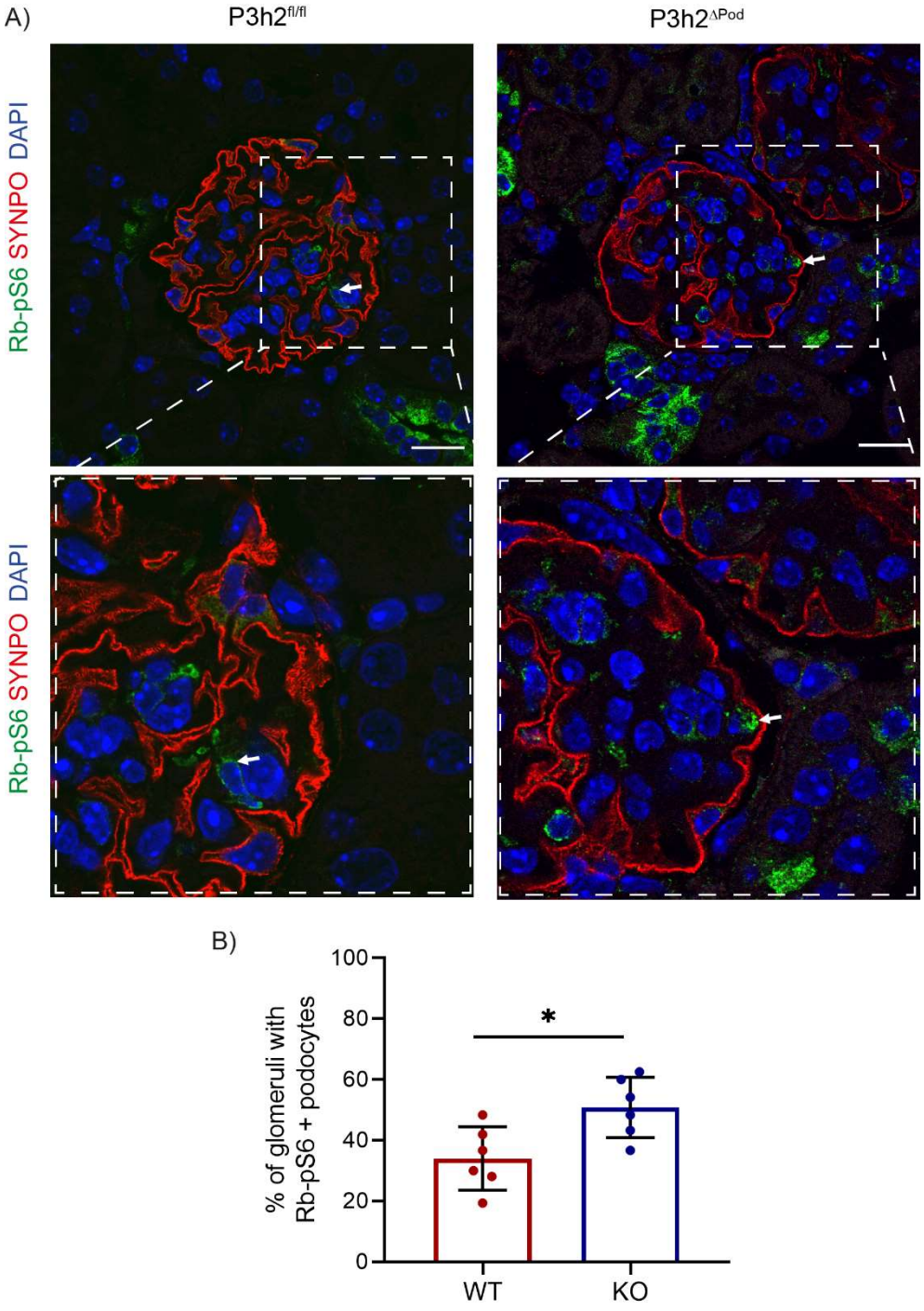

Figure 22: Podocyte hypertrophy evaluation of *P3h2*$^{\Delta Pod}$ and *P3h2*$^{fl/fl}$ mice. IF staining of the WT and the KO mice paraffin-embedded kidney tissue with Rb-pS6, SYNPO, and DAPI. A) Representative IF images showed Rb-pS6 (green) in podocytes of both WT and KO mice (white arrows). Scale bar, 20 µm. B) Quantification of IF images indicated significant increase of podocyte hypertrophy in KO glomeruli when compared with WT glomeruli. Graph shows mean ± SD, n=6, unpaired 2-tailed t-test, p-value *< 0.05.

3.4.1.8 Parietal epithelial cell activation in *P3h2*$^{\Delta Pod}$ mice

Activated PECs migrate from the outer layer of Bowman's capsule to the glomerular tuft and contribute to the formation of sclerosis [91]. We aimed to characterize the state of parietal epithelial cells (PECs) in *P3h2*$^{\Delta Pod}$ mice at the age of 48w since we observed focal sclerosis in PAS images. Moreover, we observed significant increase in Bowman's capsule thickness of KO mice at 48w during TEM micrograph analysis. The confirmation of these findings was done by IF staining of PECs via the PEC activation marker, CD44. The images were taken under a confocal microscope and quantification was done by FIJI software analysis.

Representative IF images show activated PECs (green) in KO mice. On the other hand, representative WT images show the PECs were at inactive state (Figure 23A). Quantification of IF images showed significant increase the percentage of glomeruli having activated PECs in KO glomeruli with comparison of WT ones. The mean percentage of glomeruli having active PECs for KO mice is 18.4% ± 11.2 (n=6) and for WT mice, it is 5.7% ± 3.2 (n=6). It is expected to observe some activated PECs in WT glomeruli due to the age of mice. This data showed that there is mild PEC activation in KO glomeruli being correlated with glomerulosclerosis (analysis PAS images) and increased Bowman's capsule thickness (TEM analysis) at the same age of mice.

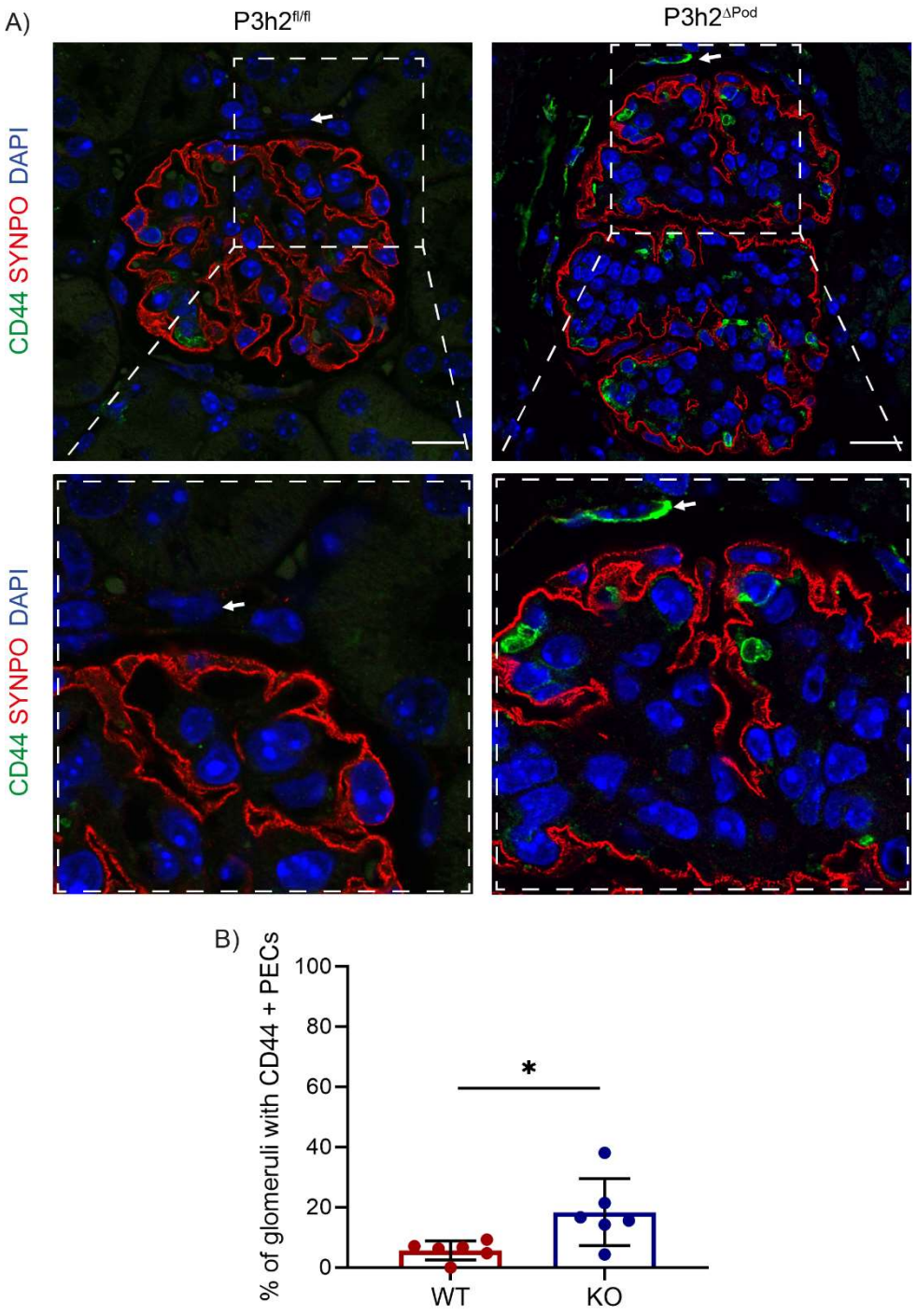

Figure 23: PEC activation of *P3h2*$^{\Delta Pod}$ and *P3h2*$^{fl/fl}$ mice. A) IF staining of WT and KO mice paraffin-embedded kidney tissue with CD44, SYNPO and DAPI. Representative IF images of KO mice showed CD44 (green) signal in PECs (white arrow) indicating PEC activation. Representative IF images of WT mice showed no signal of CD44 in PECs (white arrow). Scale bar 20 µm. B) Quantification of IF images indicated significant increase of the percentage of glomeruli having activated PEC cells in KO mice when compared with WT mice. Graph shows mean ± SD, n=6, unpaired 2-tailed t-test, p-value *< 0.05.

3.4.1.9 Quantitative GBM proteomics of *P3h2*$^{\Delta Pod}$ mice

We could get structural information of the GBM from TEM observations. However, we didn't know how the protein abundance was affected by *P3H2* deletion. Therefore, we aimed to explore protein abundance of the GBM by quantitative proteomics. Glomerulus isolation from mice was done by bead perfusion. The isolated glomeruli were decellularized by detergents to enrich the GBM. The enriched GBM was analyzed by mass spectrometry.

The enriched GBM samples were stained by Coomassie blue to check total protein separation. The GBM lane had a lot of protein of high protein weight indicating GBM enrichment as many GBM proteins are large-sized proteins. The cell's lysate lanes had protein at every size showing that many of the intracellular proteins were removed during isolation (Figure 24A). In addition, a couple of GBM, intracellular proteins, and transmembrane proteins were checked by WB to evaluate purity of the enriched GBM. The WB data indicated that the enriched GBM had a high abundance of Col4 and Laminin. On the other hand, intracellular protein (alpha-tubulin and alpha-actinin) were lacking in enriched GBM fraction when compared with the cell lysates (Figure 24B).

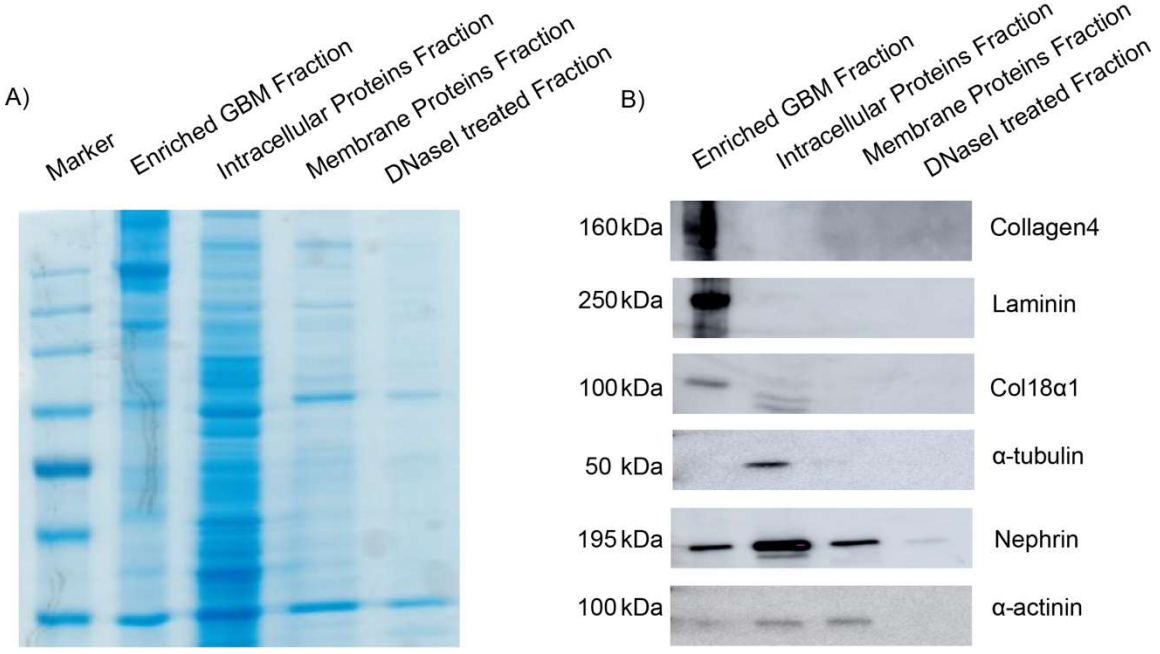

Figure 24: GBM enrichment from isolated glomeruli. A) Coomassie blue staining of enriched GBM and other fractions collected during isolation. Enriched GBM fraction had high molecular weight protein bands indicating that isolated GBM was enriched with ECM proteins. The intracellular protein fraction had protein bands in every size showing that during isolation many intracellular proteins were separated from enriched GBM. B) WB of enriched GBM and other fractions for quality control of isolated GBM. ECM proteins were detected in high abundance in enriched GBM fraction. Intracellular and transmembrane proteins were in low abundance or not detected in enriched GBM fraction when compared with intracellular and membrane protein fractions.

Regulated GBM proteins were presented in a volcano plot in which the x axis represents the log2 fold-change values of proteins and the y axis represents p values of the proteins. The comparison between WT and KO GBM components presented in the volcano plot. Significantly downregulated proteins in KO GBM was marked red at the minus side of the x-axis. The volcano plot of the GBM proteomics showed that the abundance of the main structural proteins decreased in KO GBM (Figure 25A). Col4 sub-chains, Lam521, Nidogen1 were the most affected and downregulated proteins in KO mice GBM. Relative abundance values were indicated in a dot plot analysis for each individual mouse (n=6) (Figure 25B). Therefore, before mentioned proteins could be a reason for the reduced GBM thickness observed in KO animals.

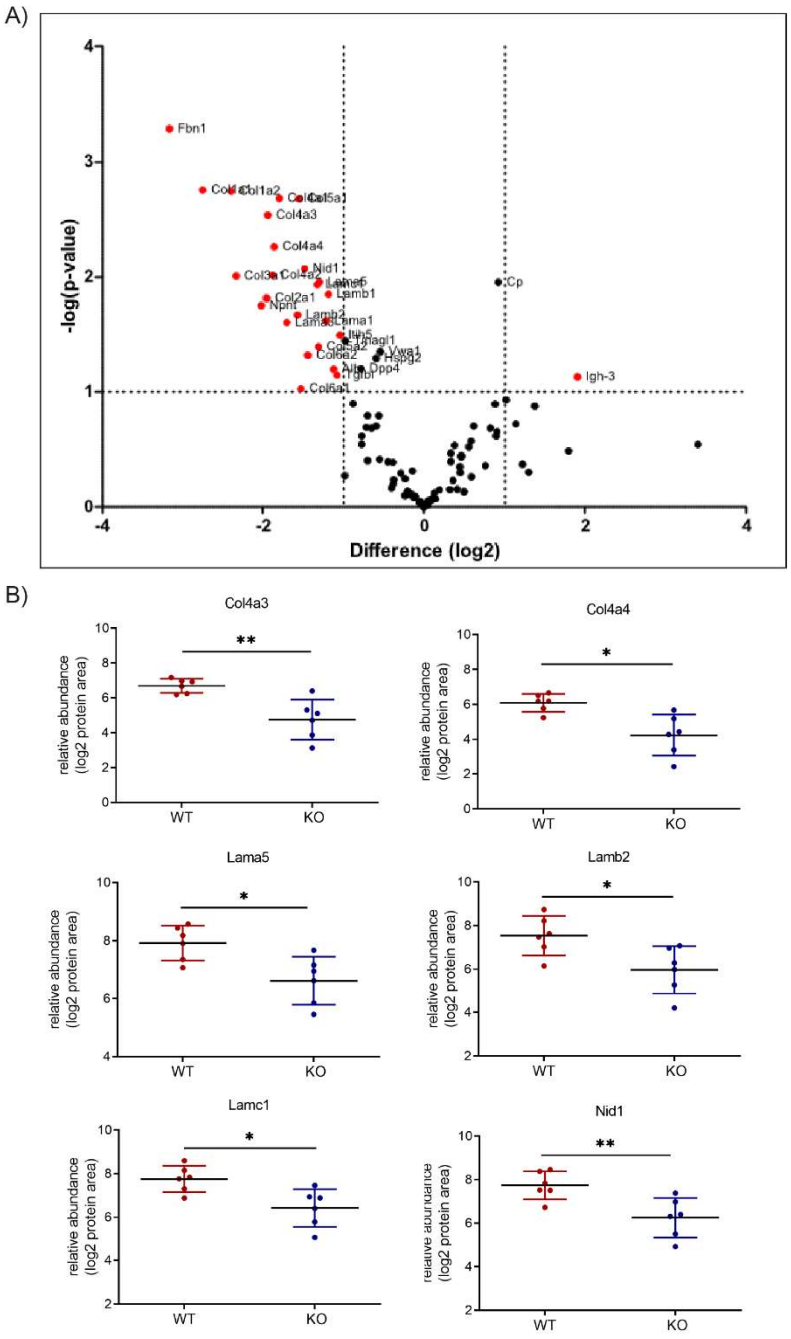

Figure 25: Quantitative GBM proteomics of *P3h2*$^{\Delta Pod}$ and *P3h2*$^{fl/fl}$ mice. A) Volcano plot of GBM proteomics. X axis showed log2 fold-changes in abundance of WT and KO GBM proteins and y axis showed the p values of the GBM proteins. Main structural GBM proteins were downregulated in KO mice indicated in the left part of the plot. B) Dot plots of the regulated structural proteins in the GBM. Relative abundance values of each mice analyzed in quantitative GBM proteomics and significant decrease in main GBM structural protein was observed. Graphs show mean ± SD, n=6, unpaired 2-tailed t-test, p-value * < 0.05, **< 0.01.

4 Discussion

In this project, we aimed to identify the effect of *P3H2* on GBM and glomerular homeostasis. An expression-based approach was applied to identify novel candidate genes in a nephrotic syndrome patient cohort. Identification of novel genes is very important for better understanding of kidney diseases, especially monogenetic kidney diseases. Characterization of monogenetic diseases can help us to better understand complex multifactorial renal diseases. With this idea, highly expressed genes in mouse podocytes were identified by omics studies and correlated with public human expression data. Podocytes were chosen for this approach since they are the predominant cell type in glomeruli which is being most affected in the progression of many kidney diseases [95]. Beside this, there are a lot of identified podocyte-specific gene mutations in nephrotic syndrome patients [69]. Therefore, it is vital to understand podocyte and glomerular homeostasis and their contribution to development and progression of kidney diseases.

With this approach a *P3H2* gene mutation was identified in a young female patient. The patient had a histological diagnosis of FSGS and a clinical one of SRNS. She had progressive kidney injury and developed ESKD. She started hemodialysis and got a kidney transplant in 2017. She also had cataract and myopia which are related with mutations in the *P3H2* gene [96] [82].

4.1 Effect of *P3H2* deletion on collagen4, extracellular matrix and basement membrane

P3H2 is a post-translational enzyme and performs 3Hyp of proline amino acids of collagens, especially Col4. Hydroxylation of proline residues of Col4 sub-chains are necessary for proper Col4 synthesis, cross-linking, flexibility and protein-protein interaction. There are two types of hydroxylation of Col4, 4Hyp and 3Hyp. 4Hyp is much more common than 3Hyp on Col4 and has been studied more intensively so far. Even though the number of 3Hyp is rare, they are evolutionary conserved and it is thought that they have an important function for Col4 biosynthesis [97]. However, the exact function of

3Hyp on Col4 biosynthesis is not known although a couple of researchers showed that it might be important for flexibility of Col4 sub-chains and protein-protein interaction [98] [99].

Quantitative ECM proteomics data showed that Col4α1 and Col4α2 abundance was downregulated. In addition, there was downregulation of the Col4 interactor protein, Col18α1. Downregulation of Col4 sub-chains and its interactor show the effect of *P3H2* deletion on Col4 biosynthesis. In addition, identified Col4 peptides in proteomics were checked for 3Hyp. However, technical limitations and difficulties in the analysis prevent the further evaluation of 3Hyp sites of Col4 sub-chains.

Quantitative GBM proteomics was performed to find out changes in GBM composition. This analysis showed that the main structural GBM proteins beside Col4 sub-chains were downregulated in KO mice. This finding might explain the thinner GBM in KO mice. However, at 48w in TEM quantification, the GBM of KO mice was significantly increased. When we checked the TEM micrographs carefully, we did observe that sclerotic regions had a thicker GBM which is a known phenomenon [100]. On the other hand, non-sclerotic part had a thinner GBM. During GBM enrichment, we might isolate more GBM of non-sclerotic parts since sclerotic, fibrous tissue is hard to digest. Therefore, our observation of thinner GBM parts in 48w KO mice is not a contradiction to the detected sclerotic lesions.

Our quantitative ECM and GBM proteomics data indicated that Col4 interactors were downregulated. These findings might also support a functional role of 3Hyp in protein-protein interaction. On the other hand, KO mice had thinner GBM and within this context all Col4 sub-chains were downregulated. Moreover, we could show decreased abundance of Col4 sub-chains in ECM of *P3H2* KO podocyte cell lines. There might be two explanation for decreased abundance levels of Col4 sub-chains in both ECM and GBM. Firstly, there might be less secretion of Col4 from podocytes to the extracellular space. Col4 is mainly secreted from podocytes [101] and lack of 3Hyp might affect its proper secretion. Second explanation might be that Col4 within the GBM had a shorter lifespan than normal hydroxylated one. Lack of 3Hyp might make them less stable or might prevent proper cross-linking inducing their degradation by MMPs. MMPs were not upregulated in our proteomics data but their activity might be increased. These two

possible mechanisms could explain low abundance of Col4 sub-chains in the ECM and GBM.

4.2 Effect of *P3H2* deletion on podocytes

Our expression data showed that P3H2 is a podocyte-enriched protein. The high expression profile of *P3H2* in podocytes should indicate a role in healthy podocyte and GBM maintenance since high expression profile of genes is correlating with their functional relevance [102].

We aimed to observe changes in cellular behavior of podocytes in an in-vitro approach. We used CRISPR-Cas9 genome editing technology to generate *P3H2* KO human podocytes by using different gRNAs. Different gRNAs targeting different exons were used to confirm findings since Cas9 nuclease might induce off-targets. Designed gRNAs were checked for possible off-targets in silico and zero off-target gRNAs were chosen. In addition, we used two different WT cells to control for off-target effects as well. One WT underwent the same procedures as KO clones and the other WT was not processed at all. Our in vitro data showed that adhesion capacity of KO cells was elevated. Adhesion is one of the most important property of healthy podocytes and elevated adhesion capacity might be a sign for stressed podocytes [26]. On the other hand, migration ability was not affected by *P3H2* deletion.

We could evaluate the response of *P3H2* deletion on an immortalized human podocyte cell line. However, there were several limitations of this in-vitro approach. One of them was the lack of a realistic in-vivo 3D morphology of podocytes. In life vertebrates, podocytes have their very special morphology with a big cell body and protrusions from the cell body to generate primary and secondary foot processes to form the SD between adjacent foot processes. However, under 2D cell culture conditions, podocyte cell morphology is completely different and there are no foot processes and SD structure. Even though our in-vitro system was good enough to evaluate basic homeostatic changes of podocytes an in-vivo system is needed for more detailed evaluation of podocytes and GFB structure.

Characterization of *P3h2*$^{\Delta Pod}$ mice indicated a mild podocyte phenotype at 28w with further progression at 48w. At 28w, FPW was significantly increased in KO podocytes. At 48w, we observed foot process effacement, podocyte loss and podocyte hypertrophy indicating podocyte stress. At earlier time points, podocyte morphology even on the ultrastructural level looked normal and healthy. The first observed ultrastructural difference in the GBM was at 6w, a time point were podocyte and glomerular morphology was completely normal. GBM alterations were more obvious at 28w and 48w and at this time points we started to observe podocyte stress and injury. Although we cannot provide further scientific evidence one could speculate that the GBM alterations are the reason of the observed podocyte phenotype in *P3h2*$^{\Delta Pod}$ mice. There are several ways to explain how GBM alteration might induce podocyte injury. Focal adhesions (FAs) are spots where podocytes attach to the GBM. FAs are known as signaling hubs and are vital for glomerular integrity. FAs keep the podocyte-GBM interaction in balance via actin cytoskeleton regulation of foot process morphology. Focal adhesion kinase (FAK) is a key enzyme within this system. Activation of FAK via phosphorylation induce FPE in podocytes. Moreover, its activation was observed in Alport syndrome mice models [103] and podocyte-specific *FAK* KO mice were protected from FPE and albuminuria [104]. Therefore, in our model, abnormal GBM composition might start FPE via activation of FAK. In addition, integrin α3β1 is another adhesion molecule linking podocytes to the GBM. Integrin signaling is a key system for podocyte inside- out signaling. Both *Itga3* and *Itgb1* podocyte-specific mouse models had severe proteinuria, GBM abnormalities and FPE [61]. Therefore, the abnormal GBM composition in *P3h2*$^{\Delta Pod}$ mice might induce podocyte stress via increased integrin signaling.

If Col4 synthesis is not properly accomplished due to *P3H2* deletion, this might induce ER stress and unfolded protein response (UPR) mechanisms in the podocytes which lead to podocyte damage over time. ER is an important organelle for post translational modification, folding and secretion of proteins. Genetic mutations can cause misfolded protein synthesis which causes ER stress and induces UPR. Inositol-requiring enzyme 1 (IRE1), protein kinase RNA-like ER kinase (PERK) and activating transcription factor 6 (ATF6) are three proteins regulating this response. Binding immunoglobin protein (BiP) is an ER chaperone which has a role in recognition of misfolded or unfolded protein and

induces UPR by interaction with three UPR proteins. Downstream of the UPR pathway, apoptosis might be activated if the misfolded protein accumulation is high [105]. ER stress and UPR response was observed in Col4 nephropathies as well as monogenetic kidney diseases. Activation of UPR response was shown in *Col4α3* KO mice and overexpression of a patient *COL4A3* mutation in podocytes [77]. Therefore, in our project, the lack of 3Hyp on Col4 sub-chains might activate ER stress and UPR since this PTM can affect proper folding and/or secretion of Col4.

At this point, we should consider mechanical forces on podocytes. There are different mechanical forces i.e. tension and shear stress. It has been shown that increased tension and shear stress induce podocyte injury. Homeostasis of GFB depends on these forces and increased pressure can surpass the limits of GFB resistance [106]. Since GBM and podocyte foot processes have to control of these pressures the changed GBM composition might elevate these forces on podocyte foot processes which could further increase podocyte stress.

4.3 *P3h2* gene deletion induces thin basement membrane nephropathy and focal segmental glomerulosclerosis

COL4 mutations cause at least two kidney diseases, Alport syndrome and thin basement membrane nephropathy. These diseases are called Col4 nephropathies. Col4 mutations cause alterations in the GBM and further progression disrupts glomerular integrity and induces FSGS [107]. Moreover, several studies showed that genetic FSGS in adulthood is related to *COL4* mutations [108]. Therefore, in the second part of the project, we aimed to examine the effect of the P3H2 modifier enzyme on GBM and GFB homeostasis by characterizing podocyte-specific *P3h2*$^{\Delta Pod}$ mice. The KO proof of generated *P3h2*$^{\Delta Pod}$ mice line was accomplished by sorting podocytes and IF staining of glomeruli. There was no *P3h2* RNA and P3H2 protein in qPCR and IF staining, respectively. Characterization of this mouse line was completed by using different approaches.

At the 6w time point, we could only observe a thinner GBM in the TEM micrographs and we couldn't detect any other abnormalities in KO mice compared with WT controls. We think, 6w is an early time point for development of a glomerular phenotype especially if

the deleted gene is a potential modifier of GBM constituents. However, we could still observe a subtle effect of P3H2 on GBM. At 28w time point, we could still observe the same finding as in 6w with a thinner GBM in KO mice indicating a TBMN phenotype. On the other hand, microhematuria is a symptom for TBMN as well. To support our findings in TEM micrographs, we checked microhematuria in *P3h2*$^{\Delta Pod}$ mice. Both dipstick and counting RBCs showed that KO mice had significantly higher urinary RBC numbers than WT controls. The counted RBCs were in the expected range of microhematuria [109]. With the findings from 6w and 28w, we could speculate that our mice might have a thin basement membrane nephropathy since thinner GBM and microhematuria are the hallmark symptoms for this disease.

At 48w, we observed a progression and a severe phenotype in KO mice when compared with earlier time points. UACR measurement showed albuminuria. UACR measurement is one of the parameters to evaluate glomerular function. Presence of albumin above a certain level in urine indicates malfunction of the GFB. Under normal conditions, albumin virtually cannot pass through the filter and in urine, can only be detected at a very low concentration. However, if the GFB is damaged or disrupted, it becomes leaky and albumin can pass through the filter. Therefore, increased UACR is a sign of GFB damage. At 36w we detected first increase in urinary albumin in the UACR measurement which further increased at 48w indicating progressive damage of the GFB.

Moreover, we observed focal sclerosis and podocyte injury in PAS staining. Focal sclerosis is a histological feature of FSGS. The scoring of glomerulosclerosis showed that we have significantly more sclerosis in glomeruli but still also have many healthy glomeruli which correlates with the modest level of albuminuria being clearly below the nephrotic range. On the other hand, we also observed few glomeruloscleroses in our WT controls which is expected given that mice were 48w old. In addition, there was variation between mice regarding number and level of glomerulosclerosis. Unfortunately, the tissues could not be collected from exactly the same part of the kidney. It is known that glomerular damage is different between different regions within the kidney. This might explain additional variation within the same groups of mice.

TEM analyses showed FPE, thickened GBM and Bowman's capsule at 48w. FPE is indicating podocyte damage and thickened GBM as well as Bowman's capsules were the result of sclerosis. In contrast to earlier time points we observed increased GBM thickness at 48w. Sclerosis could be one reason of increased GBM thickness. It could well be that sclerosis overrode the GBM phenotype that we observed at earlier time points.

Mammalian target of rapamycin complex 1 (mTORC1) signaling is important for podocytes survival and growth. Its upregulation and downregulation can induce podocyte stress and induce development of glomerular disease. One downstream mediator of mTORC1 signaling is ribosomal protein phosho-S6 (Rb-pS6). This protein has a role in the synthesis of new proteins. Overactivity of mTORC1 signaling in podocytes has been observed in many kidney diseases such as diabetic nephropathy, FSGS, and fibrotic glomerular disease. It is thought as a common stress pathway for podocytes and its overactivity causes podocyte hypertrophy [110]. In our findings, podocyte loss and podocyte hypertrophy were found in podometrics analysis and was corroborated by a positive marker (Rb-pS6) for podocyte hypertrophy in IF staining of KO mice glomeruli. We could also detect a certain level of podocyte hypertrophy in WT controls at 48w. It is expected to detect podocyte hypertrophy at this age of mice since podocyte loss and hypertrophy is a known phenomenon during normal ageing.

PEC activation can result in sclerotic glomerular lesions. To this end, activated PECs are migrating to the glomerular tuft and start sclerosis formation in glomeruli. There are many known factors and pathways involved in this process but several parts of this process are still only poorly understood preventing establishment of a complete pathophysiological concept. PEC activation is a common finding in other kidney diseases since sclerosis formation is a common pathophysiological trait [111]. In our project, we detected activated PECs in glomeruli of *P3h2*$^{\Delta Pod}$ mice at 48w. This finding shows that the common sclerosis mechanism had been activated in *P3h2*$^{\Delta Pod}$ mice.

If thinking of a filter the GBM is perhaps the most important part of the GFB. Its functional and structural importance was been further understood in recent years even though there are still many questions needed to be answered [112]. Compression of GBM is a vital process which needs to be maintained for GFB homeostasis. If its compression is not

maintained to the same level, GFB would be disrupted and induce glomerular damage. Our findings are also underlining the importance of GBM. A Col4 modifier could induce a glomerular phenotype and over time this phenotype followed a common pathologic process inducing FSGS development. Unfortunately, we were not able to evaluate our line for longer time because of animal welfare but we think at later stages of life, our mice could end up with ESKD since a progressive disease had been observed between 28w and 48w. Absence of a GBM modifier is able to disrupt GFB homeostasis. Albuminuria and microhematuria of *P3h2*$^{\Delta Pod}$ mice indicated damage of the GFB. Under normal conditions, macromolecules and cells cannot pass through the filter. However, when GFB homeostasis is disrupted, it can become leaky and cannot filtrate properly. We could show both albumin and cells in urine indicating disruption of GFB and its homeostasis.

When we compare the patient phenotype with *P3h2*$^{\Delta Pod}$ mice phenotype, they both had FSGS. However, the patient was quite young when she was diagnosed with FSGS and the *P3h2*$^{\Delta Pod}$ mice line developed FSGS phenotype only around 48w old. 48w old mice equals at least 30 years in humans. There might be several explanations for these differences in timeline during development of this FSGS phenotype. First of all, P3H2 is a modifier of Col4 and its effect on GBM might be compensated by other enzymes or pathways differently in human and mice. Different species have different metabolism and also different gene expression signatures. Therefore, the consequence of the same gene deletion might be different on a longitudinal axis. Another point is that it is known that environmental and genetic factors influence the effect of gene mutations. We have only limited information about the patient and with additional mutations or environmental factors being present the *P3H2* gene mutation might have caused a faster progression of the kidney phenotype. Last point is the genetic background of *P3h2*$^{\Delta Pod}$ mice. Our mice were on a C57BL/6 background and it is known that this background is quite resistant for development of GBM related diseases [113]. This might have contributed to a delayed phenotype in KO mice.

Comparison of *P3H2* KO human podocyte cell line findings with *P3h2*$^{\Delta Pod}$ mice findings indicated that they are supporting each other. We observed an elevated adhesion capacity in KO cell lines and podocyte detachment was observed in KO mice. Moreover,

ECM and GBM proteomics data show that Col4 sub-chains and its interactors, Col18α1 in ECM and nidogens are downregulated in both extracellular matrixes.

4.4 Potential advantages of *P3h2*$^{\Delta Pod}$ mice line

The generated podocyte specific *P3h2*$^{\Delta Pod}$ mice line might be a good model for better understanding of Col4 nephropathies. As we observed in our model, there can be development of FSGS in TBMN patients over their life time [76]. The mechanism behind this progress is not known. There are several findings which could point to candidate pathways. ER stress and UPR are strong candidate pathways that might cause FSGS development. Further characterization of this line might give us a chance to identify new pathways or describe in more detail the candidate pathways for better understanding of Col4 nephropathies.

We could show for the first time the effect of a modulator on GBM and glomerular homeostasis. The phenotype that we observed in this mouse line has in some aspects also been observed in other metabolic kidney diseases such as diabetic nephropathy or hypertension. *P3H2* might have roles in development or progression of these diseases as well. Therefore, *P3h2*$^{\Delta Pod}$ mice could serve as a model for different kinds of metabolic kidney diseases. In addition, combination of a metabolic disease model and our mouse model would be beneficial for investigating the glomerular pathology of the *P3H2* deletion.

4.5 Future perspective

In this project, we aimed to investigate the effect of *P3H2* deletion on GBM and glomerular homeostasis. Our findings showed that P3H2 induces GBM abnormalities such as local thinning and thickening and these abnormalities lead to podocyte injury. Our findings are supportive of a TBMN phenotype which in later stages progresses into a FSGS phenotype. We would like to understand the mechanisms driving the *P3h2*$^{\Delta Pod}$ mice phenotype in the second part of the project. We envisioned several approaches to delineate the disease mechanism induced by deletion of *P3H2*.

Firstly, as mentioned earlier, ER stress and UPR activation are pathways inducing podocyte injury in Col4 nephropathies. Therefore, we will examine this mechanism in

podocytes. In addition, quantitative cell proteomics can help us to identify ER stress. On the other hand, we are currently probing biobanks for expression of P3H2 in several different metabolic kidney disease entities. One challenge is to recruit enough samples of the same stage of disease. Lastly, we would like to apply a stress model to our mice to observe whether speed of podocyte injury and glomerular damage accelerates the observed disease phenotype. We plan to apply a hypertension stress model. The DOCA high salt model is one of the best established models for hypertension based on increased renin-angiotensin signaling pathway [114].

In conclusion, in our project we showed the effect of *P3H2* deletion on the GBM and GFB homeostasis. We could show that the absence of P3H2 protein changes the abundance of Col4 both in ECM of a *P3H2* human KO podocyte cell line and GBM of *P3h2*$^{\Delta Pod}$ mice. Absence of P3H2, a GBM modifier causes a TBMN phenotype in mice but by the time with progression it turned to an FSGS phenotype. It is the first time we showed that a GBM modifier can disrupt GFB homeostasis and induce a kidney phenotype. Further investigation is necessary for a better understanding of the mechanism that driven to TBMN and FSGS phenotype.

5 Summary

GFB is the decisive filter to generate primary urine. It is composed of a fenestrated endothelium, GBM, podocytes and SD. Secreted proteins (Col4, LM-521, nidogen, and agrin) from GECs and podocytes generate the meshwork structure of the GBM. It works as a scaffold to support these two cells and provides cellular cross-talk to keep the dynamic structure of the GFB in homeostasis. Disruption of the GFB leads to proteinuria and microhematuria.

A *P3H2* gene mutation was identified in a nephrotic syndrome patient cohort by using an expression-based candidate gene approach. P3H2 encodes Prolyl 3-Hydroxylase 2 (P3H2), a post-translational Col4 modifier that hydroxylases the 3' of prolines in Col4 sub-chains in the ER. P3H2's relevance for glomerular homeostasis is unknown. Therefore, we aimed to investigate its effect on GBM and GFB homeostasis. We generated *P3h2*$^{\Delta Pod}$ mice line and *P3H2* KO immortalized human podocyte cell lines. Characterization of these mice revealed that the absence of P3H2 in podocytes induces TBMN phenotype with thinner GBM than wild type mice and the development of microhematuria and microalbuminuria over time. Sclerosis in glomeruli, podocyte loss and podocyte hypertrophy were observed at 48w of age in KO mice. There was FSGS development in *P3h2*$^{\Delta Pod}$ mice over time. ECM and GBM proteomics of P3H2 KO cell lines and mice indicated a disrupted in the regulation of Col4 sub-chains and its interaction partners (Col18α1 and nidogens).

In conclusion, P3H2 is the first identified GBM modulator causing TBMN phenotype in mice and inducing FSGS over time. P3H2 might affect proper Col4 biosynthesis or stability explaining the observed phenotype on a molecular level.

6 Zusammenfassung

Die GFB ist der entscheidende Filter zur Erzeugung von Primärurin. Sie besteht aus einem fenestrierten Endothel, GBM, Podozyten und der SD. Sezernierte Proteine (Col4, LM-521, Nidogen und Agrin) aus GECs und Podozyten erzeugen die Netzstruktur der GBM. Sie fungiert als Gerüst zur Unterstützung dieser beiden Zelltypen und vermittelt zellulären Crosstalk, um die dynamische Struktur der GFB in der Homöostase zu halten. Eine Störung der GFB führt zu Proteinurie und Mikrohämaturie.

Eine P3H2-Genmutation wurde in einer Patientenkohorte mit nephrotischem Syndrom unter Verwendung eines expressions-basierten Kandidatengenansatzes identifiziert. P3H2 codiert Prolyl-3-Hydroxylase 2 (P3H2), einen posttranslationalen Col4 modifikator, der die 3'-Proline in Col4-Subketten im endoplasmatischen Retikulum hydroxyliert. Die Relevanz von P3H2 für die glomeruläre Homöostase ist unbekannt. Daher wollten wir die Auswirkungen auf die GBM- und GFB-Homöostase untersuchen. Wir erzeugten eine *P3h2*$^{\Delta Pod}$-Mauslinie und P3H2-KO-immortalisierte menschliche Podozytenzelllinien. Die Charakterisierung dieser Mäuse ergab, dass das Fehlen von P3H2 in Podozyten einen progressiven Phänotyp der dünnen Basalmembran-Nephropathie (TBMN) mit dünnerem GBM als bei Wildtyp-Mäusen und die Entwicklung von Mikrohämaturie und Mikroalbuminurie im Laufe der Zeit induziert. Sklerose von Glomeruli, Podozytenverlust und Podozytenhypertrophie wurden im Alter von 48 W von KO-Mäusen beobachtet. Im Laufe der Zeit gab es eine FSGS-Entwicklung bei *P3h2*$^{\Delta Pod}$-Mäusen. Die ECM- und GBM-Proteomik von *P3H2*-KO-Zelllinien und -Mäusen zeigte eine gestörte Regulation der Col4-Subketten und ihrer Interaktionspartner (Col18α1 und nidogene).

Zusammenfassend ist P3H2 der erste identifizierte GBM-Modulator, der bei Mäusen einen TBMN-Phänotyp verursacht und im Laufe der Zeit FSGS induziert. P3H2 könnte die ordnungsgemäße Col4-Biosynthese oder -Stabilität beeinflussen und den beobachteten Phänotyp auf molekularer Ebene erklären.

7 List of abbreviations

3Hyp	3’ hydroxylation
4Hyp	4’ hydroxylation
AA	afferent arteriole
ACE	angiotensin-converting enzyme
AFOG	acid Fuchsin Orange G
ANCA	anti-neutrophil cytoplasm antibodies
aPCV	average podocyte cell volume
APS	ammonium persulfate
Arg	arginine
AS	Alport syndrome
ATF6	activating transcription factor 6
BiP	binding immunoglobin protein
bp	base-pair
BSA	Bovine serum albumin
C	cytosine
CD	collecting duct
CD2AP	CD2 Associated Protein
cDNA	complementary DNA
CGN	crescentic glomerulonephritis
CKD	chronic kidney disease
Col II	collagenase II
Col V	collagenase V
Col4	collagen 4
CRISPR	clustered regularly interspaced short palindromic repeats
DDR1	Discoidin domain receptor tyrosine kinase 1
DE	detection enzyme
DMSO	dimethyl sulfoxide
dsDNA	double-stranded DNA
DT	distal tubules
DTT	dithiothreitol
ECL	enhanced chemiluminescence
ECM	extracellular matrix
ELISA	enzyme-linked immunosorbent assay
ER	Endoplasmic reticulum
ES	embryonic stem
ESKD	end-stage kidney disease
FA	focal adhesion

FAK	focal adhesion kinase
FBS	fetal bovine albumin
FP	foot processes
FPE	foot process effacement
FPW	foot process width
FSGS	focal segmental glomerulosclerosis
GAG	glycosaminoglycan
GBM	glomerular basement membrane
gDNA	genomic DNA
GEC	glomerular endothelial cell
GFB	glomerular Filtration Barrier
GFR	glomerular filtration rate
GN	glomerulonephritis
GO	Gene Ontology
gRNA	guide RNA
H&E	hematoxylin and eosin
HCC	hepatocellular carcinoma
HRP	horseradish peroxidase
HSP	heparan sulfate proteoglycan
IF	immunofluorescence
IQR	interquartile range
IRE1	Inositol-requiring enzyme 1
ISH	In situ hybridization
ITS	Insulin Selenite Transferrin
KO	knock-out
KTx	kidney transplantation
LM-521	laminin-521
LOH	loop of Henle
MC	mesangial cell
MEM	minimum essential medium
MET	methenamine Silver
MMP	matrix metalloproteinases
mTORC1	mammalian target of rapamycin complex 1
NC1	non-collagenous
NGS	next generation sequencing
ns	not significant
NS	nephrotic syndrome
OCT	optimal cutting temperature embedding medium
OFP	orange fluorescence protein

OsO4	osmium tetroxide
P/S	Penicillin/Streptavidin
P3H2	prolyl 3-hydroxylase 2
PAS	periodic acid–schiff
PB	phosphate buffer
PCA	principal component analysis
PCR	polymerase chain reaction
PD	podocyte density
PEC	parietal epithelial cell
PERK	protein kinase RNA-like ER kinase
PN	podocyte number
Pod	podocyte
PT	proximal tubules
PTM	post-translational modifier
qPCR	quantitative PCR
RBC	red blood cell
Rb-pS6	phosphorylated ribosomal protein S6
SD	slit diaphragm
SRNS	steroid resistance nephrotic syndrome
SSNS	steroid-sensitive nephrotic syndrome
SYNPO	synaptopodin
T	thymidine
TAE	Tris-acetate EDTA
TBMN	thin basement membrane nephropathy
TEM	transmission electron microscopy
TEMED	tetramethylethylenediamine
TIMP	tissue inhibitors of metalloproteinase
TPCV	total podocyte cell volume
TPR	tetratricopeptide repeat
TRPC6	transient receptor potential cation channel subfamily C member 6
UACR	urine albumin creatinine ratio
UPR	unfolded protein response
WB	western blot

List of Figures

List of Tables

8 References

1. Scott RP, Quaggin SE. The cell biology of renal filtration. *J Cell Biol*. 2015. doi:10.1083/jcb.201410017
2. Puelles VG, Hoy WE, Hughson MD, Diouf B, Douglas-Denton RN, Bertram JF. Glomerular number and size variability and risk for kidney disease. *Curr Opin Nephrol Hypertens*. 2011. doi:10.1097/MNH.0b013e3283410a7d
3. Christensen EI, Rennke HG, Carone FA. Renal tubular uptake of protein: Effect of molecular charge. *Am J Physiol - Ren Fluid Electrolyte Physiol*. 1983. doi:10.1152/ajprenal.1983.244.4.f436
4. Suki WN. Calcium transport in the nephron. *Am J Physiol*. 1979. doi:10.1152/ajprenal.1979.237.1.f1
5. Richard Kitching A, Hutton HL. The players: Cells involved in glomerular disease. *Clin J Am Soc Nephrol*. 2016. doi:10.2215/CJN.13791215
6. Hackl MJ, Burford JL, Villanueva K, et al. Tracking the fate of glomerular epithelial cells in vivo using serial multiphoton imaging in new mouse models with fluorescent lineage tags. *Nat Med*. 2013. doi:10.1038/nm.3405
7. Moeller MJ, Smeets B. Role of parietal epithelial cells in kidney injury: The case of rapidly progressing glomerulonephritis and focal and segmental glomerulosclerosis. *Nephron - Exp Nephrol*. 2014. doi:10.1159/000360677
8. Takano K, Kawasaki Y, Imaizumi T, et al. Development of glomerular endothelial cells, podocytes and mesangial cells in the human fetus and infant. *Tohoku J Exp Med*. 2007. doi:10.1620/tjem.212.81
9. Abboud HE. Mesangial cell biology. *Exp Cell Res*. 2012. doi:10.1016/j.yexcr.2012.02.025
10. Schlöndorff D, Banas B. The mesangial cell revisited: No cell is an island. *J Am Soc Nephrol*. 2009. doi:10.1681/ASN.2008050549
11. Masson E, Lagarde M, Wiernsperger N, El Bawab S. Hyperglycemia and glucosamine-induced mesangial cell cycle arrest and hypertrophy: Common or independent mechanisms? *IUBMB Life*. 2006. doi:10.1080/15216540600755980
12. Lennon R, Hosawi S. Glomerular cell crosstalk. *Curr Opin Nephrol Hypertens*. 2016. doi:10.1097/MNH.0000000000000221
13. Thomson SC, Blantz RC. A new role for charge of the glomerular capillary membrane. *J Am Soc Nephrol*. 2010. doi:10.1681/ASN.2010101089
14. Peti-Peterdi J, Sipos A. A high-powered view of the filtration barrier. *J Am Soc Nephrol*. 2010. doi:10.1681/ASN.2010040378
15. Deen WM, Bridges CR, Brenner BM, Myers BD. Heteroporous model of glomerular size selectivity: Application to normal and nephrotic humans. *Am J Physiol - Ren Fluid Electrolyte Physiol*. 1985. doi:10.1152/ajprenal.1985.249.3.f374
16. Ryan GB, Karnovsky MJ. Distribution of endogenous albumin in the rat glomerulus: role of hemodynamic factors in glomerular barrier function. *Kidney Int*. 1976. doi:10.1038/ki.1976.5
17. Hausmann R, Kuppe C, Egger H, et al. Electrical forces determine glomerular permeability.

J Am Soc Nephrol. 2010. doi:10.1681/ASN.2010030303

18. Fissell WH, Miner JH. What is the glomerular ultrafiltration barrier? *J Am Soc Nephrol*. 2018. doi:10.1681/ASN.2018050490
19. Salmon AH, Satchell SC. Endothelial glycocalyx dysfunction in disease: Albuminuria and increased microvascular permeability. *J Pathol*. 2012. doi:10.1002/path.3964
20. Levick JR, Smaje LH. An analysis of the permeability of a fenestra. *Microvasc Res*. 1987. doi:10.1016/0026-2862(87)90020-3
21. Sarin H. Physiologic upper limits of pore size of different blood capillary types and another perspective on the dual pore theory of microvascular permeability. *J Angiogenes Res*. 2010. doi:10.1186/2040-2384-2-14
22. Curry FE, Adamson RH. Endothelial glycocalyx: Permeability barrier and mechanosensor. *Ann Biomed Eng*. 2012. doi:10.1007/s10439-011-0429-8
23. Gottlieb RA. *Autophagy in Health and Disease*.; 2013. doi:10.1016/C2010-0-66523-0
24. Grahammer F. New structural insights into podocyte biology. *Cell Tissue Res*. 2017. doi:10.1007/s00441-017-2590-3
25. Ichimura K, Kurihara H, Sakai T. Actin Filament Organization of Foot Processes in Rat Podocytes. *J Histochem Cytochem*. 2003. doi:10.1177/002215540305101203
26. Schell C, Huber TB. The evolving complexity of the podocyte cytoskeleton. *J Am Soc Nephrol*. 2017. doi:10.1681/ASN.2017020143
27. Schell C, Rogg M, Suhm M, et al. The FERM protein EPB41L5 regulates actomyosin contractility and focal adhesion formation to maintain the kidney filtration barrier. *Proc Natl Acad Sci U S A*. 2017. doi:10.1073/pnas.1617004114
28. Michael KE, Dumbauld DW, Burns KL, Hanks SK, García AJ. Focal adhesion kinase modulates cell adhesion strengthening via integrin activation. *Mol Biol Cell*. 2009. doi:10.1091/mbc.E08-01-0076
29. Wharram BL, Goyal M, Wiggins JE, et al. Podocyte depletion causes glomerulosclerosis: Diphtheria toxin-induced podocyte depletion in rats expressing human diphtheria toxin receptor transgene. *J Am Soc Nephrol*. 2005. doi:10.1681/ASN.2005010055
30. Grahammer F, Wigge C, Schell C, et al. A flexible, multilayered protein scaffold maintains the slit in between glomerular podocytes. *JCI Insight*. 2016. doi:10.1172/jci.insight.86177
31. Kestilä M, Lenkkeri U, Männikkö M, et al. Positionally cloned gene for a novel glomerular protein - Nephrin - Is mutated in congenital nephrotic syndrome. *Mol Cell*. 1998. doi:10.1016/S1097-2765(00)80057-X
32. Ruotsalainen V, Ljungberg P, Wartiovaara J, et al. Nephrin is specifically located at the slit diaphragm of glomerular podocytes. *Proc Natl Acad Sci U S A*. 1999. doi:10.1073/pnas.96.14.7962
33. Gerke P, Huber TB, Sellin L, Benzing T, Walz G. Homodimerization and heterodimerization of the glomerular podocyte proteins nephrin and NEPH1. *J Am Soc Nephrol*. 2003. doi:10.1097/01.ASN.0000057853.05686.89
34. Solanki AK, Widmeier E, Arif E, et al. Mutations in KIRREL1, a slit diaphragm component, cause steroid-resistant nephrotic syndrome. *Kidney Int*. 2019. doi:10.1016/j.kint.2019.06.016

35. Boute N, Gribouval O, Roselli S, et al. NPHS2, encoding the glomerular protein podocin, is mutated in autosomal recessive steroid-resistant nephrotic syndrome. *Nat Genet*. 2000. doi:10.1038/74166

36. Huber TB, Schermer B, Benzing T. Podocin organizes ion channel-lipid supercomplexes: Implications for mechanosensation at the slit diaphragm. *Nephron - Exp Nephrol*. 2007. doi:10.1159/000101789

37. Tossidou I, Teng B, Worthmann K, et al. Tyrosine phosphorylation of cd2ap affects stability of the slit diaphragm complex. *J Am Soc Nephrol*. 2019. doi:10.1681/ASN.2018080860

38. Shih NY, Li J, Karpitskii V, et al. Congenital nephrotic syndrome in mice lacking CD2-associated protein. *Science (80-)*. 1999. doi:10.1126/science.286.5438.312

39. Shankland SJ. The podocyte's response to injury: Role in proteinuria and glomerulosclerosis. *Kidney Int*. 2006. doi:10.1038/sj.ki.5000410

40. Tryggvason K, Pettersson E. Causes and consequences of proteinuria: The kidney filtration barrier and progressive renal failure. *J Intern Med*. 2003. doi:10.1046/j.1365-2796.2003.01207.x

41. Byron A, Randles MJ, Humphries JD, et al. Glomerular cell cross-talk influences composition and assembly of extracellular matrix. *J Am Soc Nephrol*. 2014. doi:10.1681/ASN.2013070795

42. Suleiman H, Zhang L, Roth R, et al. Nanoscale protein architecture of the kidney glomerular basement membrane. *Elife*. 2013. doi:10.7554/elife.01149

43. Zenker M, Tralau T, Lennert T, et al. Congenital nephrosis, mesangial sclerosis, and distinct eye abnormalities with microcoria: An autosomal recessive syndrome. *Am J Med Genet*. 2004. doi:10.1002/ajmg.a.30310

44. Hasselbacher K, Wiggins RC, Matejas V, et al. Recessive missense mutations in LAMB2 expand the clinical spectrum of LAMB2-associated disorders. *Kidney Int*. 2006. doi:10.1038/sj.ki.5001679

45. Jarad G, Cunningham J, Shaw AS, Miner JH. Proteinuria precedes podocyte abnormalities in Lamb2-/- mice, implicating the glomerular basement membrane as an albumin barrier. *J Clin Invest*. 2006. doi:10.1172/JCI28414

46. Kohfeldt E, Sasaki T, Göhring W, Timpl R. Nidogen-2: A new basement membrane protein with diverse binding properties. *J Mol Biol*. 1998. doi:10.1006/jmbi.1998.2004

47. Salmivirta K, Talts JF, Olsson M, Sasaki T, Timpl R, Ekblom P. Binding of mouse nidogen-2 to basement membrane components and cells and its expression in embryonic and adult tissues suggest complementary functions of the two nidogens. *Exp Cell Res*. 2002. doi:10.1006/excr.2002.5611

48. Bader BL, Smyth N, Nedbal S, et al. Compound Genetic Ablation of Nidogen 1 and 2 Causes Basement Membrane Defects and Perinatal Lethality in Mice. *Mol Cell Biol*. 2005. doi:10.1128/mcb.25.15.6846-6856.2005

49. Groffen AJA, Veerkamp JH, Monnens LAH, Van Den Heuvel LPWJ. Recent insights into the structure and functions of heparan sulfate proteoglycans in the human glomerular basement membrane. *Nephrol Dial Transplant*. 1999. doi:10.1093/ndt/14.9.2119

50. Harvey SJ, Jarad G, Cunningham J, et al. Disruption of glomerular basement membrane charge through podocyte-specific mutation of agrin does not alter glomerular permselectivity. *Am J Pathol*. 2007. doi:10.2353/ajpath.2007.061116

51. Catania JM, Chen G, Parrish AR. Role of matrix metalloproteinases in renal pathophysiologies. *Am J Physiol - Ren Physiol*. 2007. doi:10.1152/ajprenal.00421.2006

52. Brew K, Nagase H. The tissue inhibitors of metalloproteinases (TIMPs): An ancient family with structural and functional diversity. *Biochim Biophys Acta - Mol Cell Res*. 2010. doi:10.1016/j.bbamcr.2010.01.003

53. Tveita AA, Rekvig OP, Zykova SN. Glomerular matrix metalloproteinases and their regulators in the pathogenesis of lupus nephritis. *Arthritis Res Ther*. 2008. doi:10.1186/ar2532

54. Kalluri R, Shield CF, Todd P, Hudson BG, Neilson EG. Isoform switching of type IV collagen is developmentally arrested in X- linked Aport syndrome leading to increased susceptibility of renal basement membranes to endoproteolysis. *J Clin Invest*. 1997. doi:10.1172/JCI119431

55. Khoshnoodi J, Pedchenko V, Hudson BG. Mammalian collagen IV. *Microsc Res Tech*. 2008. doi:10.1002/jemt.20564

56. Vandenberg P, Kern A, Ries A, Luckenbill-Edds L, Mann K, Kuhn K. Characterization of a type IV collagen major cell binding site with affinity to the α1β1 and the α2β1 integrins. *J Cell Biol*. 1991. doi:10.1083/jcb.113.6.1475

57. Hudson BG, Tryggvason K, Sundaramoorthy M, Neilson EG. Alport's syndrome, Goodpasture's syndrome, and type IV collagen. *N Engl J Med*. 2003. doi:10.1056/NEJMra022296

58. Cosgrove D, Liu S. Collagen IV diseases: A focus on the glomerular basement membrane in Alport syndrome. *Matrix Biol*. 2017. doi:10.1016/j.matbio.2016.08.005

59. Myllyharju J, Kivirikko KI. Collagens, modifying enzymes and their mutations in humans, flies and worms. *Trends Genet*. 2004. doi:10.1016/j.tig.2003.11.004

60. Humphries JD, Byron A, Humphries MJ. Integrin ligands at a glance. *J Cell Sci*. 2006. doi:10.1242/jcs.03098

61. Pozzi A, Jarad G, Moeckel GW, et al. β1 integrin expression by podocytes is required to maintain glomerular structural integrity. *Dev Biol*. 2008. doi:10.1016/j.ydbio.2008.01.022

62. Has C, Spartà G, Kiritsi D, et al. Integrin α3 mutations with kidney, lung, and skin disease. *N Engl J Med*. 2012. doi:10.1056/NEJMoa1110813

63. Carafoli F, Mayer MC, Shiraishi K, et al. Structure of the discoidin domain receptor 1 extracellular region bound to an inhibitory Fab fragment reveals features important for signaling. *Structure*. 2012. doi:10.1016/j.str.2012.02.011

64. Gross O, Beirowski B, Harvey SJ, et al. DDR1-deficient mice show localized subepithelial GBM thickening with focal loss of slit diaphragms and proteinuria. *Kidney Int*. 2004. doi:10.1111/j.1523-1755.2004.00712.x

65. Eddy AA, Symons JM. Nephrotic syndrome in childhood. In: *Lancet*. ; 2003. doi:10.1016/S0140-6736(03)14184-0

66. Lombel RM, Gipson DS, Hodson EM. Treatment of steroid-sensitive nephrotic syndrome: New guidelines from KDIGO. *Pediatr Nephrol*. 2013. doi:10.1007/s00467-012-2310-x

67. Kari JA, Montini G, Bockenhauer D, et al. Clinico-pathological correlations of congenital and infantile nephrotic syndrome over twenty years. *Pediatr Nephrol*. 2014. doi:10.1007/s00467-014-2856-x

68. Bagga A, Gulati A, Gulati S, Mehta KP, Vijayakumar M. Management of steroid resistant nephrotic syndrome. *Indian Pediatr*. 2009. doi:10.15406/unoaj.2017.05.00159

69. Hall G, Gbadegesin RA. Translating genetic findings in hereditary nephrotic syndrome: The missing loops. *Am J Physiol - Ren Physiol*. 2015. doi:10.1152/ajprenal.00683.2014

70. Gross O, Beirowski B, Koepke ML, et al. Preemptive ramipril therapy delays renal failure and reduces renal fibrosis in COL4A3-knockout mice with Alport syndrome. *Kidney Int*. 2003. doi:10.1046/j.1523-1755.2003.00779.x

71. Savige J, Rana K, Tonna S, Buzza M, Dagher H, Wang YY. Thin basement membrane nephropathy. *Kidney Int*. 2003. doi:10.1046/j.1523-1755.2003.00234.x

72. Dische FE, Weston MJ, Parsons V. Abnormally thin glomerular basement membranes associated with hematuria, proteinuria or renal failure in adults. *Am J Nephrol*. 1985. doi:10.1159/000166914

73. Nieuwhof CMG, De Heer F, De Leeuw P, Van Breda Viriesman PJC. Thin GBM nephropathy: Premature glomerular obsolescence is associated with hypertension and late onset renal failure. *Kidney Int*. 1997. doi:10.1038/ki.1997.219

74. Nogueira M, Cartwright J, Horn K, et al. Thin basement membrane disease with heavy proteinuria or nephrotic syndrome at presentation. *Am J Kidney Dis*. 2000. doi:10.1016/s0272-6386(00)70033-3

75. Vivante A, Afek A, Frenkel-Nir Y, et al. Persistent asymptomatic isolated microscopic hematuria in Israeli adolescents and young adults and risk for end-stage renal disease. *JAMA - J Am Med Assoc*. 2011. doi:10.1001/jama.2011.1141

76. Deltas C, Savva I, Voskarides K, Papazachariou L, Pierides A. Carriers of Autosomal Recessive Alport Syndrome with Thin Basement Membrane Nephropathy Presenting as Focal Segmental Glomerulosclerosis in Later Life. *Nephron*. 2015. doi:10.1159/000435789

77. Pieri M, Stefanou C, Zaravinos A, et al. Evidence for activation of the unfolded protein response in collagen iv nephropathies. *J Am Soc Nephrol*. 2014. doi:10.1681/ASN.2012121217

78. Pokidysheva E, Boudko S, Vranka J, et al. Biological role of prolyl 3-hydroxylation in type IV collagen. *Proc Natl Acad Sci U S A*. 2014. doi:10.1073/pnas.1307597111

79. Tiainen PI, Pasanen A, Sormunen R, Myllyharju J. Characterization of recombinant human prolyl 3-hydroxylase isoenzyme 2, an enzyme modifying the basement membrane collagen IV. *J Biol Chem*. 2008. doi:10.1074/jbc.M802973200

80. Järnum S, Kjellman C, Darabi A, Nilsson I, Edvardsen K, Åman P. LEPREL1, a novel ER and Golgi resident member of the Leprecan family. *Biochem Biophys Res Commun*. 2004. doi:10.1016/j.bbrc.2004.03.060

81. Fernandes RJ, Farnand AW, Traeger GR, Weis MA, Eyre DR. A role for prolyl 3-hydroxylase 2 in post-translational modification of fibril-forming collagens. *J Biol Chem*. 2011. doi:10.1074/jbc.M111.267906

82. Guo H, Tong P, Peng Y, et al. Homozygous loss-of-function mutation of the LEPREL1 gene causes severe non-syndromic high myopia with early-onset cataract. *Clin Genet*. 2014. doi:10.1111/cge.12309

83. Wang J, Xu X, Liu Z, et al. LEPREL1 expression in human hepatocellular carcinoma and its suppressor role on cell proliferation. *Gastroenterol Res Pract*. 2013. doi:10.1155/2013/109759

84. Lauer M, Scruggs B, Chen S, Wassenhove-McCarthy D, McCarthy KJ. Leprecan distribution in the developing and adult kidney. *Kidney Int*. 2007. doi:10.1038/sj.ki.5002269

85. Saleem MA, O'Hare MJ, Reiser J, et al. A conditionally immortalized human podocyte cell line demonstrating nephrin and podocin expression. *J Am Soc Nephrol*. 2002.

86. Häggman HM, Ryynänen LA, Aronen TS, Krajnakova J. Cryopreservation of embryogenic cultures of Scots pine. *Plant Cell Tissue Organ Cult*. 1998. doi:10.1023/A:1006104325426

87. Ferre F. Quantitative or semi-quantitative PCR: Reality versus myth. *Genome Res*. 1992. doi:10.1101/gr.2.1.1

88. Moritz CP. 40 years Western blotting: A scientific birthday toast. *J Proteomics*. 2020. doi:10.1016/j.jprot.2019.103575

89. Zhang F, Wen Y, Guo X. CRISPR/Cas9 for genome editing: Progress, implications and challenges. *Hum Mol Genet*. 2014. doi:10.1093/hmg/ddu125

90. Sielaff M, Kuharev J, Bohn T, et al. Evaluation of FASP, SP3, and iST Protocols for Proteomic Sample Preparation in the Low Microgram Range. *J Proteome Res*. 2017. doi:10.1021/acs.jproteome.7b00433

91. Puelles VG, Van Der Wolde JW, Wanner N, et al. MTOR-mediated podocyte hypertrophy regulates glomerular integrity in mice and humans. *JCI Insight*. 2019. doi:10.1172/jci.insight.99271

92. Brinkkoetter PT, Bork T, Salou S, et al. Anaerobic Glycolysis Maintains the Glomerular Filtration Barrier Independent of Mitochondrial Metabolism and Dynamics. *Cell Rep*. 2019. doi:10.1016/j.celrep.2019.04.012

93. Bechtel W, Helmstädter M, Balica J, et al. Vps34 deficiency reveals the importance of endocytosis for podocyte homeostasis. *J Am Soc Nephrol*. 2013. doi:10.1681/ASN.2012070700

94. Lennon R, Byron A, Humphries JD, et al. Global analysis reveals the complexity of the human glomerular extracellular matrix. *J Am Soc Nephrol*. 2014. doi:10.1681/ASN.2013030233

95. Assady S, Wanner N, Skorecki KL, Huber TB. New insights into podocyte biology in glomerular health and disease. *J Am Soc Nephrol*. 2017. doi:10.1681/ASN.2017010027

96. Mordechai S, Gradstein L, Pasanen A, et al. High myopia caused by a mutation in LEPREL1, encoding prolyl 3-hydroxylase 2. *Am J Hum Genet*. 2011. doi:10.1016/j.ajhg.2011.08.003

97. Rappu P, Salo AM, Myllyharju J, Heino J. Role of prolyl hydroxylation in the molecular interactions of collagens. *Essays Biochem*. 2019. doi:10.1042/EBC20180053

98. Hudson DM, Eyre DR. Collagen prolyl 3-hydroxylation: A major role for a minor post-translational modification? *Connect Tissue Res*. 2013. doi:10.3109/03008207.2013.800867

99. Montgomery NT, Zientek KD, Pokidysheva EN, Bächinger HP. Post-translational modification of type IV collagen with 3-hydroxyproline affects its interactions with glycoprotein VI and nidogens 1 and 2. *J Biol Chem*. 2018. doi:10.1074/jbc.RA117.000406

100. Nagata M. Podocyte injury and its consequences. *Kidney Int*. 2016. doi:10.1016/j.kint.2016.01.012

101. Funk SD, Bayer RH, Miner JH. Endothelial cell-specific collagen type IV-α3 expression

does not rescue alport syndrome in col4a3-/- mice. *Am J Physiol - Ren Physiol*. 2019. doi:10.1152/ajprenal.00556.2018

102. Okabe M, Motojima M, Miyazaki Y, Pastan I, Yokoo T, Matsusaka T. Global polysome analysis of normal and injured podocytes. *Am J Physiol - Ren Physiol*. 2019. doi:10.1152/ajprenal.00115.2018

103. Delimont D, Dufek BM, Meehan DT, et al. Laminin α2-mediated focal adhesion kinase activation triggers Alport glomerular pathogenesis. *PLoS One*. 2014. doi:10.1371/journal.pone.0099083

104. Ma H, Togawa A, Soda K, et al. Inhibition of podocyte FAK protects against proteinuria and foot process effacement. *J Am Soc Nephrol*. 2010. doi:10.1681/ASN.2009090991

105. Park SJ, Kim Y, Chen YM. Endoplasmic reticulum stress and monogenic kidney diseases in precision nephrology. *Pediatr Nephrol*. 2019. doi:10.1007/s00467-018-4031-2

106. Endlich K, Kliewe F, Endlich N. Stressed podocytes—mechanical forces, sensors, signaling and response. *Pflugers Arch Eur J Physiol*. 2017. doi:10.1007/s00424-017-2025-8

107. Papazachariou L, Demosthenous P, Pieri M, et al. Frequency of COL4A3/COL4A4 Mutations amongst families segregating glomerular microscopic hematuria and evidence for activation of the unfolded protein response. Focal and segmental glomerulosclerosis is a frequent development during ageing. *PLoS One*. 2014. doi:10.1371/journal.pone.0115015

108. Gast C, Pengelly RJ, Lyon M, et al. Collagen (COL4A) mutations are the most frequent mutations underlying adult focal segmental glomerulosclerosis. *Nephrol Dial Transplant*. 2016. doi:10.1093/ndt/gfv325

109. Cohen RA, Brown RS. Microscopic hematuria. *N Engl J Med*. 2003. doi:10.1056/NEJMcp012694

110. Fantus D, Rogers NM, Grahammer F, Huber TB, Thomson AW. Roles of mTOR complexes in the kidney: Implications for renal disease and transplantation. *Nat Rev Nephrol*. 2016. doi:10.1038/nrneph.2016.108

111. Al Hussain T, Al Mana H, Hussein MH, Akhtar M. Podocyte and Parietal Epithelial Cell Interactions in Health and Disease. *Adv Anat Pathol*. 2017. doi:10.1097/PAP.0000000000000125

112. Chew C, Lennon R. Basement membrane defects in genetic kidney diseases. *Front Pediatr*. 2018. doi:10.3389/fped.2018.00011

113. Kang JS, Wang XP, Miner JH, et al. Loss of α3/α4(IV) collagen from the glomerular basement membrane induces a strain-dependent isoform switch to α5α6(IV) collagen associated with longer renal survival in Col4a3-/- Alport mice. *J Am Soc Nephrol*. 2006. doi:10.1681/ASN.2006020165

114. Basting T, Lazartigues E. DOCA-Salt Hypertension: an Update. *Curr Hypertens Rep*. 2017. doi:10.1007/s11906-017-0731-4

9 Acknowledgment

I would like to thank my supervisor Prof. Dr. med. Tobias B. Huber to give me the chance to do my doctoral study at Huber Laboratory. I would like to thank Prof. Dr. med. Tobias B. Huber and my advisor PD. Dr. med. Florian Grahammer for their guidance, encouragement, help and understanding during my doctoral study. I have learned a lot from their expertise and I feel very lucky to work with them.

I am grateful for having Prof. Dr. med. Christoph Schramm and Prof. Dr. med. Heimo Ehmke as my committee and for taking time out of their schedule on my behalf and for beneficial discussion and feedback sessions during my doctoral study.

In addition, I would like to thank all Huber Laboratory members of Hamburg and Freiburg to create a productive and efficient working environment.

I would like to acknowledge the FACS sorting core facility, Mass Spectrometric Proteomics core facility and EM facility of the UKE. I would like to thank PD Dr. Oliver Kretz for EM micrographs and Dr. Christoph Krisp for the quantitative proteomics analysis.

I would like to thank my friends for their support and patience. A special thank you to my friend Serkan Sayin for English proofreading of my thesis. Last but not least, I am really grateful for having such loving and supportive parents, Ahmet & Ayten Aypek; siblings, Gamze Aypek Yagiz and Tugce Aypek Adigüzel who have always been there whenever I need them.

10 Curriculum vitae

Lebenslauf wurde aus datenschutzrechtlichen Gründen entfernt.

11 Eidesstattliche Versicherung

Ich versichere ausdrücklich, dass ich die Arbeit selbständig und ohne fremde Hilfe verfasst, andere als die von mir angegebenen Quellen und Hilfsmittel nicht benutzt und die aus den benutzten Werken wörtlich oder inhaltlich entnommenen Stellen einzeln nach Ausgabe (Auflage und Jahr des Erscheinens), Band und Seite des benutzten Werkes kenntlich gemacht habe.
Ferner versichere ich, dass ich die Dissertation bisher nicht einem Fachvertreter an einer anderen Hochschule zur Überprüfung vorgelegt oder mich anderweitig um Zulassung zur Promotion beworben habe.
Ich erkläre mich einverstanden, dass meine Dissertation vom Dekanat der Medizinischen Fakultät mit einer gängigen Software zur Erkennung von Plagiaten überprüft werden kann.

Unterschrift: .....